Analysis of Film Cooling Performance of Tripod Hole

By Sridharan Ramesh

Dissertation submitted to the faculty of the
Virginia Polytechnic Institute and State University
in partial fulfillment of the requirements for the degree of

Doctor of Philosophy
in
Mechanical Engineering

Srinath V. Ekkad, Chair
Wing F. Ng
Danesh K. Tafti
Scott T. Huxtable
Mayuresh J. Patil

8/12/2016
Blacksburg, Virginia

Keywords: Heat transfer, film cooling, anti-vortex hole, tripod hole, CFD

ABSTRACT

Analysis of performance of tripod hole film cooling

Sridharan Ramesh

The thermal efficiency of a gas turbine directly depends on the rotor inlet temperature. The ever increasing demand for more power and advances in the field of engineering enabled this temperature to be pushed higher. But the material strength of the blades and vanes can often impose restrictions on the thermal load it can bear. This is where gas turbine cooling becomes very critical and a better cooling design has the potential to extend the blade life span, enables higher rotor inlet temperatures, conserves compressor bleed air. Among various kinds of cooling involved in gas turbines, film cooling will be the subject of this study.

A novel concept for film cooling holes referred to as anti-vortex design proposed in 2007 is explored in this study. Coolant exits through two bifurcated cylindrical holes that branched out on either side of the central hole resulting in a tripod-like arrangement. Coolant from the side holes interacted with the mainstream and produced vortices that countered the main central rotating vortex pairs, weakening it and pushing the coolant jet towards the surface. In order to understand the performance of this anti-vortex tripod film cooling, a flat plate test setup and a low speed subsonic wind tunnel linear cascade were built.

Transient heat transfer experiments were carried out in the flat plate test setup using Infrared thermography. Film cooling performance was quantified by measuring adiabatic effectiveness and heat transfer coefficient ratio. In order to gauge the performance, other standard hole geometries were also tested and compared with. Following the results from the flat plate test rig, film cooling performance was also evaluated on the surface of an airfoil. Adiabatic effectiveness was measured at different coolant mass flow rates. The tripod hole consistently provided better cooling compared to the standard cylindrical hole in both the flat plate and cascade experiments.

In order to understand the anti-vortex concept which is one of the primary reason behind better performance of the tripod film cooling hole geometry, numerical simulations (CFD) were

carried out at steady state using RANS turbulence models. The interaction of the coolant from the side holes with the mainstream forms vortices that tries to suppress the vortex formed by the central hole. This causes the coolant jet from the central to stay close to the surface and increases its coverage. Additionally, the coolant getting distributed into three individual units reduces the exit momentum ratio. Tripod holes were found to be capable of providing better effectiveness even while consuming almost half the coolant used by the standard cylindrical holes.

GENERAL ABSTRACT

Analysis of performance of tripod hole film cooling

Sridharan Ramesh

The thermal efficiency of a gas turbine directly depends on the rotor inlet temperature. The ever increasing demand for more power and advances in the field of engineering enabled this temperature to be pushed higher. But the material strength of the blades and vanes can often impose restrictions on the thermal load it can bear. This is where gas turbine cooling becomes very critical and a better cooling design has the potential to extend the blade life span, enables higher rotor inlet temperatures, conserves compressor bleed air. Among various kinds of cooling involved in gas turbines, film cooling will be the subject of this study. Its primary function still serves to reduce the heat load on the gas turbine hot gas path components while creating a thin film of cooler fluid, usually bled from compressor at an intermediate stage.

A novel concept for film cooling holes referred to as anti-vortex design proposed in 2007 is explored in this study. Coolant exits through two bifurcated cylindrical holes that branched out on either side of the central hole resulting in a tripod-like arrangement. Coolant from the side holes interacted with the mainstream and produced vortices that countered the main central rotating vortex pairs, weakening it and pushing the coolant jet towards the surface. In order to understand the performance of this anti-vortex tripod film cooling, a flat plate test setup and a low speed subsonic wind tunnel linear cascade were built.

Transient heat transfer experiments were carried out in the flat plate test setup using Infrared thermography. Film cooling performance was quantified by measuring adiabatic effectiveness and heat transfer coefficient ratio. In order to gauge the performance, other standard hole geometries were also tested and compared with. Following the results from the flat plate test rig, film cooling performance was also evaluated on the surface of an airfoil. Adiabatic effectiveness was measured at different coolant mass flow rates. The tripod hole consistently provided better cooling compared to the standard cylindrical hole in both the flat plate and cascade experiments.

In order to understand the anti-vortex concept which is one of the primary reason behind better performance of the tripod film cooling hole geometry, numerical simulations (CFD) were carried out at steady state using RANS turbulence models. The interaction of the coolant from the side holes with the mainstream forms vortices that tries to suppress the vortex formed by the central hole. This causes the coolant jet from the central to stay close to the surface and increases its coverage. Additionally, the coolant getting distributed into three individual units reduces the exit momentum ratio. Tripod holes were found to be capable of providing better effectiveness even while consuming almost half the coolant used by the standard cylindrical holes.

ACKNOWLEDGEMENTS

First and foremost, I would like to thank my Research Advisor Dr. Srinath V. Ekkad for giving me the opportunity to work with him and keeping confidence in me throughout. I am grateful for his immense guidance in my research and his valuable ideas that form the foundation of this work. While working with him, I got an opportunity to learn the nuances of the field of Gas turbine cooling techniques, and also developed better understanding on aspects of experimental heat transfer. His advice on delving deeper into the research topic and being curious and excited about the work, has certainly inculcated in me the better sense of research and has helped me build self-motivation for my work.

I would like to thank my committee members Dr. Danesh K. Tafti, Dr. Wing F. Ng, Dr. Scott T. Huxtable and Dr. Mayuresh J. Patil. Their critical feedback and advice gave a fresh perspective to my work. Courses like CFD in Heat Transfer and Radiation Heat Transfer helped me lay a strong foundation for my research work. I would like to acknowledge my project sponsor, DOE-NETL and the team Mary Anne Alvin and Ed Robey, whose supervision and management helped mold this work.

I would like to thank Dr. Chris LeBlanc, Dr. Jaideep Pandit and Dr. David Gomez Ramirez for their enthusiastic participation in my research. They have provided me with invaluable guidance throughout my PhD. I am very thankful to all the present and former members in my lab, for building a strong working environment in the lab blended with fun-filled moments. Thanks to all my friends at Virginia Tech who made this journey of mine, a memorable one. Special thanks to my close friends for being my support system throughout.

This journey wouldn’t have been possible without the unconditional love and support from my mom. I would like to express deep gratitude to my dad who kept faith in me and supported me as I embarked on this career path. He has always been a great motivation and will continue to be one.

TABLE OF CONTENTS

LIST OF FIGURES

LIST OF TABLES

CHAPTER 1

INTRODUCTION

1.1 Background

The thermal efficiency of a gas turbine directly depends on the rotor inlet temperature. The ever increasing demand for more power and advances in the field of engineering enabled this temperature to be pushed higher. But the material strength of the blades and vanes can often impose restrictions on the thermal load it can bear. This is where gas turbine cooling becomes very critical and a better cooling design has the potential to extend the blade life span, enables higher rotor inlet temperatures, conserves compressor bleed air. Among various kinds of cooling involved in gas turbines, film cooling will be the subject of this study.

Film cooling technique is in practice as a gas turbine cooling methodology since the early 1970s. Its primary function still serves to reduce the heat load on the gas turbine hot gas path components while creating a thin film of cooler fluid, usually bled from compressor at an intermediate stage. The coolant or the cooler fluid is being injected through discrete holes thus providing a film of cooler medium near the blade metal surface, protecting it from direct contact with the hot mainstream gases. Research has been conducted at a steady pace to improve the performance/effectiveness of cylindrical discrete holes, even though the performance of discrete holes can never match that of a 2-D slot. One common method of improving the film effectiveness of a cylindrical hole is to modify the exit of the hole to reduce the upward momentum of the jet, mitigate jet lift-off from the surface thus provide coolant coverage close to the surface. This would be dictated by the shape of the hole exit which accounts for the interaction of the cooling jet with the hot mainstream gas. Additionally, the coolant fluid is taken from the HP/LP compressor by directing it to the turbine, which would otherwise be utilized in the combustion chamber resulting in a reduction of overall engine efficiency. Thus more coolant usage for turbine cooling will affect overall engine efficiency. Hence, improved cooling with reduced coolant mass usage is a critical issue for modern turbine design. As a result, this study focuses on designing cooling hole geometries that produce higher film cooling effectiveness while also resulting in the reduction of

overall cooling flow rates. In order to understand the performance of film cooling hole geometries, a flat plate test setup and a low speed subsonic wind tunnel linear cascade were built.

1.2 Film cooling on flat plate

Early works to maximize the potential of cylindrical holes were carried out by Goldstein [1]–[3]. Since then numerous factors affecting film cooling performance have been thoroughly studied. Bogard and Thole [4] provided a recent summary on the technology of gas turbine film cooling. Bunker [5] did a thorough review on shaped holes. A comprehensive survey on gas turbine cooling literature has been compiled by Han et al. [6]. Relevant to this study is the work conducted by Baldauf et al. [7], [8] where the authors examined local adiabatic effectiveness and heat transfer coefficients for cylindrical holes using IR thermography. Effects of blowing angle, hole spacing, and density ratio were investigated. It was observed that, for the range of blowing ratios tested, the peak value of adiabatic effectiveness lay around 0.85 to 1.0 with a momentum ratio of 0.4 and 0.5 respectively. Sinha et al. [9] also conducted flat plate experiments with cylindrical holes to study the effect of density ratio and momentum flux ratio on laterally averaged film effectiveness. Measurements were taken using a series of thin ribbon thermocouples that were attached to the test plate. The effect of density ratio on film cooling effectiveness while maintaining constant velocity ratio, blowing ratio, and momentum flux ratio was studied. Using a similar test facility, Schmidt et al. [10] performed experiments to understand the effect of compound angle on round holes and holes with diffusing expanded exits. The authors concluded that the addition of a compound angle improves effectiveness at higher momentum flux ratios while a combination of forward expansion and compound angle yielded the best results. Gritsch et al. [11] investigated film cooling performance of shaped cylindrical holes at different blowing ratios. The holes that had laid-back fan-shaped exits performed better than cylindrical and fan-shaped holes.

In 2006, Heidmann and Ekkad [12] started working on a novel concept for film cooling holes referred to as anti-vortex design. In addition to a central cylindrical hole, the coolant was also ejected through two bifurcated cylindrical holes that branched out on either side of the central hole resulting in a tripod-like arrangement. Coolant from the side holes interacted with the mainstream and produced vortices that countered the main central rotating vortex pairs, weakening it and pushing the coolant jet towards the surface. Given the size of the tripod hole arrangement, there

was one tripod hole set for every 2 cylindrical holes, which implied that tripod holes have coolant coming out at lower exit momentum for the same coolant mass flow rate. Tripod holes were investigated further by Dhungel et al. [13] where the side hole placement and branching angle were optimized. Leblanc et al. [14] further extended the work of Dhungel et al. [13] with a modified design where the side holes were of the same diameter as the main hole. With the new tripod design, Leblanc et al. [14] performed flat plate experiments that showed that a 65% increase in film cooling effectiveness over cylindrical holes with standard pitch was achievable while consuming 50% less coolant.

The development and transition of a film cooling hole concept from its design phase to its implementation in the industry is slow. Manufacturability, as well as the performance of the cooling hole with imperfections are concerns that must be fully addressed prior to incorporating a new technology in industrial designs. Johnson et al. [15] for instance, studied the impact of manufacturing techniques on film cooling effectiveness. The authors compared film cooling effectiveness of cylindrical holes which were fabricated using four different manufacturing methods, using temperature sensitive paints. The authors showed that the manufacturing technique had a noticeable impact in the performance of the cooling hole which was more pronounced at higher blowing ratios. Jovanovic et al. [16] also presented the effect on adiabatic film cooling effectiveness of hole imperfections in the form of a torus inside a cylindrical film cooling hole. The location of this torus was found to have an impact on the cooling effectiveness.

The Anti-Vortex hole design has proved to be a potential alternative to dramatically improve film cooling technologies. Manufacturability studies however are lacking and these are critical for the prompt adoption of the tripod hole technology in industry. Recently, an innovative method to manufacture tripod holes was discussed by Alvin et al. [17]. This realistic manufacturing process for the tripod hole geometry results in a modified design with chamfered corners at the hole inlet and outlet. Moreover the region where the holes bifurcate into three individual units included a webbing. The original design studied computationally and experimentally in previous studies [14] featured sharp corners which are not possible to achieve from a manufacturability stand point. Figure 1 shows an illustration that emphasizes these features. Additional details are provided in the “Film hole geometries” section. The film cooling tripod hole with the realistic manufacturing features was termed “as manufactured”. Coupons with as manufactured tripod holes, cylindrical holes, and no holes will be tested in a high temperature rig facility at NETL in the future. It is

critical to estimate the performance of the as manufactured design prior to the experimental effort and hence the realistic design was fabricated using additive manufacturing for laboratory testing. Moreover, studying the gap between the design phase of a cooling hole and the implications of its manufacturability are critical for the prompt incorporation of the technology. Therefore the thermal performance of the realistic as manufactured tripod hole design, along with the idealized tripod design were studied in the present investigation. Cylindrical and shaped cylindrical holes were also tested for comparative purposes.

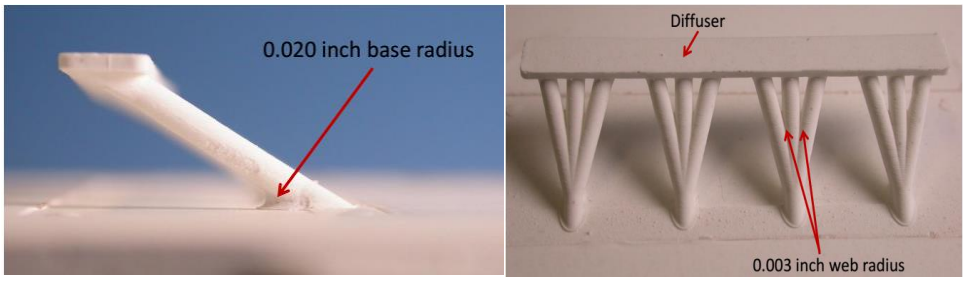

Figure 1 Example of filleting provided for hole inlet and webbing near hole bifurcation

1.3 Film cooling on an airfoil

A detailed review of all work prior to year 2000 regarding film cooling hole geometry is provided by Han et al. [6]. Another excellent summary with more recent research conducted in gas turbine film cooling was written by Bogard and Thole [4]. Of all the studies mentioned in the above literature, few contributions relevant to film cooling on turbine vanes are mentioned here. The effect of surface curvature on film cooling effectiveness was thoroughly studied by Ito et al. [18]. The relative performance on a concave or convex surface was dictated by the momentum flux ratio times the cosine square of the hole inclination angle w.r.t to the curved surface. Even at BR = 1.0, if this factor is under unity, film cooling holes on the convex wall can provide almost twice better cooling when compared to a flat or concave wall. Drost et al. [19] investigated film cooling effectiveness at various operating conditions like exit Reynolds number, density ratio, mainstream turbulence levels, and blowing ratio on pressure side and suction side of the airfoil. Zhang et al. [20] studied the effects of hole injection angles in the showerhead region and pressure side surface of the airfoil at different blowing ratios. Conventional cylindrical hole at 20° and 40°

were compared against shaped hole with 40° injection angle. For the range of bowing ratios tested (BR = 1.5, 2.0 and 2.5), it was observed that the 20° cylindrical hole was capable of delivering higher effectiveness except in the region close to the injection point where the 40° shaped hole proved to be better. Ethridge et al. [21] investigated film cooling performance on suction side of a vane that was subjected to a strong curvature as well as strong favorable pressure gradients. Film cooling effectiveness was evaluated at varying blowing ratios, turbulence intensities and density ratios. Ligrani et al. [22] studied the effect of hole shape and orientation of a film cooling hole located on the gill region on the suction side of the turbine vane. Round and shaped holes with axial, radial and compound angles were tested at two different blowing and density ratios. Results suggested that round radial holes could deliver similar adiabatic effectiveness and heat transfer enhancement in addition to the lower manufacturing costs. The study also pointed out that compound angled holes might be a better alternative than shaped holes. The impact of surface curvature at the film cooling hole location and the applicability of the scaling parameter (2r/d) was studied by Winka et al. [23]. Six different cases were tested which covered various surface curvatures and hole locations. Increasing the curvature of the surface (2r/d), from 28 to 40, caused lower area averaged adiabatic effectiveness at all blowing ratios. The normal pressure gradient on the coolant film increases with surface curvature, thereby causing the jet to stay close to the surface.

Several studies in the past have shown that cylindrical hole effectiveness diminishes at higher blowing ratios. According to Haven and Kursoka [24], the counter rotating kidney vortices result in the jet lift off by mutual induction and also causes the hot gas to get entrained near the turbine wall. The role of exit momentum flux ratio in deciding jet attachment to the wall surface has been explained in [4]. Fan shaped holes were found to be an effective solution for the lingering kidney vortices encountered in a cylindrical holes. Haven and Kurosaka [24] also took efforts to explain that the process of shaping the hole exit not only reduces the jet velocity but also widens the gap between the vortices that are formed in the jet, causing the jet to stay closer to the surface. There are however limitations to shaped film hole design mainly because of cost concerns, machining accuracy, and availability of material thickness for shaping, as noted by Bunker [5] in his review of shaped hole film cooling. Many other unique cooling hole designs have been proposed in recent years to overcome the so called kidney vortex and improve film cooling effectiveness. Ideas such as struts within the holes (Shih et al [25]), cusp-shaped holes (Papell [26]), triangular tabs at the

hole exit (Zaman and Foss [27]), trenched holes (Bunker [28], , Lu et al. [29]), double jet configuration (Kusterer et al. [30], and dumbbell and bean shaped holes (Liu et al. [31]) have been proposed and studied. Many of the proposed designs are shown to be effective in this regard, but majority of these ideas prove to be difficult to manufacture and/or produce unwanted features, such as additional solid surfaces that must be cooled or additional sharp edges that are aero-dynamic liabilities.

The anti-vortex (AV) hole or the tripod hole design intends to counteract the central kidney vortex using a much simpler approach. The holes in this design are cylindrical in geometry and therefore easy to manufacture. The 3-hole design can also provide alternate pathways for the secondary fluid to exit should there be plugging of holes due to deposition. The computational fluid dynamic (CFD) study by Heidmann and Ekkad [12] evaluated the detailed flow features associated with the tripod hole design. Various configurations of the AV hole concept were tested experimentally by Dhungel et al. [13] that included variations in the side hole ejection location relative to the main hole and side hole-to-main hole diameter ratio. The best design from Dhungel et al. and the initial anti-vortex design were studied along with the baseline cylindrical hole. It was observed that the modified anti-vortex design was capable of offsetting the counter rotating vorticity by 100%, increasing the film cooling effectiveness by 0.2. The current authors improved upon the design of Dhungel et al. [13] by aligning the hole exits in one single plane and having a uniform hole diameter for all three holes of a tripod unit. ([14], [32]). This resulted in an anti-vortex design that sports two compound angled cylindrical hole branching at 15° towards either side of the central hole. The coolant distribution through each hole at lower blowing ratios is more uniform unlike the earlier design where the majority of the coolant (~ 65%) exited through the main hole. The 15° branching angle on a hole l/d=8 causes the individual tripod holes to be placed 6 hole diameters apart. This causes the pitch to be twice as large as the convection cylindrical hole pitch of 3d.

When evaluating the film cooling performance of various holes shapes, efforts are taken to ensure that the design parameters remain consistent. Comparing an anti-vortex design with twice the pitch brings up the discussion of the amount of coolant flow rate or the blowing ratio at the hole inlets between hole geometries. Since the current anti-vortex design involves almost half the number of cylindrical holes inlets, maintaining the coolant mass flow rate doubles the blowing ratio at the inlet while maintaining the same blowing ratio results in half the amount of coolant consumed. Apart from increasing the film cooling effectiveness, one of the objectives of film cooling studies

is also to reduce the coolant consumption. Since coolant mass flow rate is a critical gas turbine design parameter, it was kept constant between hole shapes. The blowing ratio at the tripod hole inlet will be twice that of the cylindrical hole. But owing to the uniform distribution at the lower flow rates, the blowing ratio at the exit of the each hole of a tripod unit will be nearly 2/3rd of that of the cylindrical hole. This reduction in the coolant velocity owing to branching, acts favorable to the performance of the tripod hole. Since Heidmann's [12] study confirmed the offset in streamline vorticity owing to the tripod hole unit, the combined effect of lowered exit momentum and suppression of CRVPs makes the anti-vortex superior to the conventional cylindrical holes. Interestingly, in spite of having higher exit velocity at BR 2.0 and 3.0 in case of the AV hole, it still provided a better cooling compared to CY BR 0.5, suggesting that the vortex from the central hole gets subdued to a considerable extent, resulting in lower jet lift off unlike in a cylindrical hole.

Apart from the cylindrical and the anti-vortex hole, shaped cylindrical and shaped anti-vortex holes were also tested. The anti-vortex hole with and without exit shaping was found to provide better cooling when compared to the cylindrical and the shaped hole. However, the shaped cylindrical hole employed a unit area ratio since the shaping was performed at the hole exit. Future studies will focus on comparing the anti-vortex design with an industry standard hole design. But as mentioned before, unlike shaped holes which require expensive manufacturing techniques, anti-vortex holes rely only on cylindrical holes. Recently, a novel manufacturing technique has proven capable of implementing the anti-vortex design on a flat plate [17]. Evaluation of the performance of the anti-vortex hole on an airfoil will be followed by subsequent experiments at high temperatures and higher pressures, followed by a study in a rotational frame of reference.

1.4 Numerical and thermal stress analysis due to film cooling holes

Film cooling technique has remained a widely researched topic since early 1970's. In spite of consistent growth in research, the field has seen too less advancements. Pitch-to-diameter ratio, length-to-diameter ratio, coolant injection angle, shape of hole, hole location on the airfoil, blowing ratio, inlet Mach number and numerous other factors influence the performance of film cooling in their own way. The hole geometry alone has seen quite a few novel ideas. These, only a sample, include shaped, trenched, tripod, compound angled holes, usage of dumbbell or ellipse shaped holes. Though literature provides enough support to claim that the alternative designs have

thermal advantage, the aerodynamic losses, structural integrity and practical feasibility of the design need to be considered. Failure in application may be attributed to any of these issues.

The concept of tripod holes or Anti-Vortex (AV) holes was proposed by Heidmann and Ekkad [1], followed by thorough investigation by Heidmann [2] and Dhungel et al. [3]. Tripod holes have two bifurcated holes that branch out of the main hole and exit upstream of the main hole resulting in vortices that suppress the effect of the counter-rotating vortex pair (CRVP) generated by the main hole. The study tries to estimate thermal stresses, a first stage nozzle guide vane would experience if cylindrical film cooling holes were replaced with tripod holes. The nozzle guide vane receives the complete burst of hot gas ejecting from the combustion chamber, its direct exposure poses higher risk potential for failure. Thus, application of a more advanced cooling concept becomes critical in this region. References [1-4] studied various aspects of tripod hole film cooling and reported higher film cooling effectiveness, signifying potential benefits of anti-vortex holes. It becomes imperative to predict and test its effect on the blade airfoil. A numerical analysis has been performed wherein finite volume approach for a flat plate test rig is established and found to match the experimental results. Results from the conjugated CFD analysis are coupled to a finite element solver that predicts the thermal stress and strain generated on the flat plate which are later available for some discussion.

The field of computational analysis in film cooling gas turbine has seen quite a lot of literature. Earlier, numerical studies were aimed at predicting the blade temperature profile, adiabatic film cooling effectiveness, heat transfer characteristics, flow physics near cooling holes, and some understanding on mainstream-jet interaction and different vortices present inside the turbine. Some recent work have extended CFD for thermal stress evaluation. Studies that are discussed below used CFD as a tool to understand the flow behavior and explain results from experiments.

Leylek and Zerkle's [5] attempt to understand the fluidic nature of film cooling by developing a three-dimensional Navier-Stokes model was widely received. The detailed study described the complex nature of the flow inside the film hole, at exit plane of coolant jet and interaction between the hot mainstream and coolant jet. Adiabatic effectiveness performance was also reported.

Similar efforts were undertaken by Oguntade et al. [6]. They investigated a new approach in CFD where addition of hexahedral layers near the hole region gives results that are in good agreement with the expected experimental results. They also explored the effect of turbulence model and showed that standard k-ε model gave best results. Harrison et al. [7] performed a

comparative study on prediction of film cooling performance under different turbulence models. Realizable k-ε, standard k-ω (SKW) and RSM turbulence models were compared with experimental results to match laterally averaged effectiveness as well as centerline adiabatic effectiveness. It was concluded that a single best model for predicting film cooling effectiveness is not possible. The RKE model was found to predict centerline effectiveness and baseline heat transfer study but SKW model predicted laterally averaged adiabatic effectiveness better. Overall, they concluded that choice of any turbulence model would depend upon the application under examination.

Sierra et al. [8] made efforts to study the relationship between thermal stress generated on the blade and heat transfer from the hot gas path onto the blade geometry. The study comprising experimental and numerical analysis involved validation of the conjugate CFD model and added effort to perform a finite element analysis on the blade geometry to analyze the thermal stress distribution. Computations involved usage of RSM to incorporate turbulence into the system.

Kim et al. [9] followed a similar approach involving conjugate heat transfer study and stress analysis. A second row blade, made of CM247LC, with circular cooling passages was modelled in CFX-11. The SST low-Re turbulence model was reported to have been used. Results from the fluid flow analysis like temperature and pressure conditions, were coupled with the finite element module of ANSYS -11 to calculate stress distributions. Current research in this paper follows similar approach.

1.5 Numerical analysis on film cooling performance of tripod hole

Gas turbine film cooling has been in focus since the late 60s. In spite of the numerous experimental and numerical studies, this field still receives the same attention it once used to get. The biggest reason must be its application and its significance: gas turbine industry, both aero derivate and land based engines, whose continual growth relies on the research contributions heavily. Secondly, prospects for advanced cooling techniques are greatly improved by the breakthrough advancements in the manufacturing sector. Numerous film cooling hole shapes have been proposed in the past. Of all the hole geometries, cylindrical holes with shaped exits has been the major breakthrough in external cooling for a long time. Bunker et al. [33] provided a summary of proposed cooling techniques that showed potential and explained thoroughly the strengths and

weakness of each geometry. The author also explained the various quality and judgement factors based on which film cooling holes are rated. In general, higher the rating, the chances of getting adopted by the industry is higher. The anti-vortex film cooling hole proposed by Heidmann [34] and later explored in detail by Dhungel et al. [13] was also listed along with other film cooling hole concepts like shaped, funnel shaped, chevron film hole, cratered film hole, shallow trench holes, double jet film cooling holes, etc. Among the sixteen holes evaluated, Dhungel's anti-vortex holes were ranked 12. As mentioned by the author, the main contributors for the low score were the difficulties in repairing and associated costs, precise manufacturing of the side holes and flow sensitivity. From the hole geometry perspective, the above mentioned factors can be attributed to the design of the side/ligament/sister holes. The original tripod hole came with side holes whose diameter was half of central hole and its location w.r.t the central hole was varied. Dhungel et al. [13] found that three of the six variations in sister hole design, provided similar cooling performance and two of those can be considered as an alternative to the shaped hole in terms of manufacturability of the shaped hole. The current version of the anti-vortex hole has ironed out some of the inherent issues present in the earlier version. The side holes have the same diameter as the central hole and branch out from the central at the hole inlet, implying that all three holes of the unit share the same hole inlet. Recently, an innovative method to manufacture tripod holes was discussed by Alvin et al. [17]. The manufacturing process however, introduced small additional features to the tripod hole geometry results. Modifications were restricted to the hole inlet, exit where sharp corners were chamfered and the region where the holes bifurcate into three individual units included a webbing. These manufacturable AV holes were compared [32] with the original geometry and were found to provide similar cooling performance. With the advent of additive manufacturing and its reception by the gas turbine industry, numerous cooling configurations that were once shelved due difficulties associated with its manufacturing might resurface.

Computational fluid dynamics has been an integral part of film cooling research for a long time. The jet in crossflow problem has been studied by numerous scholars. Kercher [35] provided a complete bibliography of all the CFD work done prior 1996. Many scholars, since then, have evaluated the performance of various turbulence models in predicting the flow features of the cooling jet. Few such contributions relevant to the current study are mentioned here. Emphasizing the importance of turbulence closure model, Ferguson et al. [36] tested a combination of SKE, RNG-KE and RSM and near wall treatments: generalized and non-equilibrium wall functions. But

it was the final SKE with a two layer zonal model that was found to predict accurate results comparatively. The coolant jet-lift off and reattachment could be better predicted with model owing to the usage of a different length scale for the viscosity affected region close to the wall instead of applying a wall function. In their later study [37], RKE model as also included. It was observed that RKE model was capable of predicting results closer to the more superior RSM model and the actual experiments compared to the SKE and RNG-KE. The poor prediction on the airfoil profile loss was attributed to the high amounts of turbulence generated by these. Harrison et al. [38] compared various RANS turbulence models including RKE, SSTKW and RSM. It was observed that while RKE model predicted the centerline effectiveness better, laterally averaged effectiveness predicted by the SSTKW model was found be to be closer to the experiments.

Ravelli et al. [39] displayed the superior capability of the SAS model to predict the trailing edge cutback film cooling performance. The unsteady RANS model was able to capture the vortex shedding only a certain extent and the predicted streamwise film cooling effectiveness was still not close enough to the experimental value. The SAS model however, was found to match the experimental values better owing to its better prediction of vortex shedding present in this region.

In an attempt to study the effects of internal channel crossflow on film cooling, Stratton et al. [40] tested the two widely used RANS models: RKE and SSTKW. Adiabatic effectiveness at different blowing ratios were compared with the experiments conducted by McClintic et al. [41] and the LES model that was developed to understand the flow unsteadiness. Both RANS models were reported to be inconsistent in predicting the adiabatic effectiveness compared to the accuracy of the LES model but agreed on the flow features though. The authors also highlighted the pros and cons of these two RANS models. The RKE model performed better only at lower blowing ratios because of the error in predicting the jet separation and reattachment at higher blowing ratios. The SSTKW model on the contrary, works better at higher blowing ratios but could not capture the swirling flow inside the hole accurately at lower blowing ratios. These observations were noticeable in the laterally averaged effectiveness plots. Experiments showed a sudden dip around x/d=1, indicating jet separation and subsequent increase in effectiveness shows sign of coolant jet reattachment.

A commonly observed trend in all these numerical studies is that the above mentioned RANS models are capable of predicting the coolant jet-mainstream interaction only to a certain extent. Each of these models possess a drawback due to which certain flow features are not predicted

accurately. As a result, these studies are often comparative in nature. The current study also relies on one such analysis where various hole shapes (CY, AV, SH and AVSH) are compared at different blowing ratios. SSTKW model was preferred over RKE as it has proven to capture the jet separation/reattachment and predict the laterally averaged effectiveness accurately. The shaped hole used in the current study was obtained from Schroeder et al. [42]. Commonly known as the 7-7-7 shaped hole, this hole geometry was designed as a baseline hole for comparative studies. It sports a 7deg forward and lateral diffusion and 30deg hole inclination. With l/d=6, the hole is smaller than the ones employed in the current study. The lateral hole pitch is 6d, same as the AV hole, indicates same blowing ratio at the hole inlet for a given coolant mass flow rate for these two geometries.

Repko et al. [43] presented flow features of tripod hole that was proposed by Heidmann et al. [12] and optimized by Dhungel et al. [13]. Unsteady RANS simulations with k-omega turbulence model were used to understand the vortices that were generated at higher turbulence levels and its impact on the adiabatic effectiveness. It was observed that with increasing turbulence intensity from 5% to 20%, at BR=2.0 and DR=2.0, the adiabatic effectiveness of the tripod hole increases owing to the reduced vertical penetration of the coolant jet and its subsequent spreading in the lateral direction.

The double hole configuration, similar to the tripod holes, are capable of generating anti-kidney vortices, as shown by Kusterer et al. [44]. By arranging the two holes in such a way that the CRVP generated from one hole is opposite to the other, a double jet anti-kidney vortex pair was generated. They [30] showed that the double jet film cooling holes could deliver a higher effectiveness, beyond x/d=5 and at all blowing ratios, when compared to cylindrical holes and trenched holes. These holes were also shown to provide better cooling compared to shaped holes but only at blowing ratios 1.5 and above. Most recently, Chang Han et al. [45], [46] studied the effects of blowing ratio and density ratio on film cooling performance of the double jet system. Later, the double hole system was subjected to a parametric optimization where lateral hole pitch and compound angle were varied in order to maximize its cooling potential. Chi et al. [47] performed a parametric optimization study on the tripod hole with asymmetric side holes. Nine different parameters influencing the tripod hole was chosen for the study which also included position of branching, hole diameters, injection angle and streamwise and spanwise offsets of the two side

holes from the central hole. The focus here however, was to study the performance of the double jet film cooling hole system, a resultant of the orientations of the two asymmetric side holes.

A similar approach is followed in the current study where the branching angle of the tripod hole alone was being varied. The other parameters such as hole branching location, hole diameters etc. were kept constant as a part of the standard anti-vortex tripod hole system. The baseline case sports a 15° branching angle (AV15°) and has been well documented. LeBlanc et al. [48] studied the effect of tripod hole branching angle while comparing the baseline case (15°) with a 30° tripod hole (AV30°). The experimental data from these two studies [32], [48] serves as a validation for study: Effect of branching angle. Tripod holes with 12 different branching angles, starting from 5° to 30° in steps of 2.5°, are compared with the baseline case (AV15°).

1.6 Nomenclature

a	Circular cross sectional area of the cylindrical hole
ABS	Thermoplastic polymer - Acrylonitrile butadiene styrene
AR	exit-to-inlet area ratio of cooling hole
AV	Anti-Vortex hole (Tripod hole)
BR	Blowing ratio
C_{ax}	vane axial chord length, m
CFD	Computational Fluid Dynamics
CRVP	Counter rotating vortex pair
CY	Cylindrical hole
d	Hole diameter (m)
DR	Density ratio
h, hf	Heat transfer coefficient, laterally averaged (W m^{-2} K^{-1})
ho	Heat transfer coefficient, baseline, laterally averaged (W m^{-2} K^{-1})
I	Momentum flux ratio
IR	Infrared
k	Thermal conductivity (W m^{-1} K^{-1}),
k	turbulent kinetic energy (m^2/s^2)
l	Hole length (m)

L	Thickness of the test plate (m)
LES	Large Eddy Simulation
$\dot{m}$	Mass flow rate (g/s)
n, N	Number of film cooling holes
p	Hole pitch (m)
q	Heat flux due to film cooling (W m^{-2})
q_0	Heat flux for the baseline case (W m^{-2})
Δq	net heat flux reduction
R	gas constant
RANS	Reynolds Averaged Navier Stokes
RKE	Realizable *k-ε*
RNGKE	Re Normalization Group *k-ε*
Re_d	Reynolds number of the mainstream based on hole diameter
SAS	Scale adaptive simulation
SH	Shaped hole
SH-777	Baseline Shaped hole [42]
SHAV	Shaped Anti-Vortex hole
SKE	Standard *k-ε*
SKW	Standard *k-ω*
SSTKW	Shear Stress Transport *k-ω*
t	Time (s)
T	Temperature (K)
Tu	Turbulence intensity percent,
U, V	Velocity (m/s)
x	axial distance from hole leading edge/streamwise direction or axis label
y	spanwise direction or axis label

Greek

α	Thermal diffusivity (m^2/s)
ε	Turbulent dissipation
δ	Boundary layer thickness (m)

η	Adiabatic film-cooling effectiveness
ρ	Fluid density (kg/m^3)
ω	Specific dissipation
φ	overall effectiveness
μ	gas dynamic viscosity

Subscripts

avg	average
ax	axial
c	centerline
c	coolant
i	initial
in	inlet
m	mainstream
w	wall / flat plate surface
corr	corrected
i	inlet
ins	near-perfect insulated surface
main	mainstream air with no secondary gas injection or adiabatic wall temperature
sg	secondary gas
∞	mainstream air

CHAPTER 2

FILM COOLING PERFORMANCE ON A FLAT PLATE

Pervious research conducted by Leblanc et al. [14] focused on obtaining adiabatic film cooling effectiveness using steady state experimental techniques. In the present study, transient heat transfer experiments were conducted using IR thermography minimizing conduction effects around the hole exit and improving the accuracy of the measurement. The current work observed that the performance of the as manufactured design did not incur any penalty in terms of cooling performance compared to the idealized design. The studied manufacturing features are thus predicted to not negatively impact the heat transfer characteristics of the tripod cooling hole geometry. This is an important conclusion to move forward the adoption of this cooling technology to industrial systems.

2.1 Experimental Setup

Flat plate models have always been convenient to test film cooling concepts. A schematic of the flat plate test section used in this study is shown in Figure 2. The air exiting the blower passed through the mixing chamber before going through a mesh heater. The mixing chamber consisted of an array of pins stacked in a staggered configuration and a honey-comb structure close to the exit so that the air mixture was uniform and straight upstream of the mesh heater. The mesh heater was made of stainless steel and was connected to a power supply capable of supplying up to 25 kW power. The energy provided by the source was sufficient to raise the mainstream air temperature from ambient room temperature to $50 - 60$ °C. The incoming flow velocity was measured by a Pitot tube mounted 20 cm downstream of the test section inlet. The mainstream velocity was fixed at 7.9 m/s, which corresponds to a $Re_d \sim 3200$. The measured turbulence intensity was low, approximately 2%. The 101.6 cm long test section had a constant cross-sectional area of 7.62×30.5 cm (height × width). The base plate of the test section was constructed of 2.54 cm thick, low thermal conductivity ABS material ($k = 0.187$ W m^{-1} K^{-1}). A 0.47 cm diameter trip rod was located on the base plate, 5 cm from the inlet, in order to make the boundary layer turbulent. The base plate was designed with a hollow cavity which supported a mating piece with the cooling

hole geometry under study. This insert plate was replaceable and could be fabricated in a rapid prototyping machine using ABS material. The 3D printing process had a tolerance of $\pm$ 0.04 mm/mm which is lower than the dimensions of the hole features.

When sitting flush in the cavity, the holes are roughly 48 holes diameters downstream of the inlet to the flat plate setup. The normalized boundary layer thickness (δ/d) was $\sim$ 2.37 at the leading edge of the hole array. The plenum chamber for the secondary fluid, made of plastic acrylic glass, was located beneath the test insert plate. Before entering the plenum, the compressed air was metered and then directed through an inline heater with variable power output. Its temperature was monitored using a thermocouple mounted close to the outlet of one of the cooling holes. Surface temperature measurements were taken using an IR thermal imaging camera. The IR camera had a working range of -40 to 100 °C and an accuracy of ± 2 %. After further calibration, with a fast response thermocouple and accounting for emissivity of the medium and transmissivity of the stretched polyethylene sheet (IR window), the accuracy was found to be less than 1.0 °C.

2.1.1 Film Hole Geometries

The six film cooling hole geometries tested in this study are shown in Figure 3. The first geometry was a cylindrical hole (CY), 0.635 cm in diameter, with an axis inclined at 30° from the surface in the streamwise direction. The hole length-to-diameter ratio (l/d) was 8 and the pitch-to-diameter ratio (p/d) was 3. The shaped holes (SH) also had the same l/d and p/d except that the hole exits featured a 10° fan-shape angle and a 10° laidback angle. The shaping however, began at the leading edge of the hole, making the area ratio unity. The tripod hole (AV) consisted of a 3-hole unit in which the main or the central hole was identical to the first geometry but had an additional cylindrical hole on both sides that branched out at 15° compound angle and were connected together at the inlet such that the metering area at the entrance of the coolant remained circular (similar to both the cylindrical and the shaped holes). All three holes of the tripod hole set were inclined at 30° in the flow direction from the surface. For the AV holes, the l/d ratio of the center and the side holes was 8 and 8.3, respectively. The p/d ratio between the main holes was $6d$, between center and side hole $1.75d$, and between the side holes of the adjacent AV unit $2.5d$.

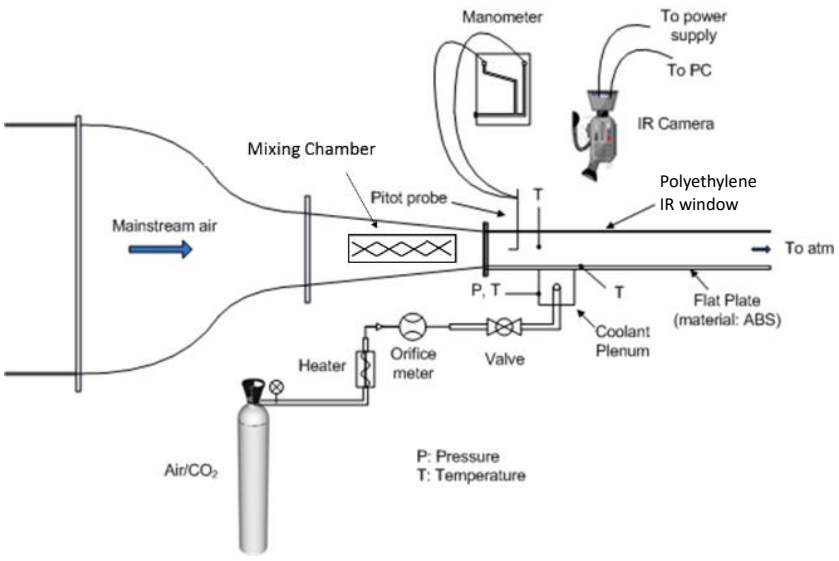

Figure 2 Schematic of the test section

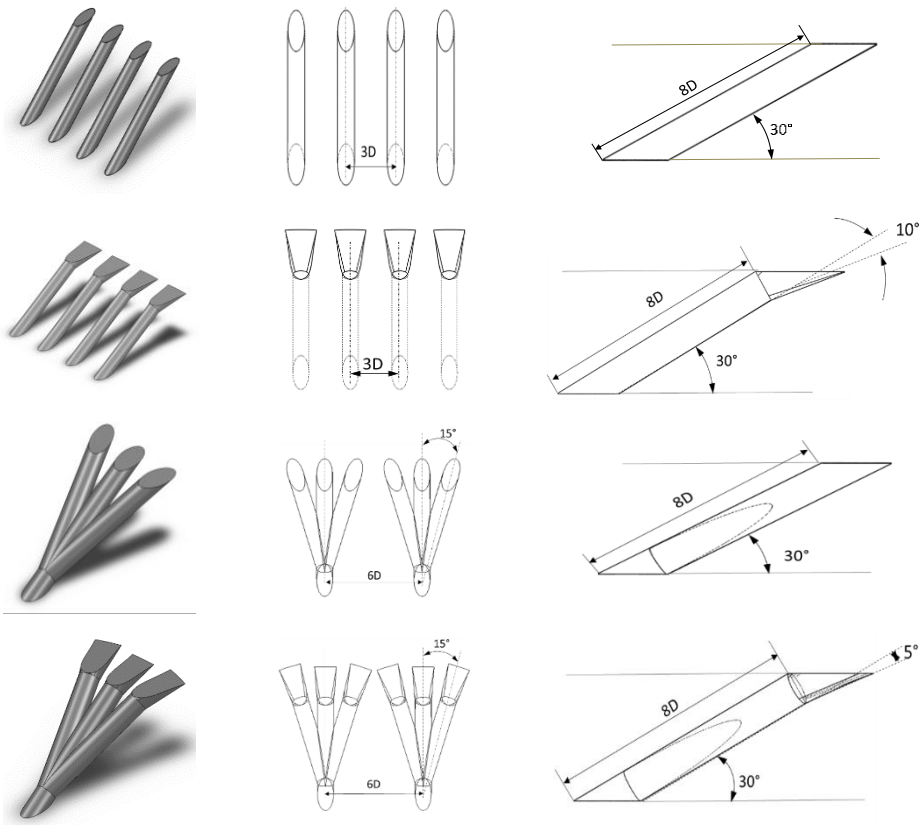

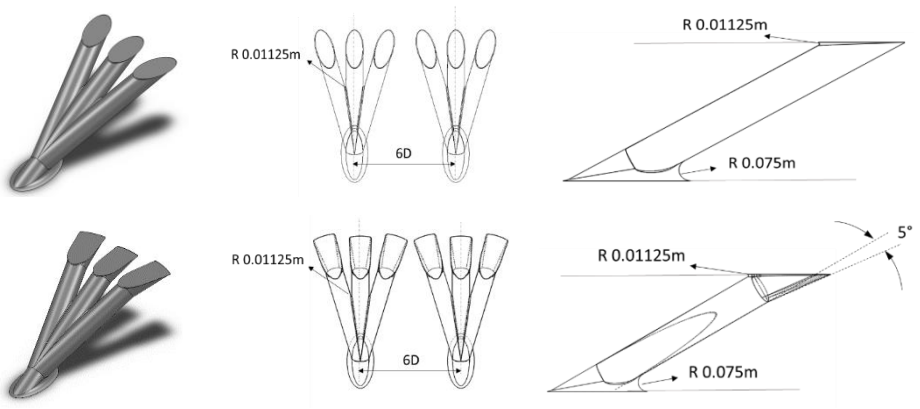

Figure 3 Film cooling hole configurations

The fourth geometry (SHAV) was also a tripod hole but had shaped hole exits. A 5° fan-shape and laidback angle was provided instead of 10°, to ensure that the adjacent side holes did not intersect. The final two geometries were modifications of the tripod hole designs (with and without shaping) that account for manufacturing features including round corners, filleted radii, and webbing between holes. Fillet radius for each location is shown in Fig. 3.

2.2 Measurement theory

The film cooling performance of these six geometries was evaluated by conducting transient heat transfer experiments in a flat plate test rig. Infrared (IR) thermography was used to obtain the surface temperature of the flat plate. Prior to the measurements, calibration of the entire IR optical system and signal was required. For this purpose a thermocouple was mounted on the test surface using aluminum tape, located outside the measurement region to avoid interference with the area of interest. The test surface was sprayed with flat black paint to increase its emissivity to a value close to 1.0. The IR camera was focused on the test surface, the field of view of which also encompassed the surface thermocouple. The temperature recorded by the thermocouple was compared to that of the IR camera and the emissivity was adjusted to match both measurements. A number of temperatures were used to determine the correct emissivity of the test surface. During the emissivity calculation, the polyethylene sheet (IR window) was removed. In order to determine the transmissivity of the polyethylene window, a similar test was conducted with the window in

place. With the known emissivity from the prior test, transmissivity of the window was altered until the IR camera readings coincided with the thermocouple readings. The emissivity of the black painted test surface was of 0.98. The calibrated transmissivity for the polyethylene sheet was 0.9.

The test began by setting the mainstream air to the proper inlet velocity (7.9 m/s), corresponding to a Reynolds number of ~ 3200 based on the cooling hole diameter. Upstream of the cooling holes a thermocouple was placed to measure the mainstream temperature (T_m). The coolant (secondary fluid) temperature (T_c) was measured by a thermocouple located near the exit of one of the film cooling holes. All thermocouples were connected to a data acquisition system. The coolant supply loop consisted of an inline heater element, a rotameter, and a valve. The secondary fluid was set to the appropriate blowing ratio using the rotameter.

Two sets of experiments were conducted in order to capture the film cooling effectiveness and heat transfer coefficient accurately. In the first experiment both the mainstream and coolant were sent at a relatively close temperature of about 50 °C. The coolant film as a result also remained close to the mainstream temperature. In the second run, the mainstream temperature was retained (~ 50 °C) while the secondary fluid was sent at room temperature (22 °C). It was assumed that the heat transfer coefficient (h) and the adiabatic film cooling effectiveness (η) were the same in both experimental runs. The transient evolution of the surface temperature (T_w) was recorded using the IR imaging system as the mainstream and coolant flowed over the flat plate. For the regions on the flat plate where there was no coolant, both experimental runs would yield a similar T_w time evolution. For regions with large coolant presence, T_w would increase faster for the hot run. Each run lasted ~ 60 seconds, within the time duration for which the 1D semi-infinite heat conduction assumption was valid. The time taken for the heat flux to penetrate a one inch thick plate can be found using Equation 1.

$$t < \frac{c\,L^2}{\alpha} \tag{1.1}$$

where $c \approx 0.077$, $L = 0.0254\ m$ and $\alpha = 1.2e-7\ m^2/s$

$$t < 413.952\ s$$

The 1D semi-infinite transient heat conduction equation with film cooling for run 1 and 2 is shown below, for an initial surface temperature of T_i.

$$T_w - T_i = \left[1 - e^{\frac{h^2 \alpha t}{k^2}} erfc\left(\frac{h\sqrt{\alpha t}}{k}\right)\right](\eta\, \mathrm{T}_c + (1-\eta)\mathrm{T}_m - T_i) \quad (1.2)$$

Run 1: $T_m = T_c \approx 50$ °C, $T_i \approx 22$ °C

Run 2: $T_c = T_i \approx 22$ °C, $T_m \approx 50$ °C

This equation corresponds to the response of the surface temperature to a perfect step in the mainstream flow temperature from T_i to T_m. During the experiment, the mainstream temperature varied from 22 °C to a final value of ~ 50 °C and hence Duhamel's superposition technique was implemented [12] using the step response. The heat transfer coefficient (h) and adiabatic film cooling effectiveness (η) were found by solving the above equations simultaneously at different times (t).

2.2.1 Test Conditions

As shown in Table 1, a total of 19 experiments were conducted to study the effect of blowing (BR) on adiabatic film-cooling effectiveness. The blowing ratio (BR) and momentum flux ratio (I) are defined as

$$BR = \frac{(\rho V)_c}{(\rho V)_m}, \; I = \frac{(\rho V^2)_c}{(\rho V^2)_m} \quad (1.3)$$

where V_m is the mainstream air velocity, V_c is the coolant bulk velocity based on the nominal hole diameter 'd', ρ_c and ρ_m are the densities of the coolant and mainstream respectively. Defining the blowing ratio based on the nominal hole diameter instead of the hole exit or the inlet area will alleviate the issues related to multiple exits (tripod hole) and chamfered inlets (as manufactured design). The coolant mass flow rate for the ideal tripod hole and the "as manufactured" design was matched for a better comparison. The mass flow rate ($\dot{m}$) per hole entrance for a given blowing ratio is given Equation 4.

$$\dot{m} = BR \cdot (\rho V)_m \cdot a_{in} \quad (1.4)$$

The flow rates given in Table 1 are per hole entrance. Since the number of AV holes required is half that of traditional cylindrical or shaped holes (to cover the same span), AV holes operate at twice the blowing ratio to achieve the same flow rate through each hole inlet. Equivalently, at the same blowing ratio, the AV holes require half the coolant used for the cylindrical and shaped holes.

Table 1: Summary of experimental conditions

Hole	**BR**	**$\dot{m}$ per hole entrance (g/s)**
CY, SH	0.5, 1.0, 2.0	0.15, 0.3, 0.6
AV, AVSH	1.0, 2.0, 4.0	0.15, 0.3, 0.6
AV-Cham, AVSH-Cham	1.0, 2.0, 4.0	0.15, 0.3, 0.6
No holes	-	-

2.2.2 Experimental Uncertainty

Uncertainties were estimated based on the procedure described by Kline and McClintock [49]. The mainstream velocity was measured using a pitot tube and a hand held digital manometer. The accuracy of this manometer (HHP-90) at 7.9 m/s is ± 0.5076 mmH_20. This in turn resulted in an uncertainty of 6.65% in the mainstream velocity and 9.4% for the blowing ratio. This uncertainty was primarily due to the full scale range of the chosen manometer. Based on a thermocouple accuracy of ± 0.5 °C and an accuracy of ± 1 °C for the IR measurements, the uncertainty in heat transfer coefficient was $\pm 12.3\%$, $\pm 15\%$ for the adiabatic film cooling effectiveness and $\pm 17.5\%$ for the heat flux ratio for $1 < x/d < 15$. Beyond this region, since the effectiveness values are lower, the uncertainties are higher and hence in this paper, the focus is only on the near downstream region where a statistically significant difference between various holes was observed.

2.3 Results and Discussion

2.3.1 Baseline cases

Figure 4 shows the effectiveness distribution for the cylindrical holes on the flat plate. Typically, cylindrical holes are operated at blowing ratios from 0.5 to 1.0. Even though the momentum flux ratio has an impact on jet separation and hence effectiveness, at higher blowing ratio conditions, cylindrical holes may not be the apt choice for film cooling. This can be ascertained with the existing literature [4]. Figure 4 of this study shows that higher effectiveness was achieved at the lowest blowing ratio (0.5). Moreover, increasing blowing ratios led to regions of low effectiveness which were observed immediately downstream from the hole exit, indicating jet separation (most evident for a momentum flux ratio of $I = 3.653$ in Figure 4). In order to validate the experimental technique, the laterally averaged effectiveness at $BR = 0.5$ was compared with data provided in the literature (Figure 5a). The present study matches the results obtained by Sinha et al. [9], Rallabandi et al. [50] and follows a similar downward (compared to other studies) sloping trend after $x/d = 5$. In the far downstream region, fluctuations in the laterally averaged effectiveness were observed, which originated from the errors associated with the temperature measurement. The difference between hole geometries downstream of $x/d = 15$ are within the uncertainty in the data and hence limited information can be concluded from those observations. Figure 5b compares the normalized heat transfer coefficient for the test case CY BR 1.0 with other studies in the literature. Comparison with Gritsch et al. [51] and Hay et al. [52] shows that the current study matches well with the previous work by these authors. It also shows that the momentum flux ratio might serve as an important parameter while comparing heat transfer coefficients.

	BR	DR	I
	0.5	1.095	0.228
CY	1.0	1.095	0.913
	2.0	1.095	3.653

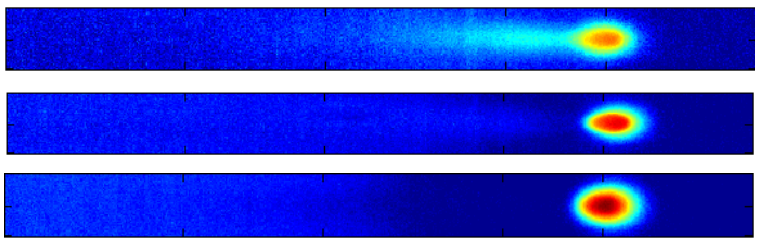

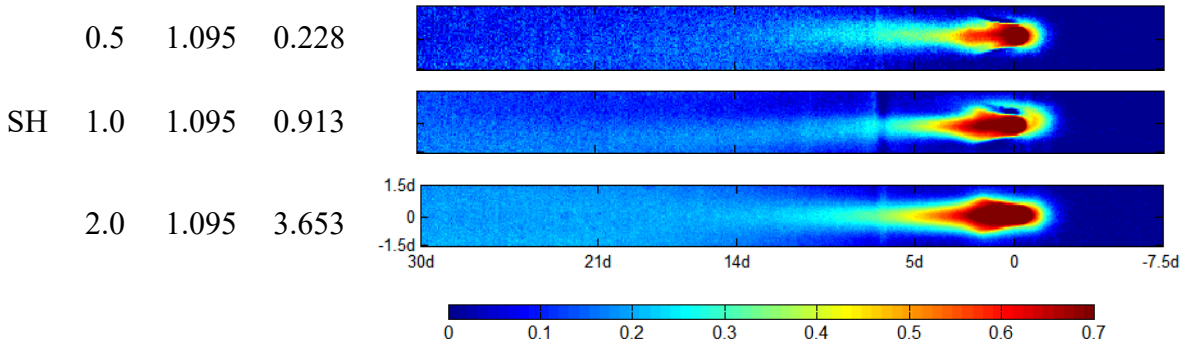

Figure 4 Adiabatic film cooling effectiveness of Cylindrical and Shaped holes at various blowing ratios

Since shaped holes have replaced the cylindrical holes in industrial gas turbine blades, newly proposed film cooling hole designs are compared with the performance of the shaped holes. The shaped hole Figure 4 shows the higher film cooling effectiveness of shaped holes compared to the cylindrical holes at all blowing ratios. A spanwise distribution of the cooling effectiveness over the entire flat plate is shown in Figure 5c for the shaped hole at a blowing ratio 2.0. The hole exits are also displayed at the bottom of the figure. The repeating pattern of effectiveness in the spanwise direction demonstrates uniform coolant and mainstream distribution around the holes. Hence it was sufficient to present the results over a single hole pitch.

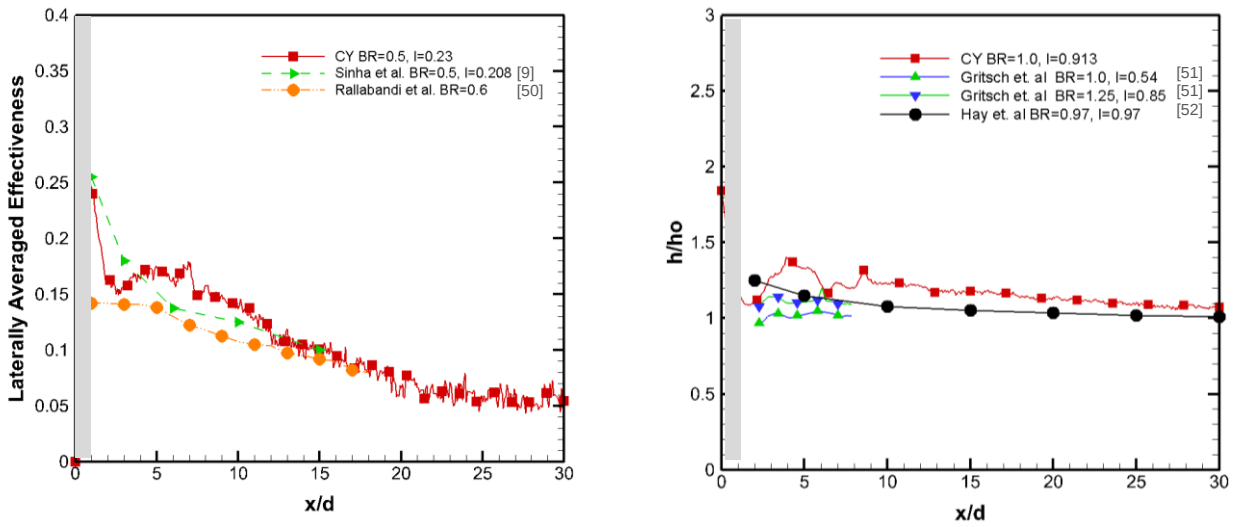

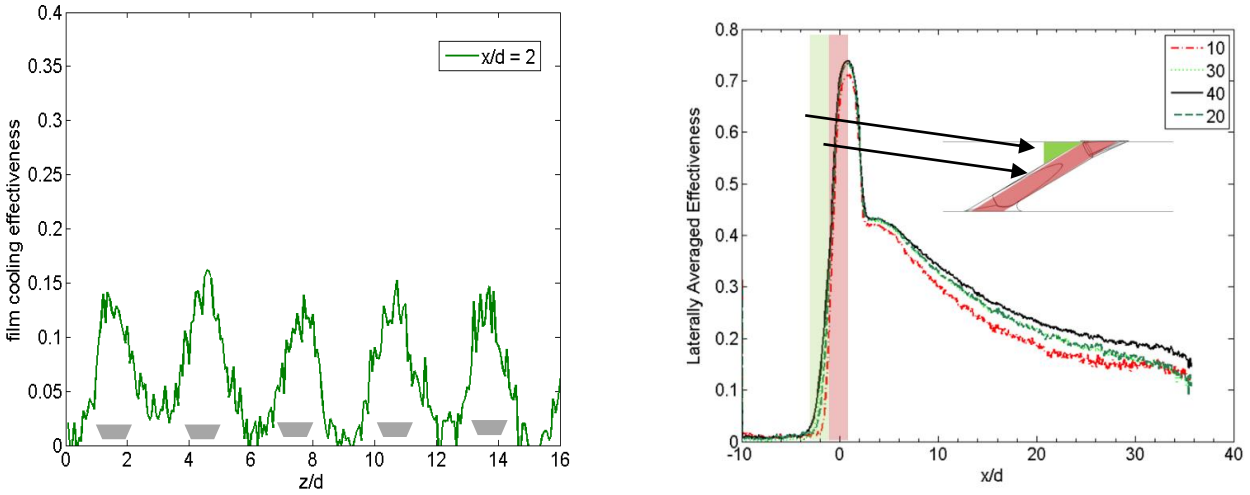

Figure 5. a) Adiabatic effectiveness: comparison with other studies; b) h/ho: comparison with other studies; c) Lateral variation in effectiveness at x/d = 2 for SH BR 2.0 test case; d) Laterally averaged effectiveness vs. x/d for AVSH BR 2.0 at 10, 20, 30 and 40s to illustrate the conduction losses

Film cooling experiments which are aimed at measuring adiabatic effectiveness usually suffer from conduction losses, unless a technique based on the mass transfer analogy is employed. In spite of the low thermal conductivity of ABS and strictly adhering to the 1D semi-infinite assumption, a finite amount of heat loss does occurs in the region close to the film cooling holes and especially in between them (holes) for the tripod geometry. This can be observed in all the contours presented in the current study. Figure 5d explains this phenomenon for the case of chamfered AVSH holes at BR 4.0. Despite the entire experiment lasted 60 s, only the first 40 s of data were used for the analysis. Moreover, since the Duhamel's superposition principle was applied, it was sufficient to process only one data point (time, temperature pair at each location) to obtain heat transfer coefficient and adiabatic effectiveness. In order to improve the accuracy, multiple data points in intervals of 10 s were analyzed. The laterally averaged effectiveness (Fig. 5d) obtained from all these data points were found to be overlapping within the uncertainty, implying consistency for the data obtained during the experiments.

The effectiveness behind the trailing edge of the hole ($-3 < x/d < -1$) was greater than zero in the absence of the coolant. This region experienced heat loss owing to the presence of the holes beneath the surface. Due to the nature of the tripod holes, the surface area in contact with the coolant is higher, making it easier for the heat to diffuse into the solid. This explanation would

equally apply for the region present in between the holes of any tripod hole unit. The region in front of the holes ($1 < x/d < 2$) would also experience some losses due to conduction but the effect would not be as pronounced as observed in the region $-3 < x/d < -1$. The effectiveness line plots start to diverge after $x/d > 4$. This can only be due to the uncertainty in the temperature measurement since the time taken for the heat to diffuse through a distance as small as 2 hole diameters inside ABS is roughly 103.2 s (using Equation 1).

One of the primary objectives of this paper was to analyze the effect of the newly proposed manufacturing technique [17] on the thermal performance of the tripod hole. Figure 6 and Figure 7 present the results for all the tripod hole variants studied. These contours indicate that the chamfered holes provide similar or better cooling compared with the ideal tripod design (sharp edges). The difference is not significant, which is critical as it corroborates that the as manufactured design can replace the original design without any penalty in performance. At the lowest blowing ratio, all three individual holes of a tripod hole set seem to contribute (effectiveness) equally, suggesting approximately equal coolant mass flow rate distribution. The coolant presence can be observed till roughly 10 hole diameters in both the cases but the tripod hole with chamfered (as manufactured design) corners was found to yield higher effectiveness in this region. One of the reasons could be the hole inlet chamfer affecting the coolant flow pattern and reducing the jetting effect inside the hole. Leylek and Zerkle [53] have pointed out that this phenomenon exists within a cylindrical hole (sharp corners) wherein most of the coolant entering the hole tend to concentrate towards the leading edge of the hole. The turning coolant inside the hole was also found to be responsible for the vortices present inside. Burd and Simon [54] have studied the effect of coolant supply geometry on film cooling effectiveness. Though the present study sports an unrestricted plenum, the coolant entry pattern can be affected by the inlet chamfer. Studies to confirm these plausible reasons will form part of the future analysis on the flow pattern inside the cooling hole. Hence for this paper, the analysis is restricted strictly to the thermal performance of the various hole geometries.

2.3.2 Comparison between various tripod holes

At $BR = 1.0$, the downstream region very close to the hole exit experienced high effectiveness for both AV and chamfered AV hole. At higher blowing ratios, especially at $BR = 4.0$, the effectiveness contour appears to indicate that the coolant jet separated from the surface and

reattached downstream. The low effectiveness region observed in the case of a cylindrical hole is absent here, which may be contrasting given the same momentum flux ratio ($I = 3.653$). Owing to the nature of the tripod hole, the coolant getting distributed into three different units lowers the effective blowing ratio and momentum flux ratio at the exit of each hole. In this study, blowing ratio was defined using the cross-sectional (circular) area at the inlet of the cooling hole.

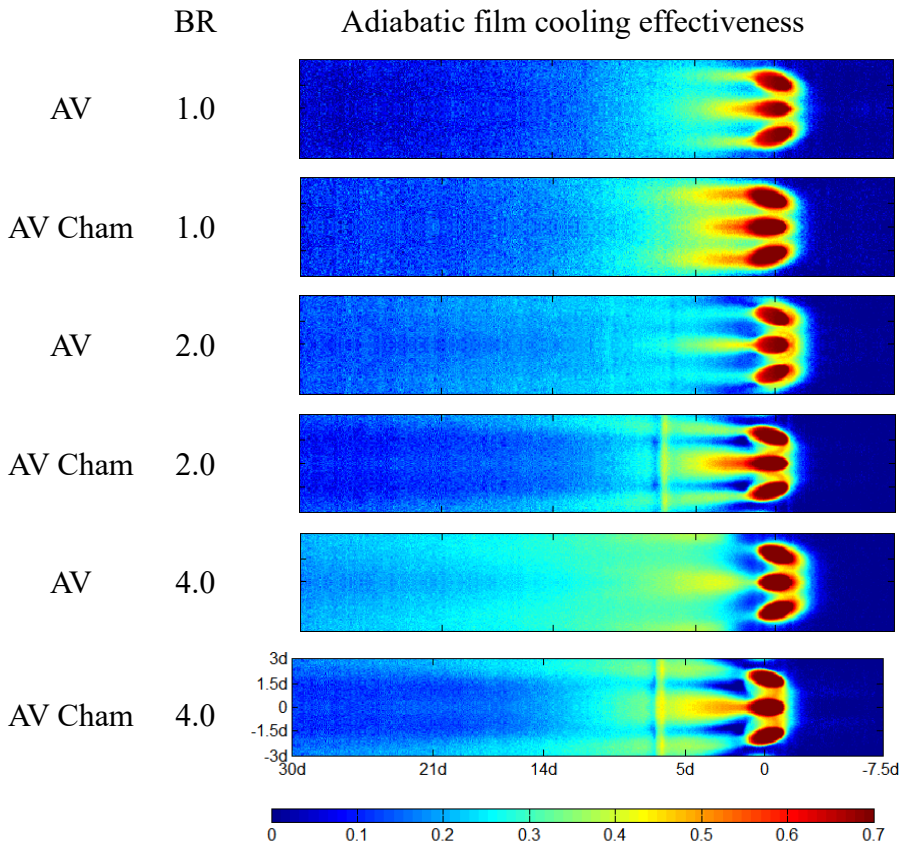

Figure 6. Tripod holes (AV and AV Cham) film cooling effectiveness at various blowing ratios

This indicates that the exit momentum flux ratio was $I = 0.34$ instead of 0.913 at the lowest blowing ratio ($BR = 1.0$), given equal distribution of the coolant to all three holes of a tripod. As far as the shaped tripod holes are concerned, the chamfered holes mostly outperformed the original design (AVSH refer to Figure 7) and this difference was distinct at lower blowing ratios. Similar to the shaped cylindrical holes, with increasing blowing ratios, the cooling ability of the shaped tripod holes also improved, irrespective of the chamfering.

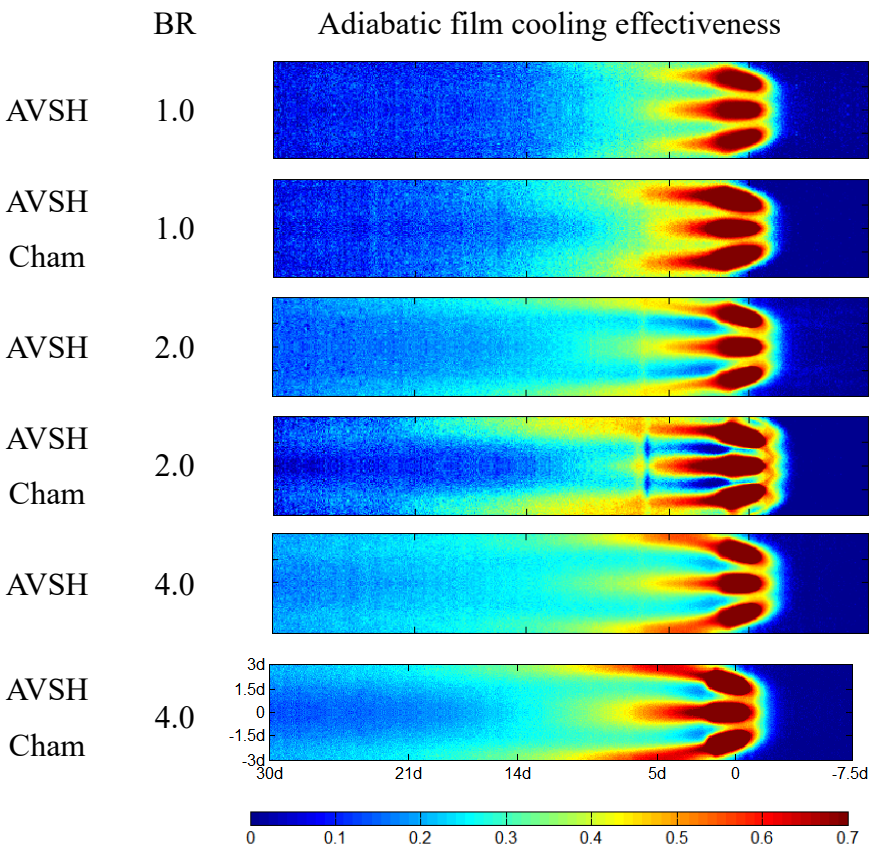

Figure 7. Shaped tripod (AVSH and AVSH Cham) hole film cooling effectiveness at various blowing ratios

Some of the effectiveness contours in Figure 6 and Figure 7 display a small discontinuity in the region $6 < x/d < 8$. The insert carrying the film cooling holes was flush with the test plate and the ridge caused at the interface was filled with gypsum plaster and sanded down, ensuring a smooth continuous flat surface. Figure 8a highlights this region for the case of a CY hole, showing that the aforementioned ridge was properly treated, producing a smooth transition from the insert to the test plate. In spite of the efforts taken, the plaster surface is distinctly visible, forming a streak or seam on the temperature contours. Figure 8b displays the surface temperature of the test surface with cylindrical holes (raw/unprocessed experimental data). This feature (seam) was clearly visible for all the 19 test cases studied in this paper. Plausible reasons could be the a) emissivity of the plaster which absorbed the black paint (used for IR thermography, refer to Figure 8a); b) height mismatch resulting in tripping of the boundary layer and c) not accounting for the plaster properties in the 1D model.

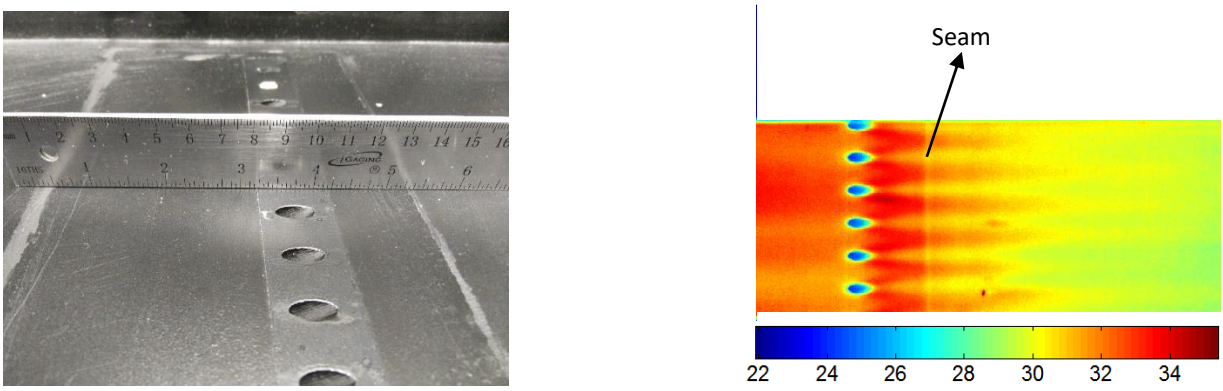

Figure 8. a) Test surface after finish on either ends of the insert; b) Surface temperature IR data after 30s

The plaster absorbing the black paint could have altered the emissivity of that region and hence the surface temperature. Any change in the emissivity would be independent of the blowing ratio and must affect all the test cases equally. It is hence not clear why only selective cases were affected, which makes this explanation unlikely. Similarly, any step change in height of the test surface would increase the heat transfer coefficient for all the holes, this is not observed thus the effect cannot be due to a disturbance in the boundary layer. Moreover, Figure 8b shows surface temperature contours undergoing a smooth transition before and after the seam. Change in the thermal diffusivity of the test section (gypsum plaster) will alter the surface temperature and this change in properties is not accounted for in the data analysis. In any case, it is clear that the boundary layer was not affected by the presence of the seam and its effect seems to be confined in the region $6 < x/d < 8$. As a result, for the current study, the data presented in Fig. 6 and 7 for $6 < x/d < 8$ was trimmed for the line plots in Figure 9 and Figure 10.

2.3.3 Film cooling effectiveness

Figure 9 shows laterally averaged effectiveness for all the test cases conducted, summarizing the results and aiding in the comparison of the performance of different geometries. As previously discussed, there are roughly twice as many cylindrical hole inlets as there are inlet tripod holes; hence the blowing ratios for tripod holes will be twice that of the cylindrical holes (the individual plots are matching coolant mass flow rate).

Figure 9a compares all the holes at their lowest blowing ratio ($\dot{m} = 0.15$ g/s). The tripod holes provided better film cooling coverage compared to the cylindrical holes as previously observed by Dhungel et al. [13]. For cylindrical and shaped holes, the peak effectiveness value ($\eta \approx 0.25$) was located at $x/d = 1$ after which it started to decrease. The effect of shaping becomes apparent at $1 < x/d < 3$, where the cylindrical hole effectiveness decreased while the shaped hole provided improved cooling. Beyond $x/d = 9$, shaped holes showed a higher effectiveness compared to cylindrical holes. The AV hole geometry and its variants on the other hand, showed remarkable cooling performance compared to both CY and SH holes. This dominance in performance started at $x/d = 1$ and extended until $x/d \approx 13$. Close to the hole exit, the anti-vortex hole showed at least 20% increase in effectiveness when compared to the shaped or cylindrical holes. Beyond $x/d = 15$, the line contours start overlapping each other and no distinct difference in effectiveness can be concluded. Interestingly, the as manufactured tripod hole (AV Cham) seemed to provide better cooling, 25.67% increase in the area averaged effectiveness over a distance of 10 hole diameters, when compared to the idealized AV hole. A similar relationship was also observed from the results of AVSH and AVSH Cham, although the difference was marginal (7.25%). This was also noted in the effectiveness spatial distributions shown in Figure 7. Even more impressive was the effect of shaping on the tripod holes. SHAV and SHAV Cham showed roughly 33% and 13% improvement in effectiveness compared to their non-shaped counterparts.

At higher blowing ratios, the effect of the shaping played a vital role (Figure 9b). The sudden dip and subsequent increase in the laterally averaged effectiveness for CY, AV and AV Cham holes occurred as a result of coolant jet separation and its reattachment. Coolant jet separation from the surface has been cited in [4] for a cylindrical hole at these flow conditions. This effect is pronounced at $\dot{m} = 0.6$ g/s (Figure 9c) when the merits of AV hole started to fade ($1 < x/d < 3$) when compared to the SH hole, in spite of having a higher area averaged effectiveness ($+16\%$ over 10 hole diameters). The cylindrical geometry of the hole exit is what seems to be causing this since SH, AVSH and AVSH Cham holes do not show this characteristic decrease in effectiveness close to the hole exit.

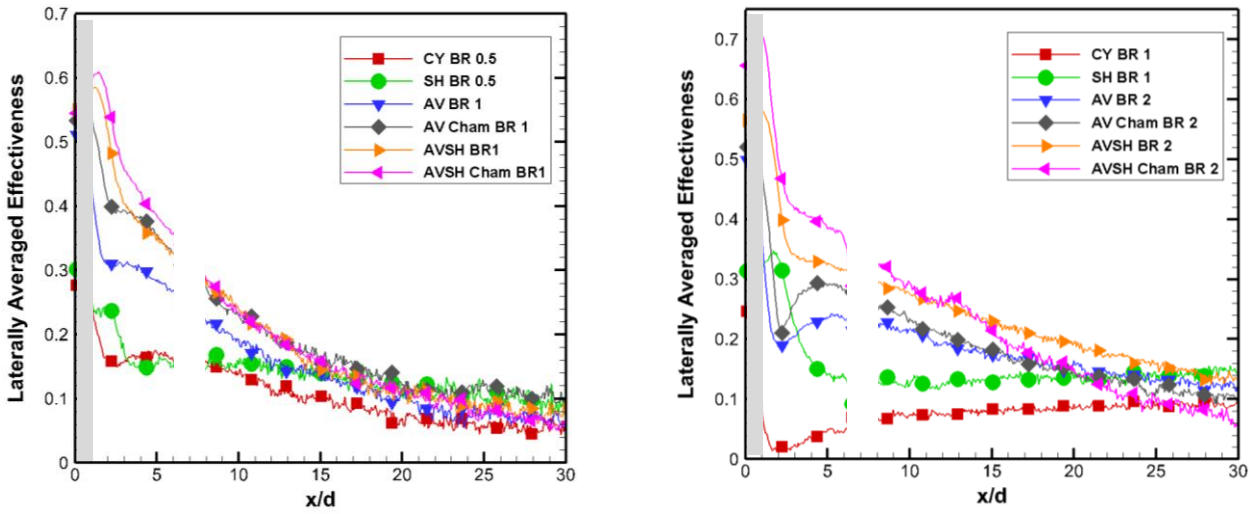

Figure 9. Laterally averaged film cooling effectiveness for all the holes at a) $\dot{m} = 0.15$, b) $\dot{m} = 0.3$, and c) $\dot{m} = 0.6$ g/s

The shaping angle is important to the effectiveness of a shaped hole. Recall that the shaping angle is larger for the traditional shaped holes compared to the shaped AV holes (to avoid hole overlap). The trends between SH and AVSH therefore will not be similar. Lower effectiveness values for the SH hole when compared to AV or AVSH could have originated from three different aspects a) the anti-kidney vortices present in AV holes which lower the strength of the CRVPs, decreasing jet lift off b) the effective coolant velocity (and momentum) at the hole exit, for a SH

hole with $BR = 1.0$ and an AV hole with $BR = 2.0$ was different, since the coolant was distributed through three different holes for the tripod hole, and c) the transition region typically present in shaped holes lies very close to the exit which restricts the expansion of the coolant jet. At both $BR = 1.0$ and 2.0 (w.r.t. CY/SH), the AV holes were more effective than the SH holes in the region from $3 < x/d < 20$ with AVSH and AVSH Cham holes providing the best performance. It is interesting that in general the AV holes with manufacturing features (AVSH Cham and AV Cham) were exhibiting a better film cooling effectiveness compared to their idealized counterparts (AV and AVSH designs). From the manufacturability perspective, the AV Cham and AVSH Cham designs provided a more realistic design with no penalty (and in fact a gain) in thermal performance.

2.3.4 Heat transfer coefficient

Figure 10 displays laterally averaged heat transfer coefficient ratios for all the test cases. These were obtained after normalizing the laterally averaged local heat transfer coefficient (h) with respect to the laterally averaged heat transfer coefficient of the baseline case (ho), which corresponds to a flat plate devoid of any cooling holes. The heat transfer coefficient ratio near the hole exit was higher compared to the far downstream region and this effect seems to be predominant up to $x/d = 7$ to 8. This trend is consistent with what was observed by Dhungel et al. [13]. After roughly 15 hole diameters the effect of coolant on the heat transfer coefficient diminished, as observed by the h/ho values approaching unity. The coolant at this point would have diffused laterally and most of it would have mixed with the mainstream. This can also be noticed by the low film cooling effectiveness after 15 hole diameters (Figure 9). As the coolant exits the hole, its interaction with the mainstream increases the local heat transfer coefficient, followed by a quick decrease in the h/h_0 ratio. Past ~ 5 hole diameters, h/ho continued to gradually decrease approaching unity. At any coolant flow rate, the tripod holes caused a higher heat transfer coefficient when compared to the cylindrical holes. Among the tripod holes, the shaped ones resulted in the highest ratio in the region close to the hole exit. Due to the uncertainty past 2 hole diameters, the increase in the heat transfer coefficient is not significantly different for the holes tested in this study (expect CY BR 2.0).

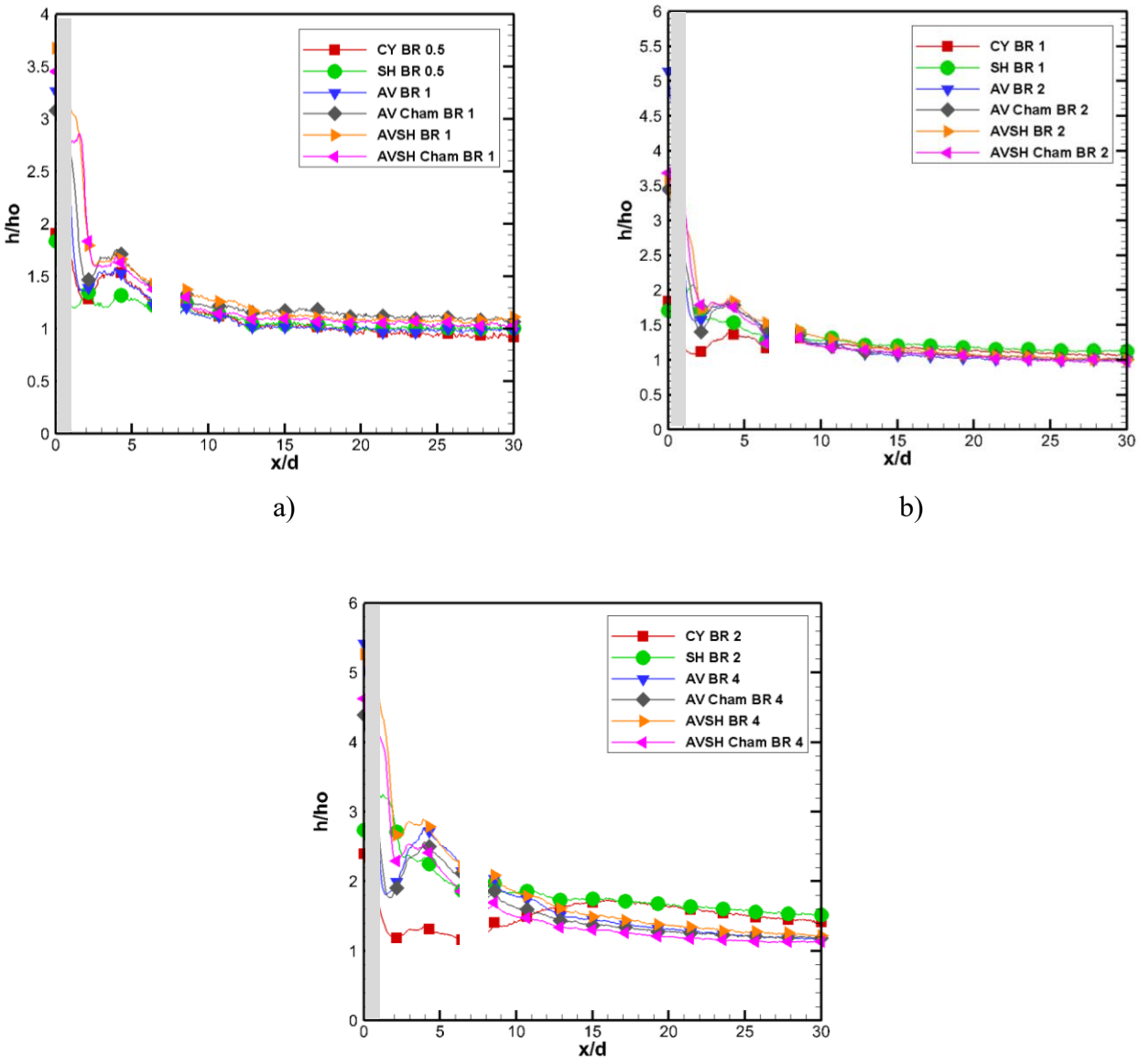

Figure 10. Laterally averaged heat transfer coefficient for all the holes at a) $\dot{m}$ = 0.15, b) $\dot{m}$ = 0.3 and c) $\dot{m}$ = 0.6 g/s

2.3.5 Overall heat flux ratio

Figure 11 presents the area averaged heat flux ratio on the flat plate for all the test cases conducted. The area used to represent the film cooling effectiveness distribution was that shown in Figure 4, Figure 6, and Figure 7. The heat flux ratio is essential to determine the amount of heat flux that will enter the surface if film cooling holes were used, compared to a surface with no film

cooling holes. It depends on the heat transfer coefficient ratio and the ratio of adiabatic effectiveness to overall cooling effectiveness (normalized metal temperature similar to adiabatic effectiveness) as defined below:

$$\frac{q}{q_0} = \frac{h}{ho}\left(1 - \frac{\eta}{\varphi}\right) \tag{1.5}$$

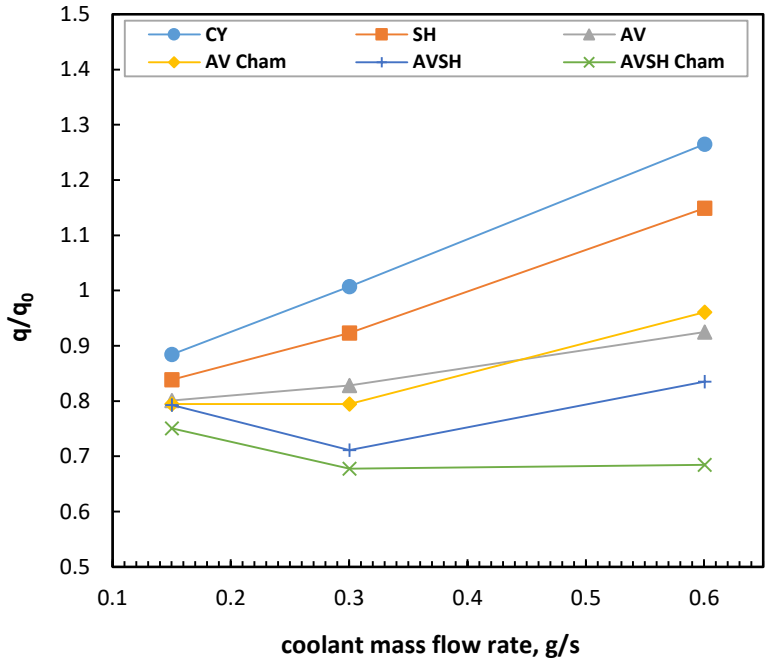

Figure 11. Area averaged heat flux ratio for all the holes at a) $\dot{m}$ = 0.15, b) $\dot{m}$ = 0.3 and c) $\dot{m}$ = 0.6 g/s

Typically, the overall cooling effectiveness (φ) is difficult to measure and in this study, a value of 0.6 [13] was used to calculate the heat flux ratio. This definition also implies that it is desirable for a film cooling hole to have a heat flux ratio < 1. From Figure 11 it can be noticed that at the lowest coolant flow rate, all the holes tested caused lower heat flux on the flat plate. The trends in heat flux ratio observed between various holes was consistent with the trends observed for the film cooling effectiveness at the respective flow rates. Shaped tripod holes with chamfered exits yielded the lowest heat flux on the flat plate, while cylindrical holes provided the highest. Tripod hole variants caused a lower heat flux ratio compared to the cylindrical and shaped holes. For the most part, the chamfered tripod holes resulted in lower heat fluxes compared to the tripod and shaped

tripod holes. At the highest flow rate, only cylindrical and shaped holes showed a higher heat flux (heat flux ratio > 1) while all the tripod holes resulted in a heat flux reduction to the flat plate. Tripod holes and its variants can hence deliver a significant improvement compared to cylindrical holes in terms of reducing the heat flux entering the flat plate.

CHAPTER 3

FILM COOLING PERFORMANCE ON AN AIRFOIL

The current chapter focuses on the performance of this tripod hole design on the suction and pressure sides of a GE E^3 first stage vane in a cascade. The experimental setup consists of a low-speed wind tunnel and scaled up five-vane linear cascade, with measurements taken on the center vane using steady-state infrared thermography technique. Additional measurements are performed using a rake of pressure taps to determine the flow velocity profile upstream and downstream of the center vane. Several coolant-to-mainstream blowing ratios are tested experimentally to examine the effects of greater coolant ejection velocities at the same mainstream velocity. Both CO_2 and air were used as coolants to examine the effect of the density difference between the mainstream and coolant flows. These experiments were conducted with the center blade having the standard cylindrical hole and the tripod anti-vortex hole configuration at the same locations on the pressure and suction surfaces. The results from the two tested configurations are then compared to illustrate the advantages of the tripod anti-vortex injection holes.

3.1 Experimental setup

An open loop flow channel consisting of a blower, an inlet section, a combustor section (90° annular section), a nozzle, and a 5-vane linear cascade is shown in Figure 12. The blower (Cincinnati Fans, 900 CFM max. capacity) is fitted to a 15-HP motor having a maximum speed of 3525 RPM. The motor is controlled by a Rockwell Automation V-TAC controller and can be adjusted to provide to the required inlet flow velocity for the vane cascade. The blower pushes air into the inlet section comprising of a settling chamber, a converging nozzle, and a diffuser. The linear vane cascade is comprised of five E^3 vanes, built from low conductivity ABS resin by fused deposition method. This method allows complex geometries to be built at fraction of the machining cost. The vanes are scaled up four times their original size to match the size of the upstream combustor geometry. The resultant vane chord, height, pitch, and absolute flow angle are 0.1349m, 0.1524m, 0.1778m, and 73.1˚, respectively. The walls of the vane test section are made of clear acrylic material to permit obstruction-free optical measurements, and with viewing windows cut

normal to the throat region on the suction surface for IR thermography. The maximum flow velocity that can be obtained at the inlet of the vane cascade is 20m/s.

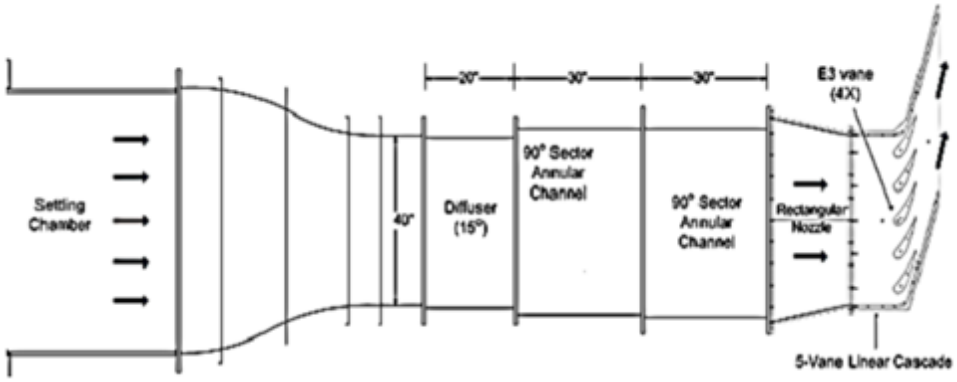

Figure 12.Sub-sonic Wind Tunnel with 5-Vane Linear Cascade

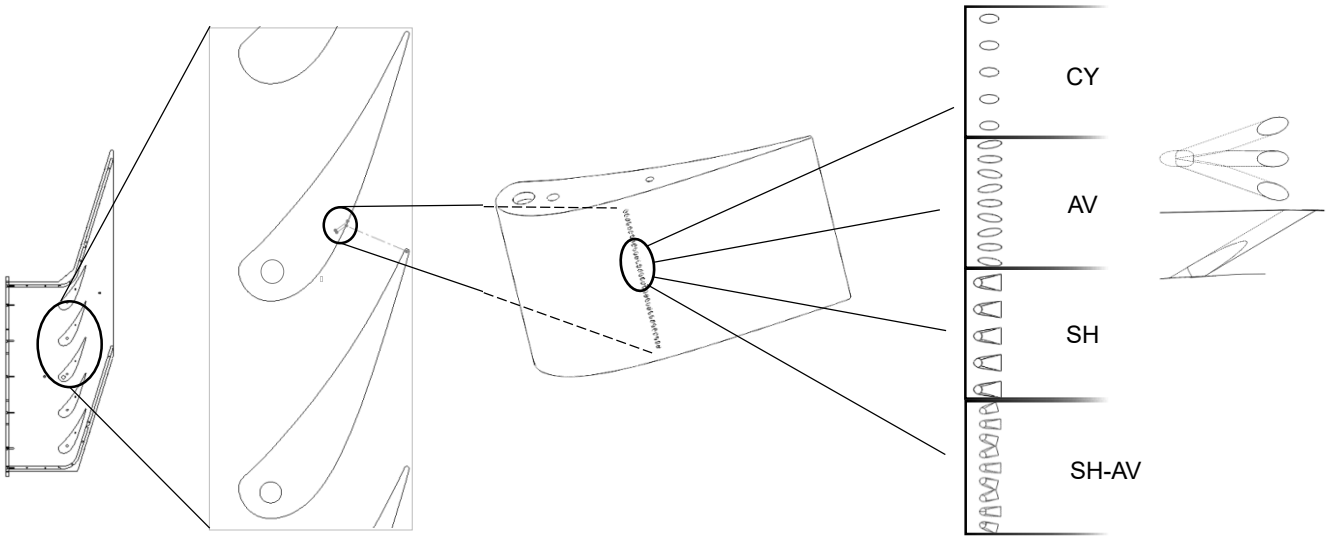

Figure 13.Film cooling hole location on the suction side of the airfoil: an exploded view

3.1.1 Film hole geometries

Four film hole geometries shown in Figure 13 were used in the experiments. With an intention of capturing the effects of coolant jet and its coverage on the suction side near mid-span region to the trailing edge, it was decided to have the holes near the throat region. Solid airfoils (without any hole geometry) were assembled in the cascade and the throat region was located as shown in Figure

13. This region lies at around 0.1905m from the tip of the trailing edge. Coolant holes were then designed near this location. Figure 13 presents a detailed view of the construction of coolant hole geometry and the way it is assembled in the linear cascade shown in Figure 12.

The first geometry is a simple CY hole of diameter 2 mm and axis inclined at 30˚ from the surface in the streamwise direction. The hole length-to-diameter ratio (l/d) is 4.0 and the pitch-to-diameter ratio (p/d) is 3. There are total of 23 holes on the vane. The second hole (AV) is a 3-hole unit in which the main or the central hole is identical to the first geometry but has an additional compound CY hole on either side that branch out at 15˚ angle and connected together at the inlet such that the metering area at the entrance of the secondary flow is circular and similar to both the cylindrical and shaped holes. The top and side view of one tripod hole unit is shown in Figure 13 while the details of this design can be found in [7]. All three holes are inclined at 30˚ angle in the flow direction from the surface. The l/d ratio of the center and the side holes is 7.5 and 7.7, respectively. The p/d ratio between the main holes is 6d, between center and side hole is 1.75d, and between the side holes of the adjacent AV unit is 2.5d. There are total 11 sets of AV holes on the vane. The design is akin to removing alternate holes in the CY design and adding two angled holes to each of the remaining holes.

The third geometry (SH) is a conventional shaped hole with 10° fan diffuser exits laterally on either side of a hole and 10° laidback angle, diffusing into the surface. Expect for the shaping, the rest of the design looked similar to that of the CY hole, including ratios l/d and p/d, resulting in a total of 23 identical shaped holes. The final geometry (SH AV) is a modification of the previous one, more of a combination of the second and third geometry. In this case, all the holes of the anti-vortex geometry are provided with shaped exits. The exits diffuse out at angle of 5° on all three sides (laidback and fan angle of 5° on either side). The l/d ratios of each hole as well as the p/d ratios are similar to that of case 3, the third geometry. This gives us 11 sets of 15° tripod holes with 5° shaped exits, exiting the surface at an angle of 30°. The geometry tries to absorb the merits of shaping and breaking down of the kidney bean vortices (CRVP). Potentially this should result in wider coverage of the jet on the blade surface, provide higher film cooling effectiveness as well as reduce the amount of coolant flow from the compressor. All geometries were created with the rapid prototyping technique because of the ease with which complex geometries can be built in quick time at a fraction of the machining cost.

3.2 Measurement theory

To obtain the surface temperature data, Infrared (IR) thermography technique was used. Prior to actual thermal measurements, calibration of the entire thermography system and the IR signal is required. A thermocouple is mounted on the test surface using Aluminum tape. Its location is outside the measurement region to avoid the interference caused by the aluminum tape. The test surface is then sprayed with flat black paint to increase its emissivity. The IR camera is focused on the test surface, the field of view of which also encompasses the thermocouple. The test surface is then heated by mixing of the cold mainstream air and the hot air from the secondary loop which consists of an inline heater element, an orifice meter and an adjustable tap in the order mentioned. Thermocouple reading which is mounted on the suction side of the airfoil, is noted until the plate comes to a steady state. Next, the temperature recorded by the thermocouple is compared to that by the IR camera. A number of factors, such as distance between the front lens and the test surface, relative humidity, and background temperature affect the temperature measured by the IR system. Multiple calibrations at different temperatures should be carried out to minimize the error that creeps in because of these factors.

A number of temperatures are used to determine the correct emissivity of the test surface. During the emissivity calculation, polyethylene sheet window was not used. So, the transmissivity value used was 1. In order to determine the transmissivity of the polyethylene window, a similar test was conducted with the window in place. With the known emissivity from the prior test, transmissivity of the window was altered until the IR camera readings coincided with the thermocouple readings. The emissivity of the black painted test surface when viewed without the window is 0.99. The calibrated transmissivity for the polyurethane sheet was 0.9.

The test begins by setting the mainstream air to the proper inlet velocity. A pitot tube is present upstream of the blades on the other side of Figure 12. The V-TAC controller can be used to provide the required inlet velocity near the blower. An inlet velocity of 12 m/s was set for the mainstream air just upstream of the leading edge of the cascade airfoils. For the given configuration of the linear cascade, this velocity provides a cascade inlet Reynolds number of about 100,000 based on airfoil axial chord. After about 20 minutes when the mainstream air reaches steady state, the IR camera captures 11 consecutive images of the suction surface of the blade which includes the film cooling holes, at its maximum operating speed. This set is labeled as T_{main} and it is same as the

normally labeled adiabatic wall temperature. Next, the secondary fluid is set to the right blowing ratio and provided to the test section at the proper mass flow rate. Orifice meter present before the inline heater meters the required coolant mass flow depending on the blowing ratio. The secondary fluid is heated close to a temperature of 45-50˚C in all the tests, compared to a mainstream temperature of 22-25˚C. The mainstream air, secondary gas, and the plate surface temperature are continuously monitored. When steady state condition is reached, the second set of 11 images is captured and labeled as T_{wall}. The fluid temperature inside the holes, T_{sg}, is noted simultaneously using a data acquisition system. A thermocouple connected to the data acquisition system, is placed at the hole entrance of one of the holes to measure the secondary flow temperature. The adiabatic film-cooling effectiveness is then calculated using the following equation:

$$\eta = \frac{T_{wall} - T_{main}}{T_{sg} - T_{main}} \tag{2.1}$$

T_{main} was used in the equation in place of the more common, T_∞, to eliminate surface non-uniformities in lighting and paint. Two IR images, one from each set T_{main} and T_{wall}, are converted into a readable format and post processed using MATLAB. It has been tested that any image from the set of 11 images corresponding to T_{wall} and T_{main} can be randomly picked for post processing the data and it still yields similar effectiveness as long as the images captured do not show any presence of recalibration.

3.2.1 Test conditions

As shown in Table 2, a total of 16 experiments were performed to study the effects of blowing (BR) on adiabatic film-cooling effectiveness. The blowing ratio is defined as

$$BR = \frac{(\rho V)_{sg}}{(\rho V)_\infty} \tag{2.2}$$

where V_∞ is the mainstream air velocity at the film hole location on the airfoil and V_{sg} is the nominal average velocity at the injection hole inlet. This is to ensure that the metering area is the same for all the geometries as the hole inlet areas are identical. The mass flow rate for a given blowing ratio is given by

$$\dot{m} = \sum_{i=1}^{n} BR.(\rho V)_{\infty}.a_i \quad (2.3)$$

For any given blade geometry there will be almost twice as many CY holes as compared the AV holes. So it can be noticed that the mass flow rate required with AV holes is only about half that of CY holes for any given blowing ratio.

Table 2: Summary of Experimental Conditions

Exp.	Hole	BR	$\dot{m}$ (kg/s)
1	CY	0.5	0.0008035
2	CY	1.0	0.0016070
3	CY	1.5	0.0024105
4	CY	2.0	0.0032140
5	SH	0.5	0.0008035
6	SH	1.0	0.0016070
7	SH	1.5	0.0024105
8	SH	2.0	0.0032140
9	AV	1.0	0.0008936
10	AV	2.0	0.0017872
11	AV	3.0	0.0026808
12	AV	4.0	0.0035744
13	AV-SH	1.0	0.0008936
14	AV-SH	2.0	0.0017872
15	AV-SH	3.0	0.0026808
16	AV-SH	4.0	0.0035744

3.2.2 Flow characterization

Flow characteristics upstream of the airfoil and around the airfoil were determined to evaluate the local blowing ratio for coolant injection. A solid vane with pressure taps was placed in the central

vane location and measurements were taken to determine the velocity profile on both the vane surface and the spanwise velocity profile upstream of the cascade.

Figure 14a shows the spanwise velocity profile (boundary layer) upstream of the cascade and Figure 14b shows the vane velocity profile along the surface for the cascade. As shown in the figures, the flow is smooth over the vane with no separation, and the spanwise flow is steady throughout the central region of the vane where the data is to be collected. The rhombus marking near $x/C_{ax} = 0.63$ on Figure 14b symbolically represents the cooling hole location on the suction side of the GE E3 airfoil. Blowing ratio is defined based on mainstream velocity at this location, where Mach number is 0.1361. The subsonic wind tunnel observes a peak Mach number of 0.1433, at x/Cax ~ 0.4.

3.2.3 Experimental uncertainty

Uncertainties were estimated based on the procedure described by Kline and McClintock [49]. The mainstream velocity was kept constant within ±1.3%. Uncertainties in setting the blowing ratios were ±3%. Based on accuracy of ±0.5˚C for thermocouple measurements and accuracy of ±1˚C for IR measurements, the uncertainty in effectiveness amounted to ±0.5% for η=0.5 and ±1.0% for η=0.15.

3.2.4 Conduction effect

Due to the blade geometry, conduction through the wall from the plenum side to the mainstream side has a significant effect. A correction factor to allow for comparison to adiabatic surface conditions was developed using a CFD model representative of the actual geometry. Two cases were compared for each blowing ratio, one using the properties of ABS plastic, and one with near-perfect insulated surface. The temperature difference between the two cases was then used to calculate an effectiveness correction factor. This correction factor is the temperature difference between the two cases divided by the difference in temperature between the main-stream and coolant inlets.

$$\eta_{corr} = \frac{T_{plastic} - T_{ins}}{T_{sg} - T_{main}} \tag{2.4}$$

The greatest amount of correction is required in the region between and just upstream and immediately downstream of the holes of the hole exits, especially in the upstream of the hole where the adiabatic cooling effectiveness is theoretically zero as there is no presence of the coolant.

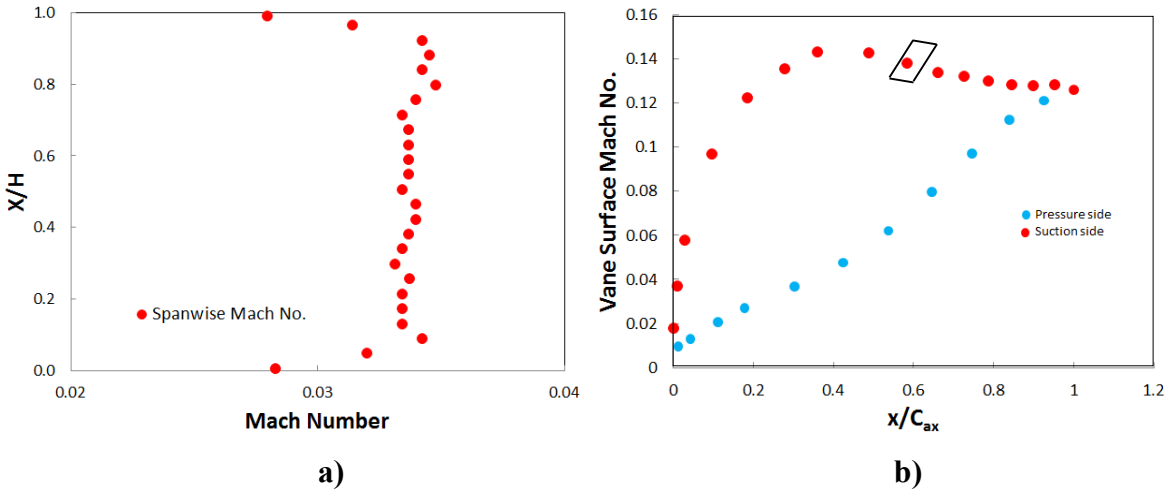

Figure 14.Velocity profile: a) spanwise; b) near vane surface

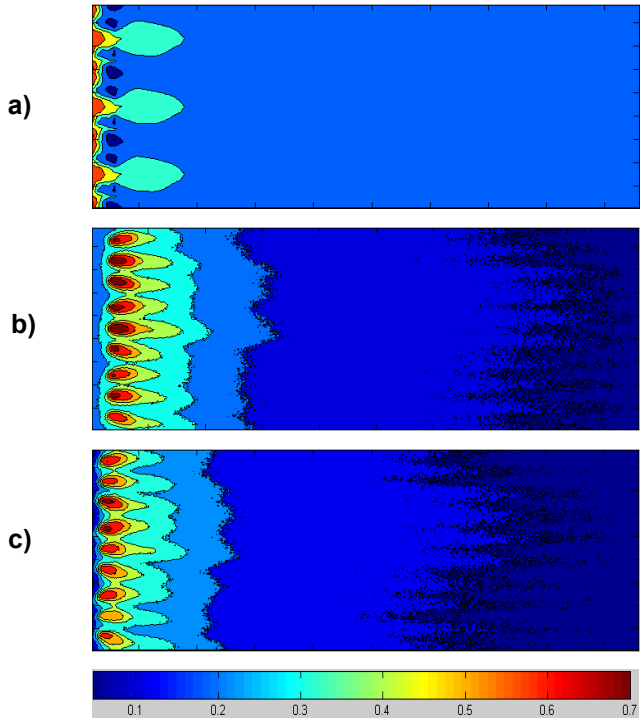

Figure 15.Effectiveness contour for AV hole, BR=1.0: a) correction contour; b) pre-correction; (c) post-correction

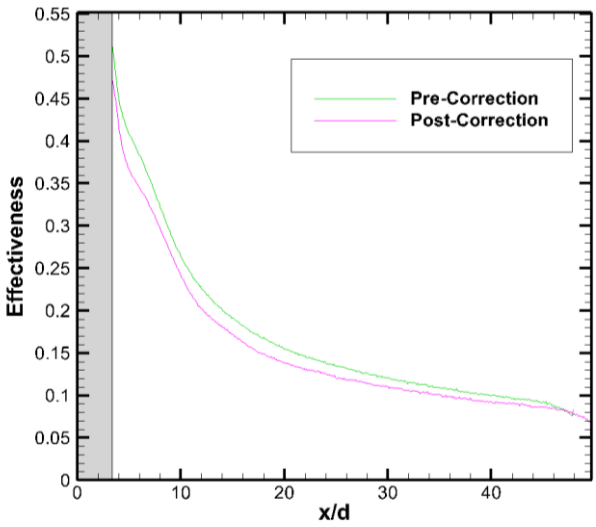

Figure 16.Effect of conduction correction on laterally averaged effectiveness for AV hole at BR = 1.0

The required correction is very small far down-stream of the fluid injection location. Once applied to the data, this correction factor results in a reduced effectiveness compared to the raw experimental data. Figure 15a shows an example temperature correction contour for the tripod hole BR=1.0 case, while Figure 15b and Figure 15c show the effectiveness results pre and post-correction for the tripod hole BR=1.0 case. Figure 15c, which is the corrected data, is obtained by deducting the correction factor from Figure 15a from Figure 15b. The blue region (Figure 15a) indicates that there is no conduction correction needed in that region. Pre and post-correction results are also plotted for laterally averaged film cooling effectiveness as shown in Figure 15 for the same tripod hole at BR = 1.0. From both Figure 15 and Figure 16, it can be noted that the effect of conduction is more significant in the upstream region owing to the location of coolant flow inside the cavity shown in Figure 13. This effect, more or less, is the same for all the cooling hole geometries and would change the effectiveness values slightly by less than 10%. Since, the results are presented as a comparison between the various hole geometries, conduction correction effect on effectiveness data is not presented in the results.

3.3 Results and discussion

Experiments were run at four different blowing ratios for all the geometries shown in Figure 13. Blowing ratio is defined based on average hole inlet area (cylindrical hole). Figure 17 shows detailed film cooling effectiveness contours for all the geometries at different blowing ratios. Side views of the blades are also shown in Figure 17a. Effectiveness contour is present on the right side of the airfoil and it is roughly aligned with the start of the hole location on the blade. The height of the contour plots correspond to the distance covered by the coolant jets on the suction side of the airfoil, capturing effectiveness data up to 46 hole diameters.

Figure 17b shows the detailed contours of film effectiveness for cylindrical holes. At the lowest blowing ratio (BR = 0.5), the near downstream region, adjacent to the holes observes high effectiveness. In the far downstream region, however, the effect of the coolant jet diminishes resulting in an effectiveness as low as 0.15. As blowing ratio increases, increased exit momentum resulting in jet lift off lowers the effectiveness distribution near the holes. The effect doesn't seem to be strong owing to the curvature of the blade on the suction side and the contours look closely similar. This in turn causes the far downstream region to notice very little improvement in the effectiveness at higher blowing ratios. Very high mainstream velocity on the suction side might also carry away the coolant jet resulting in lower effectiveness spread over a large distance. At all blowing ratios, individual streak lines were clearly distinguishable up to 10 hole diameters.

Figure 17c shows the effect of the blowing ratio on film cooling effectiveness for the tripod anti-vortex holes. For all blowing ratios, the downstream region sees almost uniform coverage of coolant. However at the lowest blowing ratio, the jet does not carry sufficient momentum to travel far downstream. This can be noticed by the presence of low effectiveness region (blue colored) far downstream. The overall film cooling effectiveness for the tripod hole is better than that of the cylindrical at any corresponding blowing ratio because the anti-vortex hole geometry reduces the strength of the kidney bean vortex (CRVP) observed in a CY hole [55]. The additional set of holes on either side of the main hole creates vortex that weakens the counter vortex from the central hole, tending to push the coolant exit towards the wall. Moreover, presence of additional side holes means more coolant coverage in the spanwise direction. This is illustrated by the absence of distinct streamlines present Figure 17b. Diffusion of coolant exiting the adjacent side holes results in coalescence, formation of a single downstream jet which in turn increases effectiveness in those

regions. Also it should be noted that the anti-vortex holes consume half as much coolant as cylindrical hole does since there are half as many tripod hole inlets present on the airfoil when operating at same blowing ratio.

Figure 17d presents the film cooling effectiveness for the shaped holes. At the lowest blowing ratio, the shaped holes performs exceedingly better than cylindrical holes and the anti-vortex hole, especially in the downstream region adjacent to the holes where regions of high effectiveness, as high as 0.8 are observed. Shaped hole exit area being twice as much as compared to a CY hole should reduce the jet exit momentum by the same factor, for an incompressible flow. SH holes also observe better jet diffusion in the lateral direction. The coolant exiting the holes thus tends to stick with the blade surface, providing better cooling. Aspect ratio can be defined in terms of effective exit to inlet area for the cooling hole geometries. SH holes, in spite of having a lower aspect ratio compared to tripod holes (exit area includes side holes), the change in ejection angle near the hole exit or shaping results in higher effectiveness. This effect however seems to be nullified at higher blowing ratios. The incremental change in the blowing ratio from BR = 0.5 to BR = 1.0 might have impacted the jet momentum, causing lift off resulting in the entrainment of hot gas near to the surface. Individual streaks observed in CY holes were present and under these conditions, the tripod holes show high film cooling effectiveness.

Figure 17e presents the film cooling effectiveness for shaped exit tripod holes. It appears that shaping of the exits changes the pattern of cooling distribution on the surface drastically. The shaped exits help increase the film effectiveness for BR = 0.5 and as BR increases, the effectiveness decreases with clear jet streaks which was not seen for unshaped tripod holes in Figure 17c. As seen in AV holes, adjacent side holes results in a single coolant jet over the blade surface but it is unclear why the SH-AV geometry produces spanwise non-uniformity in film effectiveness.

Figure 18 compares the effect of coolant-to-mainstream blowing ratio on laterally averaged cooling effectiveness for different coolant hole geometries. Figure 18a shows that for cylindrical holes, the film cooling effectiveness decreases with increasing blowing ratio, peak value at blowing ratio 0.5 was 0.51, at the exit of the hole location, x/d ~ 2.

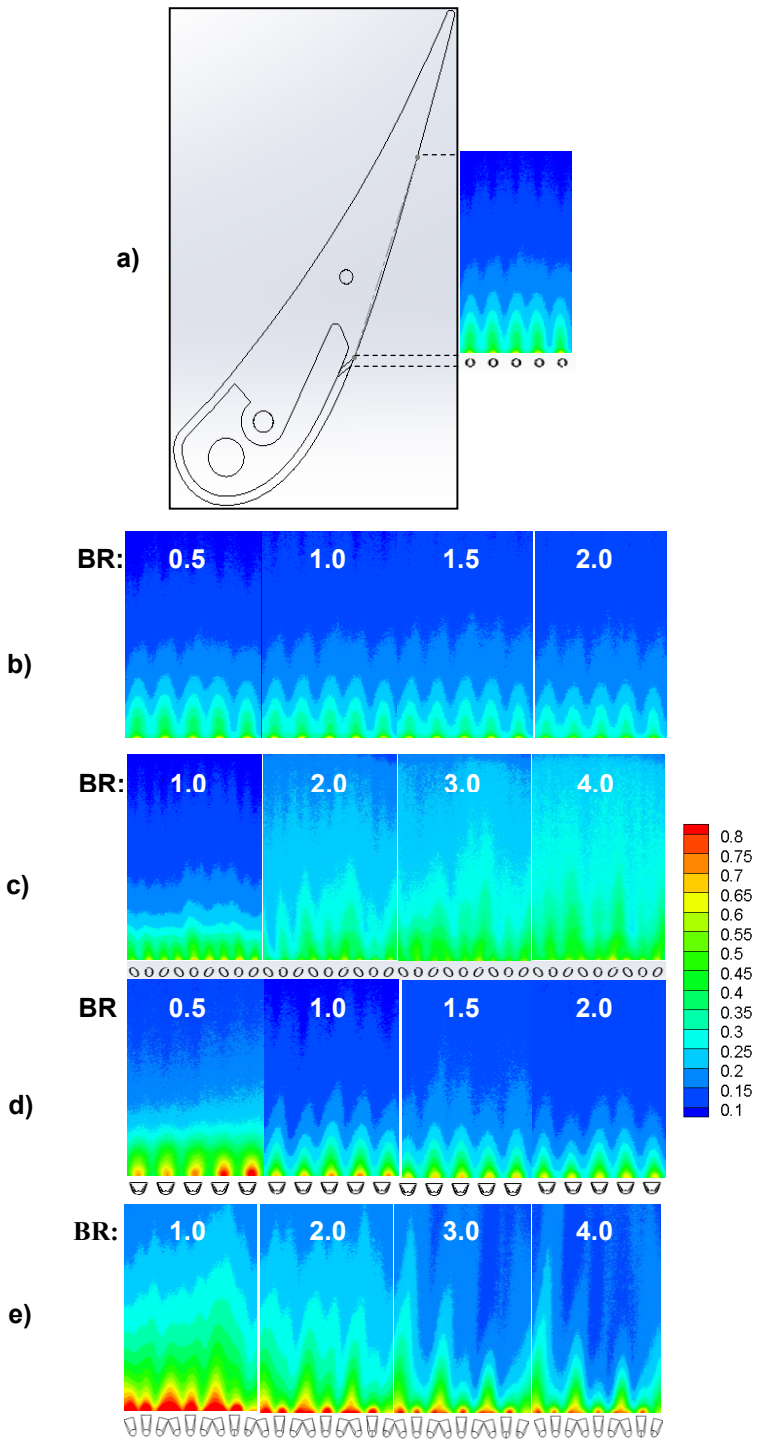

Figure 17. Steady state experimental results: a) side view of an airfoil along with a sample result; b), c), d), e): film cooling effectiveness for CY, AV and shaped and shaped AV holes respectively

However the change in effectiveness was minimal enough to conclude that change in blowing ratio has little effect on film cooling effectiveness for this hole location. As expected, at a given blowing ratio, the averaged effectiveness decreases drastically in the initial downstream region ($x/d < 10$). This could be attributed to the jet lift off phenomenon. On the contrary, for the AV holes (Figure 18b), the peak value was observed at the highest blowing ratio BR = 4.0, equivalent for BR = 2.0 for CY hole. This value was around 0.61 for BR = 4.0 (at $x/d \sim 2$) and dropped to 0.55 for BR = 1.0 showing an increasing trend for the laterally averaged effectiveness with blowing ratio. The effect of blowing ratio on film effectiveness for tripod holes was quite significant when compared to a cylindrical hole case. Shaped hole trends were similar to cylindrical, in terms of decreasing effectiveness with increasing blowing ratios. However the effectiveness value, at the lowest BR = 0.5, was higher than that of the tripod hole BR = 4.0 cases in the initial downstream region ($x/d < 10$) by a significant margin. This distance moves close to the hole location as blowing ratio increases, $x/d \sim 8$ and 6 for BR = 1.0 and 2.0. Past this region, the effect of shaping is greatly reduced as the jet loses its effect and tripod holes were found to be performing better by a margin of ~ 0.1 by spreading the coolant in both lateral and in the flow direction.

Figure 18d shows the effect of BR on shaped AV cooling holes. The trend is very similar to regular shaped holes but the decrease in effectiveness with increased BR is not dramatic as seen for shaped holes. Effectiveness just downstream of the hole are close to 1.0 for shaped AV holes. It appears that shaping the exit of the tripod holes has significant effect on coolant jet-mainstream interactions at this location. Also, all geometries present a trend for effectiveness that changes with blowing ratio, except for CY hole. The scale chosen for representation of laterally averaged effectiveness does not clearly distinguish individual lines in Figure 18a. Moreover, the aspect ratio of the film cooling hole for any other geometry (AV, SH and SH-AV) is almost greater than two. As a result, CY holes experience higher exit momentum or momentum flux ratio. This might have an effect on dependency of the CY hole effectiveness with blowing ratios.

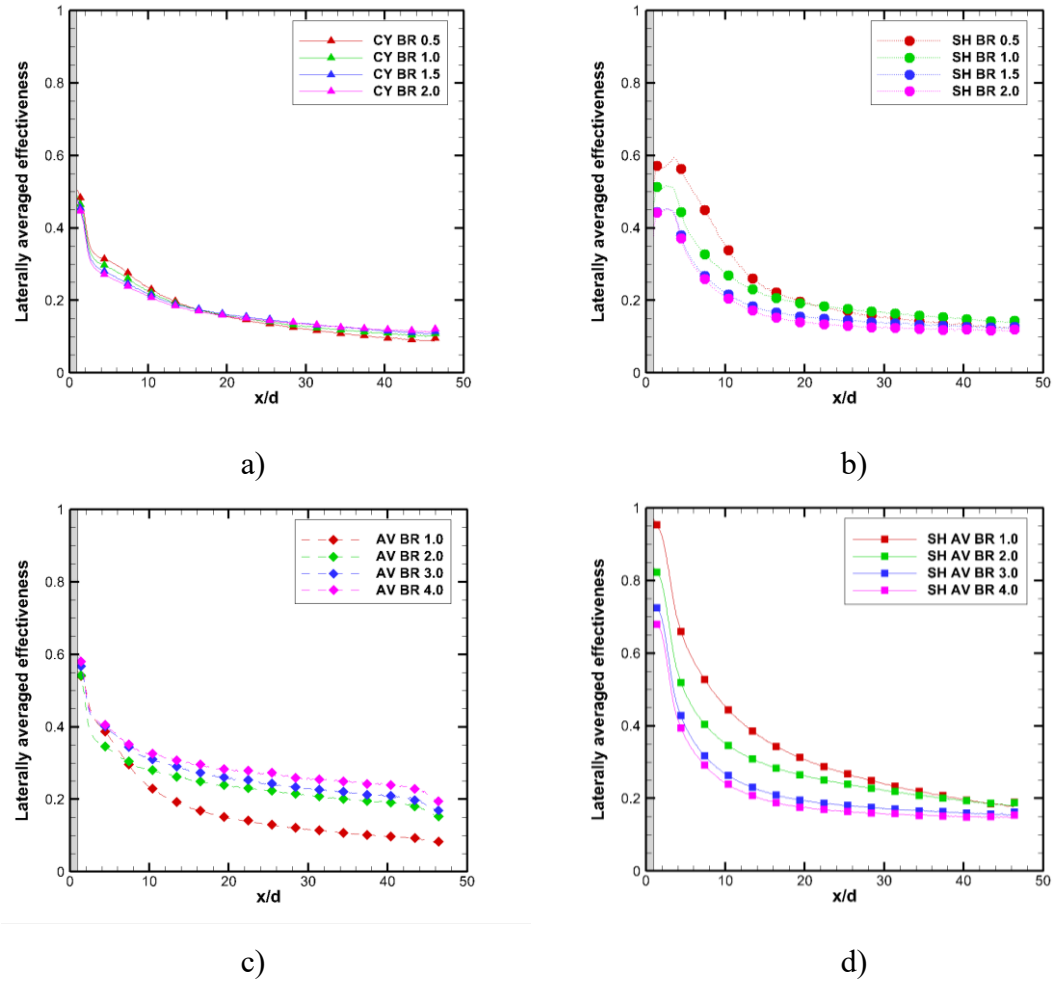

Figure 18.Effect of blowing ratio on laterally averaged film cooling effectiveness for different cooling holes: a) CY; b) SH; c) AV; d) SH-AV holes

Figure 19 shows the effect of coolant mass flow rate on laterally averaged effectiveness. Effectiveness contour provided in Figure 17 is used for spanwise averaging and the resulting data is expressed in terms of hole diameters. Each plot displays the effectiveness for all four geometries shown in Figure 13 and tested under similar coolant flow rates. Mass flow rates are provided in Table 1 and increases as we move from Figure 19a to Figure 19d. At the lowest flow rate case, shaped tripod holes and shaped cylindrical holes outperform non-shaped counterparts. Even at BR = 2.0, the shaped tripod seem to provide the best test results. However with increasing flow rates, two significant trends were noted. Only tripod hole geometry was found to have an average effectiveness data that was noticeably increasing. Shaping of holes provides only marginal

improvement in these conditions. We should remember that at any given mass flow rate condition, a tripod hole will see twice as much velocity as compared to a cylindrical or shaped hole.

Figure 20a and Figure 20b provide comparison between various geometries at a given blowing ratio. Irrespective of the blowing ratio, the shaped tripod holes seems to deliver the best performance. At BR = 1.0, the lowest mass flow rate case, effect of shaping seems to lower the blade temperature. However, at BR = 2.0, AV holes are found to have a better performance for most of the part of the downstream.

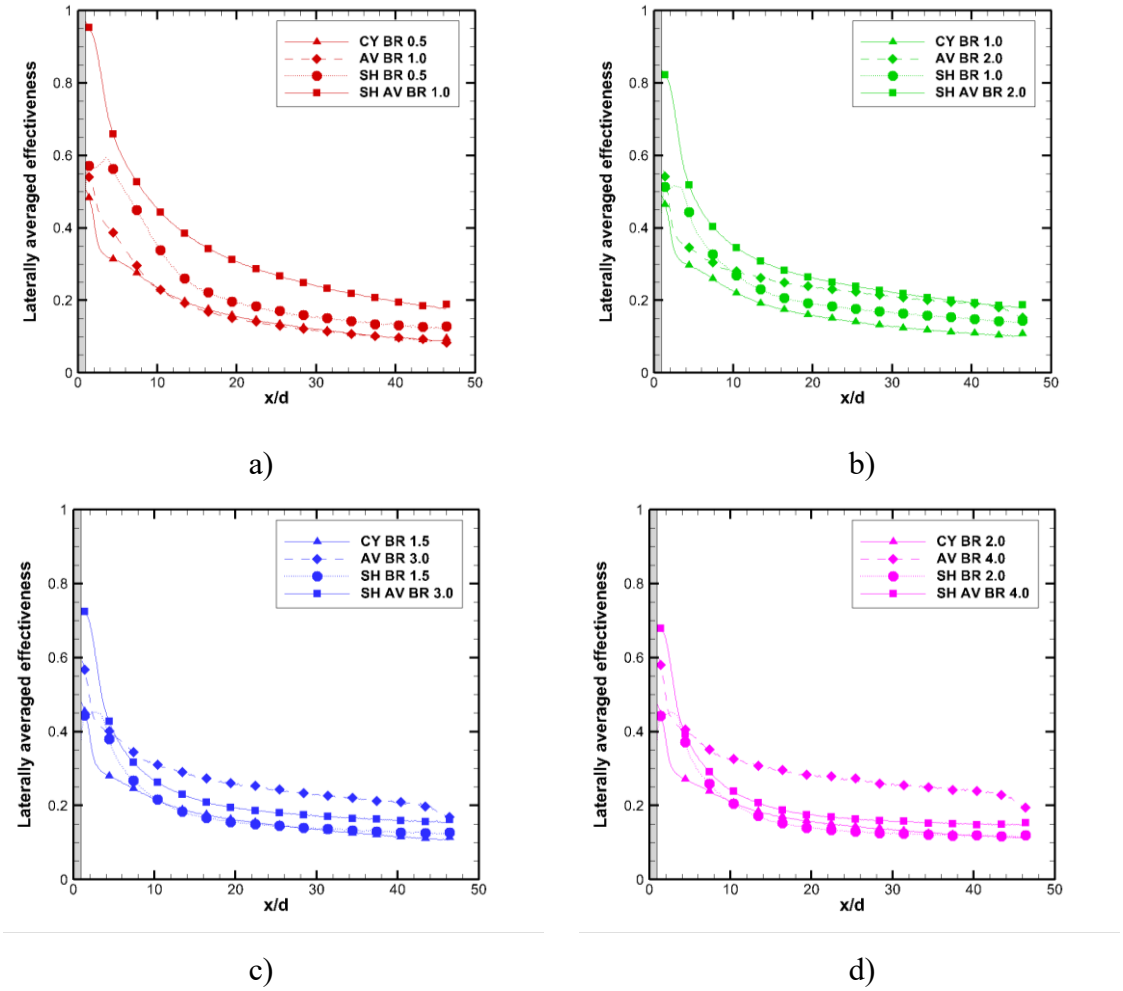

Figure 19.Effect of coolant flow rate on laterally averaged film cooling effectiveness for different cooling holes: a) $\dot{m} \sim 0.0008$ b) $\dot{m} \sim 0.0016$; c) $\dot{m} \sim 0.0024$; d) $\dot{m} \sim 0.0032$

The blowing ratios are based on CY hole and at any given BR similar coolant flow rates can be observed in different hole geometries, as shown in Table 2.

Results for cylindrical and shaped holes are in agreement with [9]. At the lowest Mach number case, at x/d ~ 30, both cylindrical and shaped holes were reported to provide a film cooling effectiveness of about 0.15 which is same as seen from Figure 18a and Figure 18b. Consistency with prior studies establishes that tripod hole geometries, both shaped and non-shaped perform better than the SH or CY holes, except at BR = 0.5 where tripod hole has lower effectiveness. This can be seen in Figure 21 which shows the area averaged effectiveness at different blowing ratios for the test cases discussed above with respect to blowing ratio and coolant mass flow rates. Effectiveness contours from Figure 17 were used for averaging.

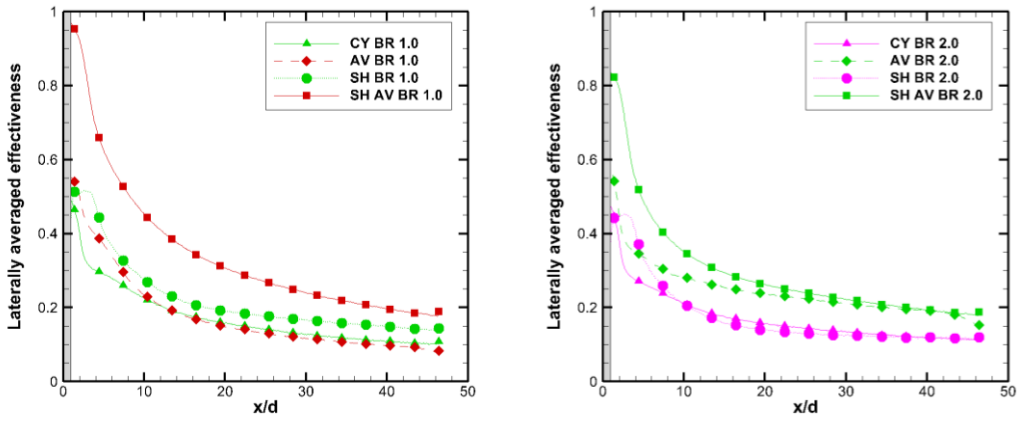

a) b)

Figure 20.Effect of coolant flow rate on laterally averaged film cooling effectiveness for different cooling holes: a) $\dot{m}$ ~ 0.0008 b) $\dot{m}$ ~ 0.0016; c) $\dot{m}$ ~ 0.0024; d) $\dot{m}$ ~ 0.0032

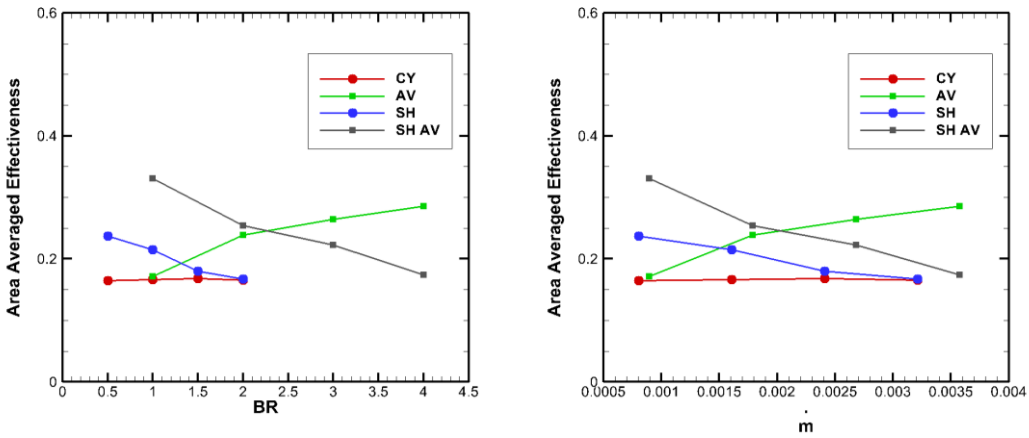

a) b)

Figure 21. Area averaged effectiveness for different cooling hole geometries w.r.t. a) BR; b) $\dot{m}$

CHAPTER 4

NUMERICAL AND THERMAL STRESS ANALYSIS ON A FLAT PLATE

A numerical model was built to simulate the experiments conducted by LeBlanc et al. [14]. The description on the airfoil geometry along with the test setup is available in [14]. This chapter presents experimental adiabatic film cooling effectiveness for cylindrical and tripod cooling holes, its variation with x, effect of blowing ratio and density ratio and mainstream-jet interaction using CFD.

For the current study the test setup including the hole geometries, was designed in ANSYS-14 Design Modeler. The material properties of ABS and experimental boundary conditions were injected into the code. While some of above mentioned studies tried k-ε model to solve the turbulence equations, others have recommended standard k-ω, k-ω shear stress transport model or other RANS models. In spite of significant amount of effort put into this field, as mentioned in [7] these models may not be universally applicable. Most commonly used k-ε model was sought for all the simulations. Numerical predictions weren't accurate but were close to the experimental results and similar procedure was followed for Haynes230, a nickel based single crystal alloy, at engine conditions. Comparison of the thermal stress on the blade near the cooling hole area are provided for all the hole geometries to evaluate thermal stress behavior under realistic conditions.

4.1 Numerical modelling

All computations were run using ANSYS 14. CFX module performs basic fluid flow analysis using finite volume technique and Static Structural module to solve stress equations using finite element technique. Flat plate model shown in Figure 22 resembles the experimental setup described in [14]. Two different hole geometries namely, cylindrical and anti-vortex holes along with the flat plate form a part of the solid domain while hotter mainstream and coolant together constitute the fluid domain, resulting in a conjugate system. Different test cases are summarized in Table 3.

As a result, both these domains are meshed with unstructured tetrahedrons using patch conforming method, totaling around 5 million elements. In order to capture the wall effects, inflation layers are added both on either side of the blade surface as shown in Figure 23. Addition of inflation layers replaces default tetrahedrons with hexahedral elements that align in the flow direction. As shown in Figure 23 close to the wall, the size of the element is negligibly small and it grows in the normal direction at the rate of 1.2. Since velocity and temperature gradient is much larger in the normal direction, presence of inflation layers captures more information with few elements. Wall shear stress and wall heat transfer coefficient are related to the velocity and temperature gradient near the surface.

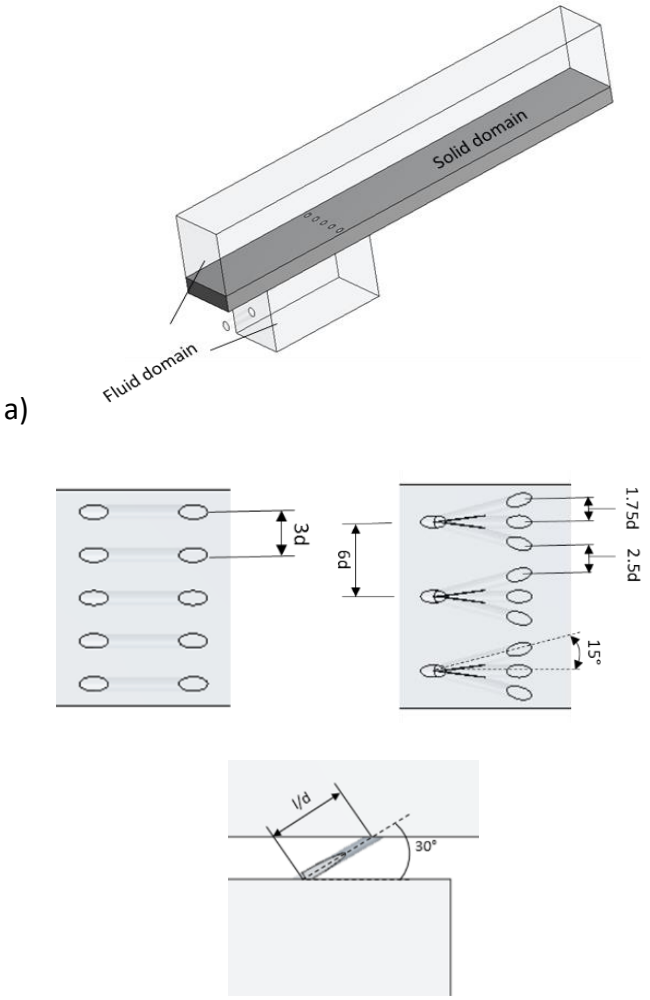

Figure 22 CFX design model: a) CFD domains, b) hole geometries: CY and AV

Inlet boundary conditions were prescribed at mainstream and plenum inlet locations, Table 3. Mainstream inlet is 24 holes diameters upstream of the main hole leading edge while exit location is situated 60 hole diameters downstream. Coolant velocity was varied depending on the blowing ratio. Experimental setup included a strip rod located upstream of hole exits to increase the turbulence in the mainstream. This was accounted by setting the turbulence intensity levels roughly at 5%. Incompressible Reynolds-Averaged Navier Stokes equations were solved that included total kinetic energy equation as well. ANSYS solves standard k-ε model with scalable wall function for near-wall treatment.

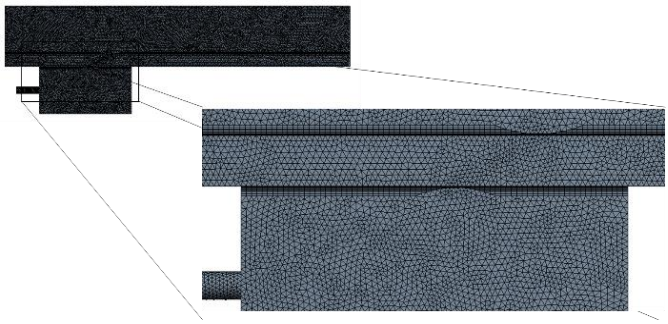

Figure 23.Unstructured tetrahedral mesh with inflational layers

Laterally averaged adiabatic film cooling effectiveness is compared with experimental results from [4]. Numerical prediction isn't expected to match with literature perfectly, but visual comparison of the contours suggests usage of the model for simulating with Haynes-230 alloy at engine temperature conditions. Moreover, objective of the paper lies in developing a tool to predict stress distributions on blade surface.

CFD with Haynes-230 alloy at engine temperature conditions is modeled with the same setup shown in Figure 22. Hot mainstream is designed to flow past the surface at 1400 °C while the blade is being cooled by the coolant at 900 °C. Similar blowing ratios are maintained for Haynes230. The density ratio in these working conditions is approximately around 1.25, a little higher than the one used for validation. But effect of density ratio has already been discussed in [14] and very little change in film cooling effectiveness was noticed.

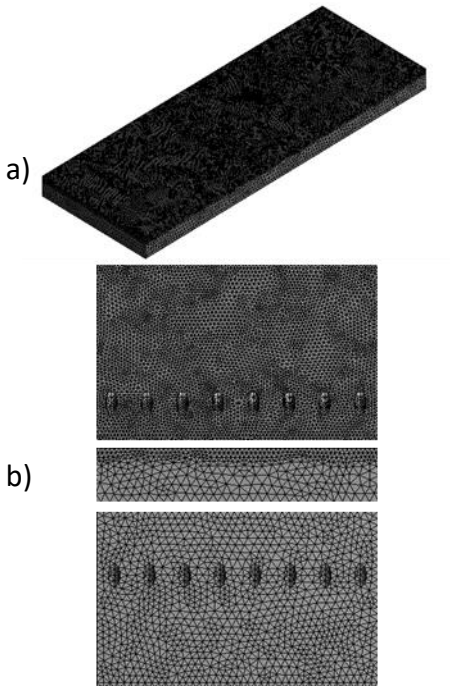

Figure 24.Unstructured tetrahedral mesh: a) flat plate with 600,000 elements, b) mesh refinement as seen from top, side and bottom view

Table 3. Design data for computation

Parameter	Validation
CY AV	d – 2 mm; l/d – 4.0; d – 2 mm l/d (center)– 7.5; l/d (side) – 7.7
BC: mainstream inlet	Fluid: air; V = 9.8 m/s; T = 298.15 K
BC: plenum inlet	Fluid: air; CY: BR = 0.5 &1.0; AV: BR = 1.0 & 2.0; T = 323.15 K
BC: exit	Pr – atm. Pr
Material	ABS

CFD is now coupled with stress analysis tool. The imported solid domain along with its body temperatures is meshed using patch conforming tetrahedrons. Meshed flat plate containing

600,000 tetrahedral elements is shown in Figure 24. The blade surface facing hot gas path has been refined further. Refinement serves two purposes: captures finer stress levels on the blade surface; secondly, it impacts adjacent cells present along the thickness of the plate since cell sizes do not differ by a factor of 1.2. Various loads, acceleration and supports can be provided to the flat plate, depending on the type of system under consideration - a nozzle guide vane. The entire body is thus restrained from any motion. Imported solution from CFD is applied as a boundary condition for the finite element system.

4.2 Results and discussion

LeBlanc et al. [14] varied blowing ratio from 0.5 to 2.0, in steps of 0.5, for cylindrical hole film cooling experiments. Two extreme conditions from the above reference are being considered in this study. As a result, BR of 0.5 and 2.0 for CY and 1.0 and 4.0 for AV were used in CFD. Even before the actual simulations started, initial results were tested for grid independence. For this sake, AV holes were run at 6 different grid sizes, starting from 3 million tetrahedral elements to 8 million, with increments of 1 million per case. Refinement beyond 5 million elements did not seem to have a significant effect on the effectiveness. Henceforth, all future design cases were meshed with 5 million unstructured tetrahedral elements. Figure 25 shows the predictive improvement with number of grid points.

Experimental results from [14], for tripod holes, along with the CFD values are provided for comparison in Figure 26. Experimental data reduction employed MATLAB and as result the effectiveness data were presented in RGB color map. ANSYS CFX, on the other hand, uses Rainbow color map by default. Figure 26 focusses on laterally averaged film cooling effectiveness based on CFD and experiments for tripod hole case at BR 1.0. The k-epsilon model seems to over predict and in general does not seem to predict the coolant jet diffusion in the spanwise direction. Figure 27 illustrates the presence of counter-rotating vortex pairs and anti-kidney vortex pairs in cylindrical and tripod holes respectively, signifying other capabilities of the model. It is important to note that the numerical model was not designed to capture flow physics associated with these film cooling holes. In spite of a conjugate analysis, low thermal conductivity of ABS and increased thickness of the flat plate provided more resistance to heat flow through the blade and hence the absence of any effect due to conduction.

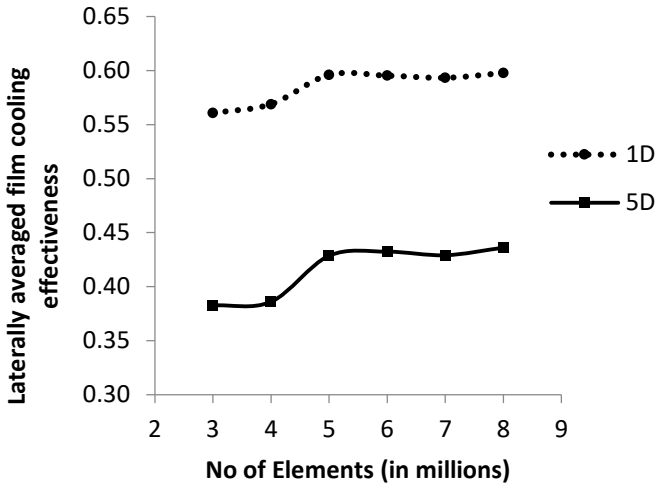

Figure 25.Test of grid independence for AV hole at BR 1.0

Cylindrical and tripod holes were run again at two different blowing ratios, BR 0.5 and 2.0, this time with a new material for the flat plate: Haynes-230 alloy. Different blowing ratios were chosen this time to predict range in variation of thermal stress in a blade in an actual turbine. Results for Haynes-230 alloy are more accurate than those run with ABS, since convergence criteria for RMS residuals were set $4x10^{-5}$. Also residual values as low as $4x10^{-7}$ were noticed throughout the domain except near the bottom wall of the plenum, where residuals just managed to lie below the set convergence level.

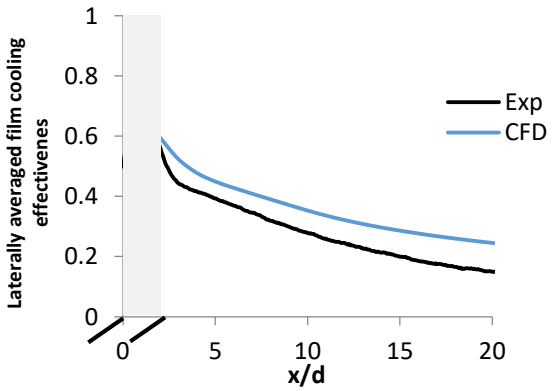

Figure 26.Validation of CFD with experiments: laterally averaged film cooling effectiveness for AV hole at BR 1.0

Owing to higher thermal conductivity of Haynes-230 alloy, temperature distribution was more uniform. Higher ‘k’ also causes the coolant to heat up even before it reaches the blade surface. Figure 28 presents coolant temperature streamlines. Near the trailing edge of the tripod hole, coolant temperature raises to ~1400 K. The amount of heat gained by the coolant will vary with blowing ratio, generally decreasses as blowing ratio increases and depends on hole configuration as well, cylindrical holes will observe higher temperatures. To compare the heat flux flowing from the hot side to the cold side, Biot number needs to be evaluated. The non-dimensional number will provide an estimation of heat flux and temperature distribution for different cases and acts as a good scaling parameter. Typical gas turbine values varies between 0.15 and 1.5 for the hot side of the blade and around 0.15 - 0.3 for the cold side. Cylindrical hole CFD cases had a Bi of 0.063 near the hole.

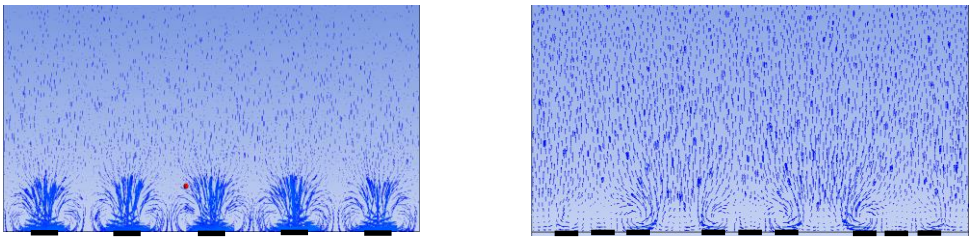

a) b)

Figure 27.Vortex structure at x=3d downstream from center of the holes in case of: a) CY holes, b) AV holes

Body temperature imported from CFX is shown in Figure 29a while numerical result is presented in Figure 29b. Effect of conduction is evident in the stress contours, Figure 30, and clearly locates the position of holes present within the solid blade. The region upstream of holes also suffer higher stress when compared to near hole region. Again heat flow into the blade to plenum chamber reduces body temperature, as seen in Figure 29. This in turn causes higher temperature gradient local to that region, causing higher thermal stress levels. If same amount of coolant is injected, tripod holes will have double the blowing ratio when compared to cylindrical holes.

Figure 30 displays equivalent (Von-Mises) stress for CY: BR 0.5 , 2.0 and AV: BR1.0 and 4.0. In Figure 30a and Figure 30b, highest temperature gradients are recorded inside the holes. This region suffers from high stresses, as seen by local red spots. Surface far away from the cooling

zone observes very little temperature change and hence the low stress levels near the end of the flat plate. For both geometries at lowest blowing ratio, blade temperature within the hole doesn't exceed 1175°C. From Table 4, even at 1205°C the ultimate tensile strength of Haynes230 alloy is 65MPa. At the highest blowing ratio, temperature inside the holes is less than 1300K or 1027°C for both AV and CY holes. Linear interpolation of test temperature between 1095°C and 980°C, yeilds a tensile strength of 190MPa at 1037.5 °C. At BR 2 for CY, tripod holes seem to have favorable stress contour and both these holes lie within the tolerable limitIn all these cases, a small low stress region near the trailing edge of cooling holes could be noticed. This may be due to the flow separation from the surface. *k-ε* model with scalable wall function may not be the best for near wall modeling but still recognizes these features. CY BR 2.0 seems to have a high stress region downstream of cooling holes because of usage of unique range for each test case. Equivalent stress in this region for CY and AV, shown in Figure 30, explains this.

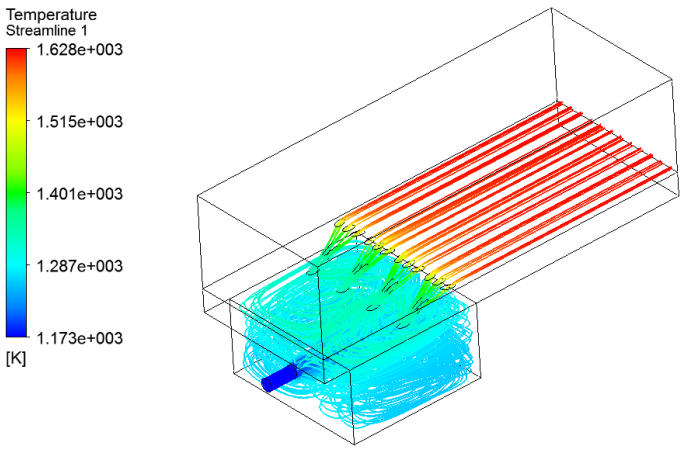

Figure 28. Temperature streamlines of coolant jet for AV hole at BR 1.0

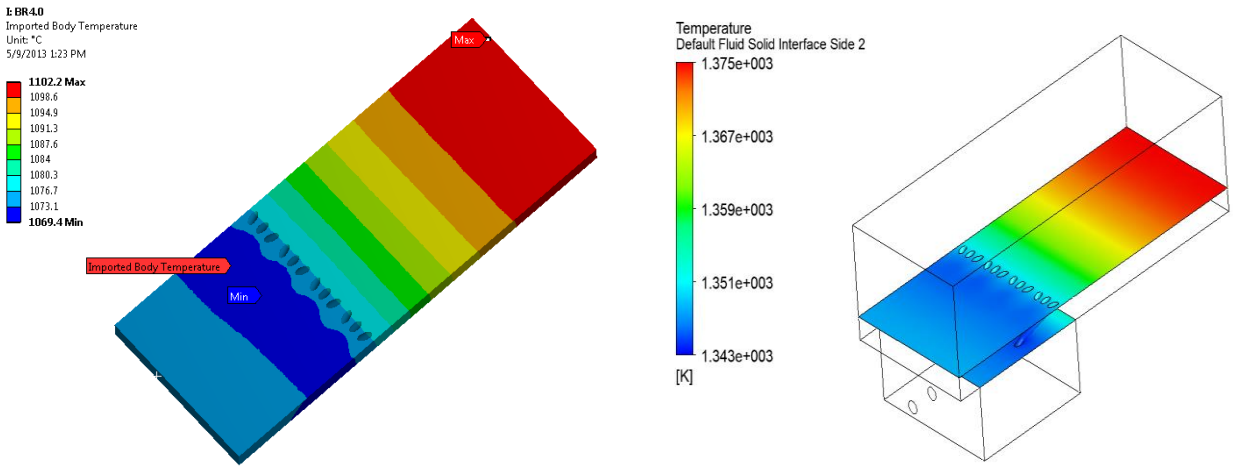

a) **b)**

Figure 29.Temperature distribution on the flat plate: a) imported body temperature in static structural module, b) CFX

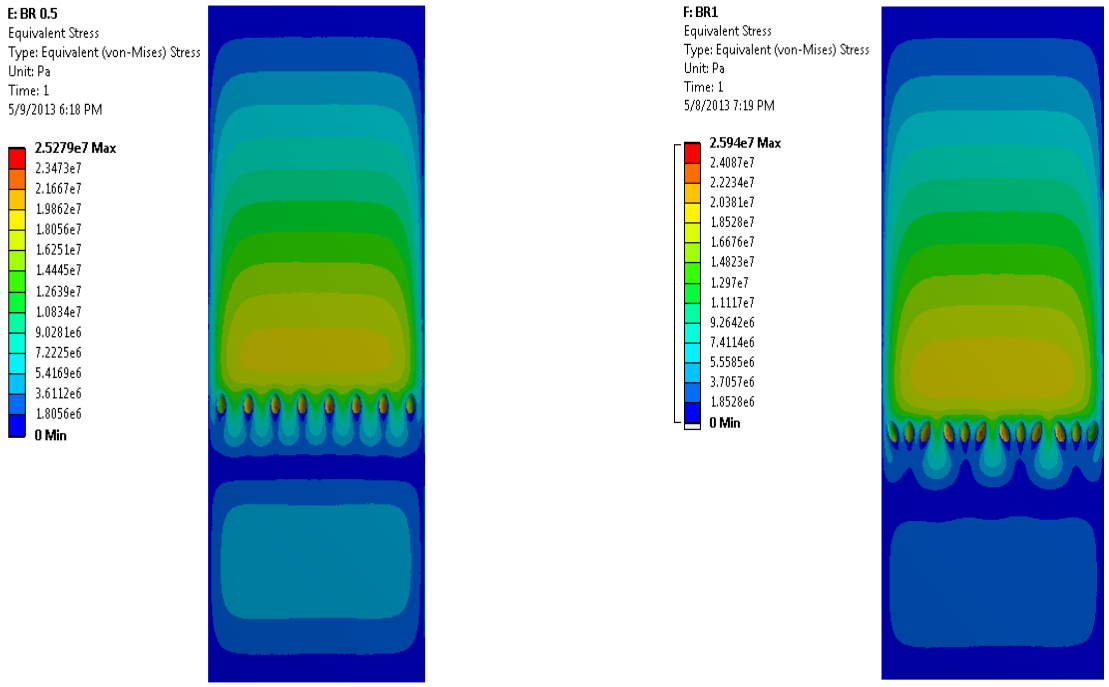

a) **b)**

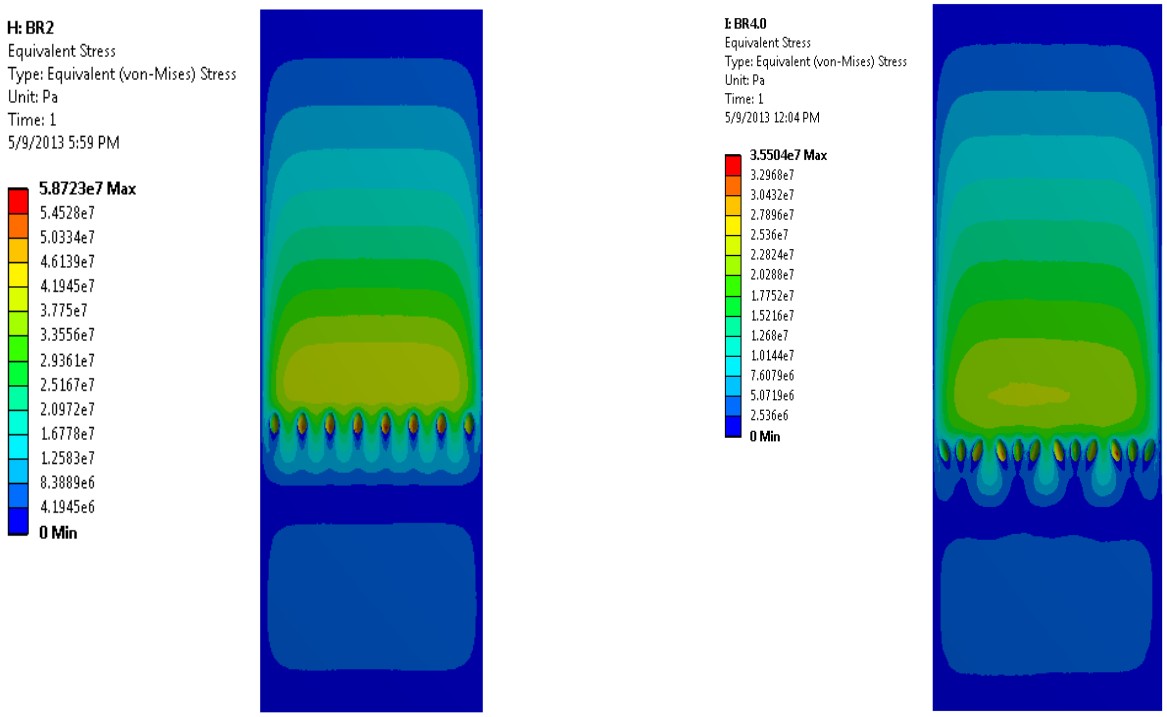

c) **d)**

Figure 30.Thermal stress distribution on the flat plate: a) CY BR 0.5, b) AV BR 1.0, c) CY BR 2.0 and d) AV BR 4.0

Table 4: Typical tensile properties of haynes230 alloy

Test Temperature		Ultimate tensile strength	
°F	°C	Ksi	Mpa
Room	Room	125	860
1000	540	103	705
1200	650	98	675
1400	760	88	605
1600	870	63	435
1800	980	35	240
2000	1095	20	140
2100	1150	13	91
2200	1205	9	65

4.3 Conclusion

Tripod holes have already been tested for better film cooling performance. Application of such cooling method would also require careful consideration of its impact on aerodynamic losses and

induced thermal stresses. A relatively new technique for studying thermal stress was implemented in this paper. While CFD provided agreeable comparison between experimental and numerical results, stress analysis showed that cylindrical holes can be replaced with tripod holes but the performance depends on working conditions. For both working conditions (CY: BR 0.5 and 2.0), CFD predicts safe function of cooling holes. But caution must be exercised while using these data since CFD over predicted temperature distribution. Moreover, the test section is a simplified version of a gas turbine engine. Even for flat plate testing, usage of actual inlet Reynolds numbers, thermal barrier coating and variation in any parameter attributed with a film cooling hole might have huge implications on thermal stress behavior. For the current study, at any blowing ratio, maximum stress region was seen inside the hole and cylindrical holes seems to create more stress on the blade compared to the tripod holes.

CHAPTER 5

NUMERICAL ANALYSIS OF TRIPOD HOLE FILM COOLING AT LAB SCALE CONDITIONS

5.1 Numerical model

5.1.1 Design

The design model for numerical analysis of film cooling hole performance shown in Figure 31 comprises of a single fluid domain with 2 inlets: one for the hot gas and another for the coolant and one common outlet. Mainstream hot gas and coolant are modeled with air which was treated as an ideal gas. This design focuses on the performance of a single film cooling hole. The various cooling shapes studied here are shown in Figure 32. The width of domain is the same as half of the hole pitch. In case of the cylindrical hole, the domain width was 3d while the tripod and the 7-7-7-shaped hole domain was 6d wide. As mentioned in the experimental section, cylindrical and tripod holes of length, l = 8d are inclined 30° to the surface in the streamwise direction. The side holes of the tripod hole unit are also inclined 30° to the surface in the streamwise direction. The numerical model shown in Figure 31 was design so as to replicate the film cooling experiments conducted at Virginia Tech's flat plate test rig. The results of these experiments were already discussed in the second Chapter.

The hot gas/mainstream inlet is located roughly 48 hole diameters upstream from the leading edge of the hole. The experimental test rig had a trip wire close to the hot gas inlet (8d) in order to trip the boundary layer and make it turbulent. The velocity boundary layer thus developed will be representative of the experiments. As mentioned above, the design shows two chambers: one on the top where the hot gas enters from the left and exits from the outlet, also known as mainstream section; another one on the bottom where the coolant enters, also called as plenum. The coolant exits the plenum, entering the film cooling hole and eventually mixes with the hot mainstream gas. This design was further divided into smaller sections, as shown in the Figure 31, for the convenience of meshing. The domain was divided into 5 sections, 3 of which are attached to the flat plate. Other

details regarding the dimensions of the numerical model and hole geometries are provided in Figure 31a, Figure 31b and Figure 32.

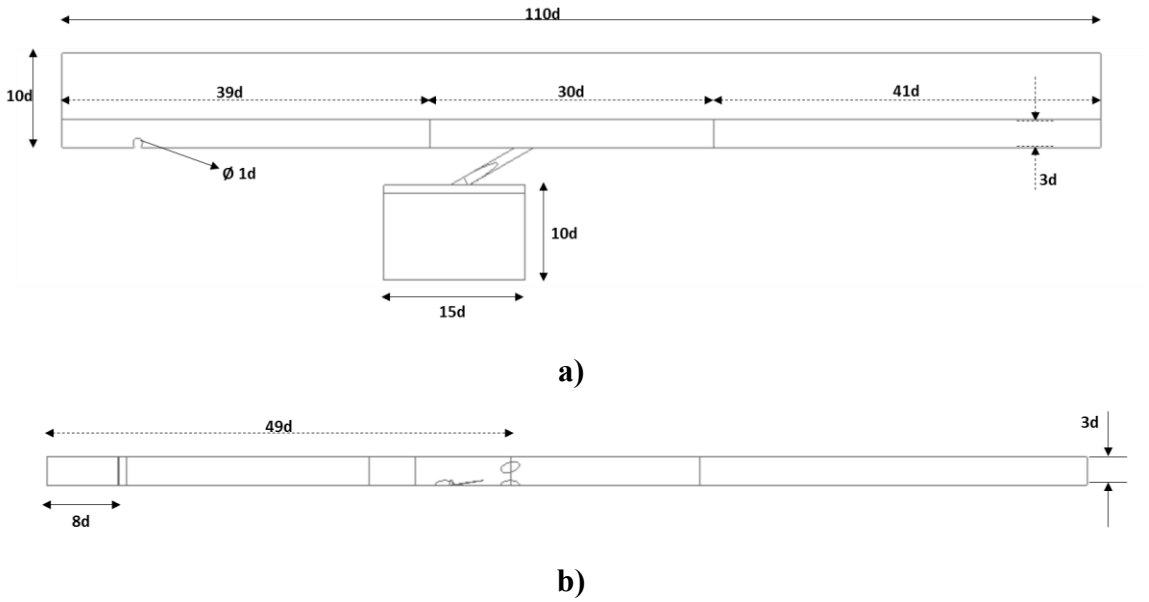

Figure 31 Numerical model: a) side view; b) top view

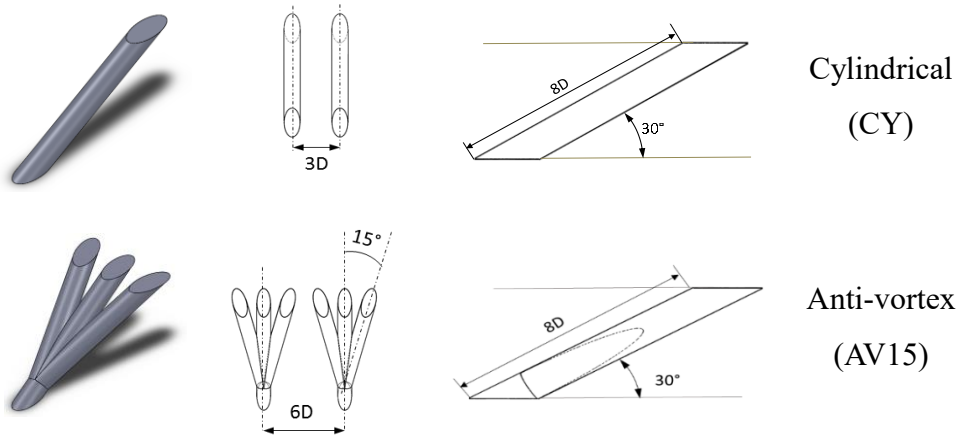

Figure 32 Film cooling hole shapes studied

5.1.2 Meshing process

The meshing process for the current model was performed using ANSYS CFX. The choice of the meshing software was understandable since ANSYS tetrahedral mesher is known for generating

high quality elements for geometries involving complex shapes (tripod holes in this case). The entire domain was meshed with unstructured tetrahedral elements (Figure 33) using patch conforming method which ensures a conformal mesh even when the domain is meshed part by part. The outer parts of the domain, namely the hot mainstream gas and coolant plenum, were meshed with coarse elements of size same as the hole diameter (d). The remaining parts, ones closer to the flat plate wall and the film cooling hole, were meshed with finer elements of size = d/6.25. In order to resolve the boundary layer, inflation layers were added to all walls surface such that y+ ~ 1. Addition of inflation layers replaces default tetrahedrons with hexahedral elements that are aligned in the flow direction. The requirement of y+ ~ 1 had to be met because of the turbulent closure model (SST-KW) chosen for the current study. 22 inflation layers were added as a result, with a first layer cell thickness of 0.001in (= d/250). The growth rate (1.12) had to be adjusted according to the hole diameter and the number of inflation layers. Values of the parameters discussed above are universal and applicable for inflation layers present on all the wall surfaces. Based on the experience, it was observed that using different parametric values for different inflation layers results in a poor mesh in regions where two inflation layers would meet. One such example would be the inflation layer present inside the hole and one for the flat surface. There is a higher chance of having poor quality elements in the region close to the hole exit in this case. This was avoided by using a single inflation layer setting for the entire domain. Overall, roughly 3.3 million tetrahedral elements were used to the mesh the domain. A preliminary numerical study was performed as a part of the grid independent study. Parts of the domain closer to the flat wall, with a finer mesh were refined further. This resulted in 5 different grids whose size ranged from ~1 million to ~7 million tetrahedral elements. When the laterally averaged adiabatic effectiveness was compared for all these meshes, it was noticed that mesh independence was not satisfactory. Even though the effectiveness values were much closer as the mesh count went above 6 million, the gradients in flow variables like velocity, temperature, turbulent kinetic energy, vorticity etc. were still large enough. The overall process of obtaining a mesh independent result by uniformly lowering the mesh size, close the region of interest, still looked futile. The temperature gradient especially, close to the hole exit where the coolant mixes with the mainstream hot gas could not be captured accurately. Resorting to refine the mesh further to capture these critical flow details will result in a huge mesh which would be computationally expensive to run. Since the duration of each simulation had to be kept as small as possible, mesh adaptation technique was employed. Mesh

adaption technique in CFX is based on the gradients of the variable chosen. As such this technique requires only few essential parameters and these can be optimized based on the flow physics that is being solved. The mesh adaptation strategy followed by ANSYS CFX is shown in Figure 34.

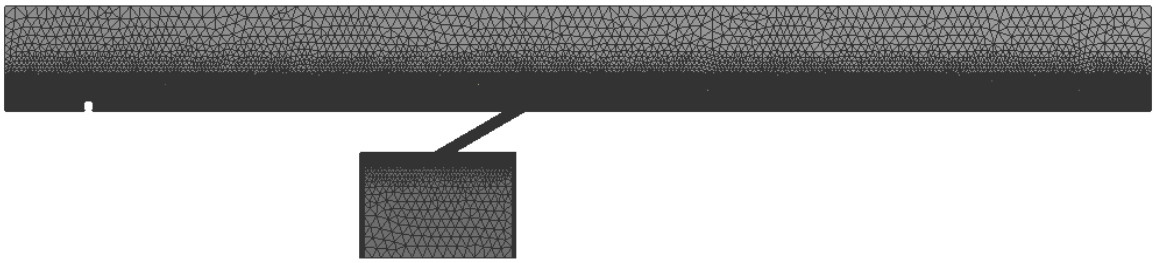

a)

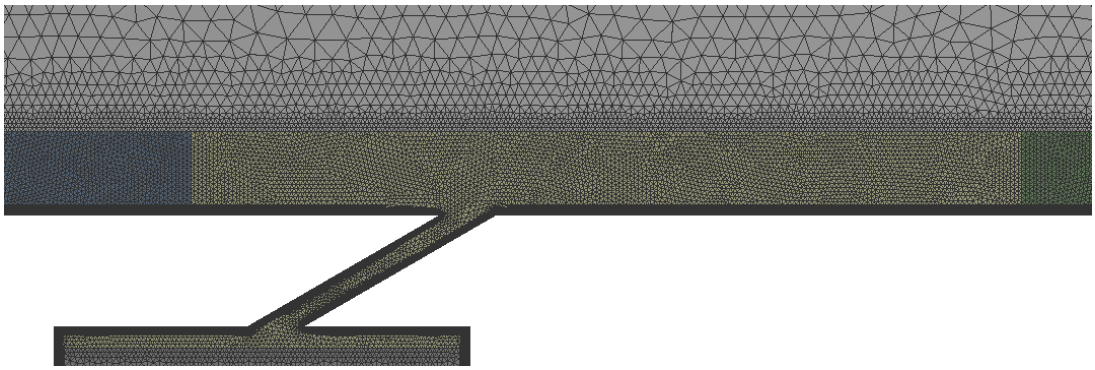

b)

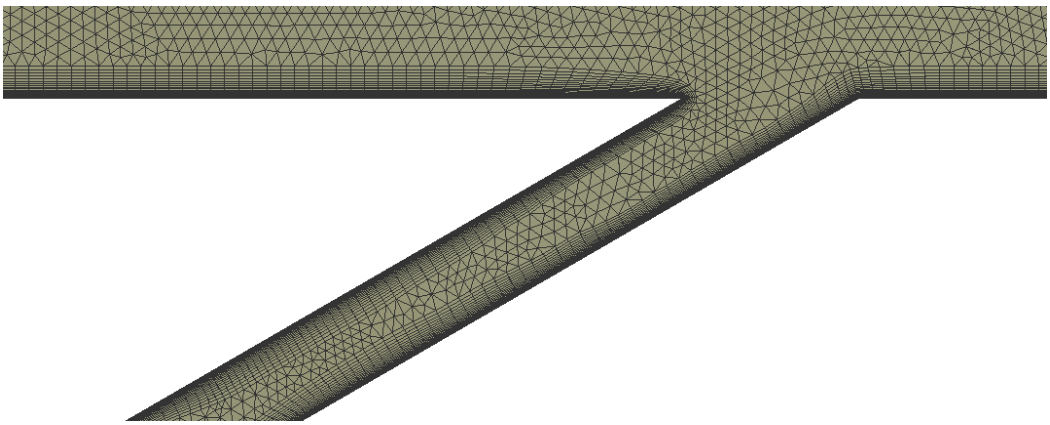

c)

Figure 33 Tetrahedral mesh: a) side of the entire model; b) exploded view of the mesh showing the finer mesh details close to the wall; c) mesh distribution inside the film cooling hole (inflation layers)

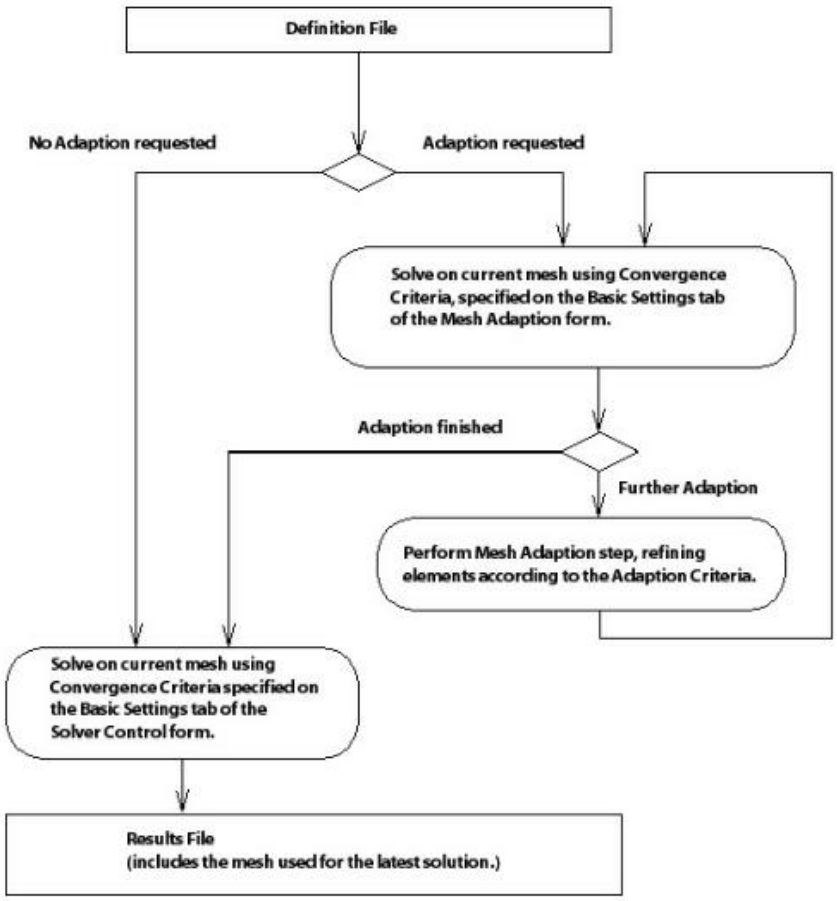

Figure 34 Mesh adaption flow chart followed by ANSYS CFX [user's guide]

The method employed by ANSYS CFX is incremental meshing where an existing mesh is modified depending on the adaption criteria set by the user. This technique is much faster than re-meshing the entire domain at every adaptation step. The adaption algorithm used in this incremental adaption method is known as hierarchical refinement or h-refinement in short. The results of mesh adaption will be discussed shortly.

5.1.3 Boundary conditions

The hot gas inlet shown below was provided with a constant velocity inlet boundary condition. The hot gas velocity and temperature were taken from the experimental data presented in Chapter 2. A mainstream velocity of 7.9 m/s at 323.15 K was modeled at the inlet. The experimental test setup employed a mesh heater to uniformly raise the mainstream temperature from ambient room

temperature to ~ 323.15 K. The stainless steel mesh is known to break down the large vortices and in one of the earlier experiments performed on a similar mesh heater, reported a turbulent intensity of roughly 2%. The value is quite low compared to realistic gas turbine engines where values more than 10% can be expected near the first stage vane. To be on the conservative side, the hot gas inlet turbulent intensity was set at 5% for the current study.

The coolant inlet plenum was provided with a mass flow rate inlet boundary condition. The coolant mass flow rate depends on the blowing ratio and density ratio. Though the coolant was supplied at room temperature ~ 22 °C during experiments, a slightly higher value of 298.15 K was used for the numerical simulations. Since the objective of this study is to predict the adiabatic effectiveness, which is normalized w.r.t. the hot gas and coolant temperature, the actual coolant temperature should not impact the study as long as the density ratio is close to the experimental value. The coolant plenum was also supplied with a similar turbulent intensity of 5%. The gas turbine film cooling review paper by Bogard and Thole highlights important factors affecting film cooling performance and its impact on the adiabatic effectiveness. One such parameter was the mainstream/hot gas turbulent intensity but in the one of the study cited in this review paper, it was observed that even doubling the turbulent intensity from 3.6% to 7.5%, caused less than 10% change in laterally averaged effectiveness. At some blowing ratios, this difference was as low as 0.02. As a result, it expected that the values of mainstream and coolant turbulent intensity at their respective inlets, should not affect the results significantly. Moreover, these values are consistent for all hole shapes and at all blowing ratios. A comparative study between hole shapes can still provide insight on the relative film cooling performance.

The ability to study a wide variety of test cases in a relatively shorter amount of time is one of the biggest advantages of CFD over experiments. The time taken for a particular numerical simulation is always the key deciding factor. In order to achieve this, few assumptions are generally made while designing the numerical model. The experimental test setup employed approximately 11 cylindrical hole with a p/d=3. The numerical model however, simulates only one half of this cylindrical hole. Symmetry boundary conditions were used on either side to reduce the size of the computational domain. The top wall of the domain was also modeled with a symmetry boundary condition even though it was located far above the flat wall surface/film cooling hole exit. Assigning a wall boundary condition in place of a symmetric BC, would result in a growth of the boundary layer on the top wall which could now alter the mainstream velocity profile. Owing to the steady

state nature of the CFD, the symmetry boundary condition should be able to replicate the experiment accurately. For studies involving transient flow features, it is more appropriate to model the entire film cooling hole and assign periodic boundary conditions on either side of the hole.

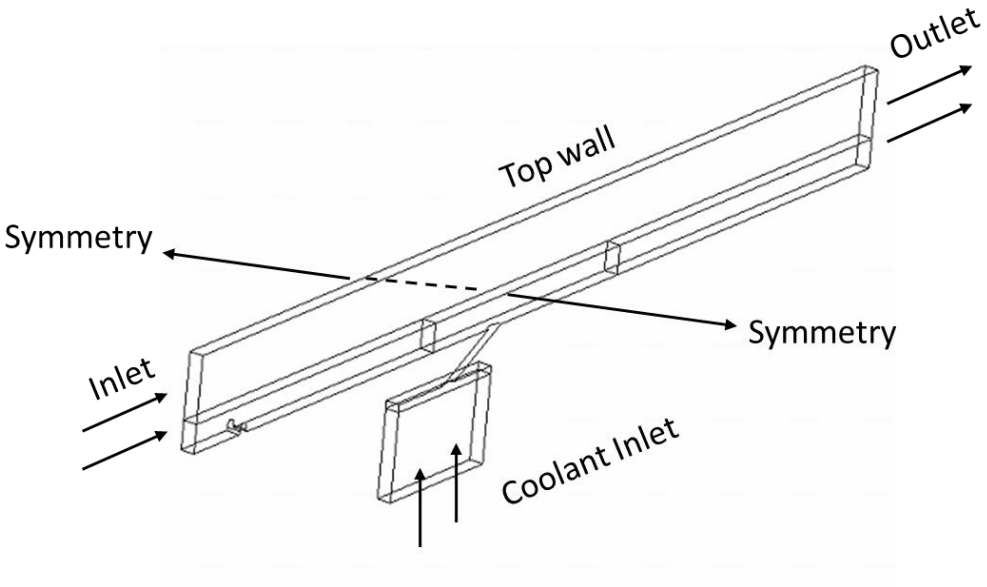

Figure 35 Numerical model with appropriate boundary conditions

5.2. Mesh adaption results

5.2.1 Grid independent study

As a first step towards numerical analysis of performance of film cooling holes, a solution independent of the grid size was sought. The numerical domain shown above was meshed using five different element sizes. The size of the tetrahedral element was chosen such that it will result in an overall mesh count ranging from 1 million to 7 million. Laterally averaged effectiveness was obtained for all mesh cases and summarized in the figure shown below. Surprisingly the effect of a finer mesh element (on the solution) could not be observed in Figure 36. The difference effectiveness between a 0.84 million mesh and 7.2 million element was almost negligible. The element size in the region close to the flat plate was reduced from 0.08 in to 0.0225 in between these two extreme cases. It appears that a similar solution can be by using a coarser mesh even

though the discretization errors are higher. Though the differences are easily noticeable, results summarized in the table below, clearly recommends the finest mesh used. Table 5 compares the percentage difference in area averaged effectiveness with the mesh adapted solution as the reference. It can be seen that the finest mesh case with 7.2 million elements predicts a solution closer to the mesh adapted effectiveness (~1%) while the coarsest mesh with 0.84 million elements predicted effectiveness is higher by more than 6%.

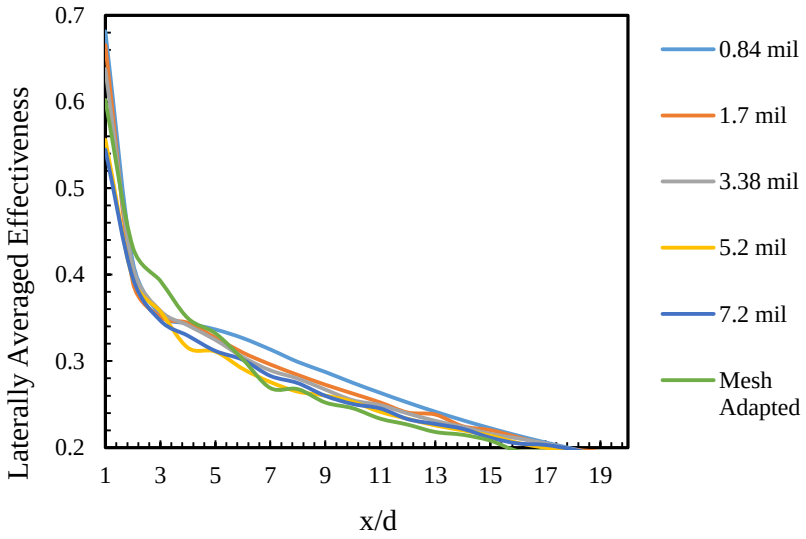

Figure 36 Effect of grid independent study on laterally averaged effectiveness

Table 5 Percentage difference in area averaged effectiveness w.r.t. mesh adapted solution

Location\Mesh	0.84mil	1.7 mil	3.38 mil	5.2 mil	7.2 mil	Mesh Adapted
x/d: 0 - 20	***6.28***	***3.48***	***2.46***	***-1.71***	***-1.13***	-
x/d: 0 – 5	1.02	-1.37	-1.77	-8.20	-8.52	-
x/d: 6 – 10	13.48	7.90	5.73	2.16	3.59	-
x/d: 10 - 20	7.88	6.34	5.38	3.29	3.80	-
Element size	0.08 in	0.055 in	0.04 in	0.0275in	0.022 in	0.04 in

In spite of the proximity of the solution predicted by the finest mesh, Figure 37 and Figure 38 clearly illustrate the shortcomings of a simple grid independent study and showcases the benefits

of mesh adapted solution. The usage of tetrahedral elements as compared to the hexahedral element, greatly limits the resolution of the gradients present in the solution. In regions like film cooling hole exit where the coolant jet and hot mainstream gas interact, a thin mixing layer with temperature gradients dictated by the hot gas and coolant temperature is formed. From Figure 38 and Table 5, it can be noticed that while the coarsest mesh results in an effectiveness closer (1%) to the mesh adapted result in the region $0 < x/d < 5$, the finest mesh with 7.2 million element results in an error of almost 8.5%.

The grid independent study typically performed on an unstructured tetrahedral mesh poses a great risk of not capturing critical flow features. Instead of a uniform refinement throughout the domain, it might be quicker and efficient to focus regions of large gradients and perform selective refinement. The effect of local refinement achieved through mesh adaption is discussed in the following sub-section. Three different regions are examined here. The first region chosen was the flat wall surface where adiabatic effectiveness contour are plotted. These contours are helpful in understanding the coolant coverage on the surface of the turbine blade, flat plate in this case. The second region is when the coolant exits the film cooling hole and interacts with hot gas mainstream. This critical region where fluids at two different temperatures mix together results in large gradients in temperature over a small distance. Finally, the film cooling hole and hole entrance are inspected where turbulent kinetic energy contours are plotted. Leylek and Zerkle [53] observed that this region is critical in determining the production of counter rotating vortex pairs and coolant jet turbulence in general.

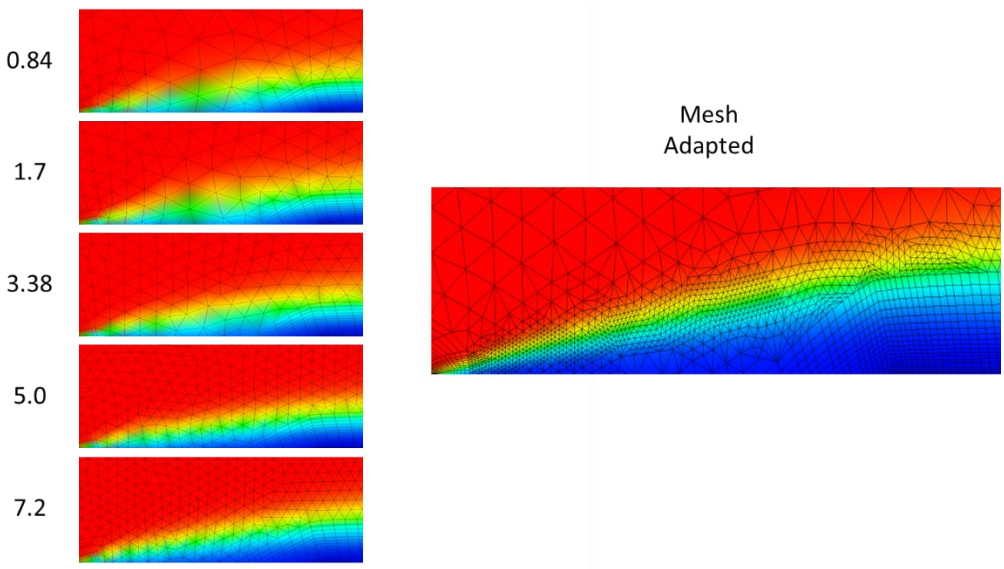

Figure 37 Effect of GIS and mesh adaption on coolant jet temperature distribution

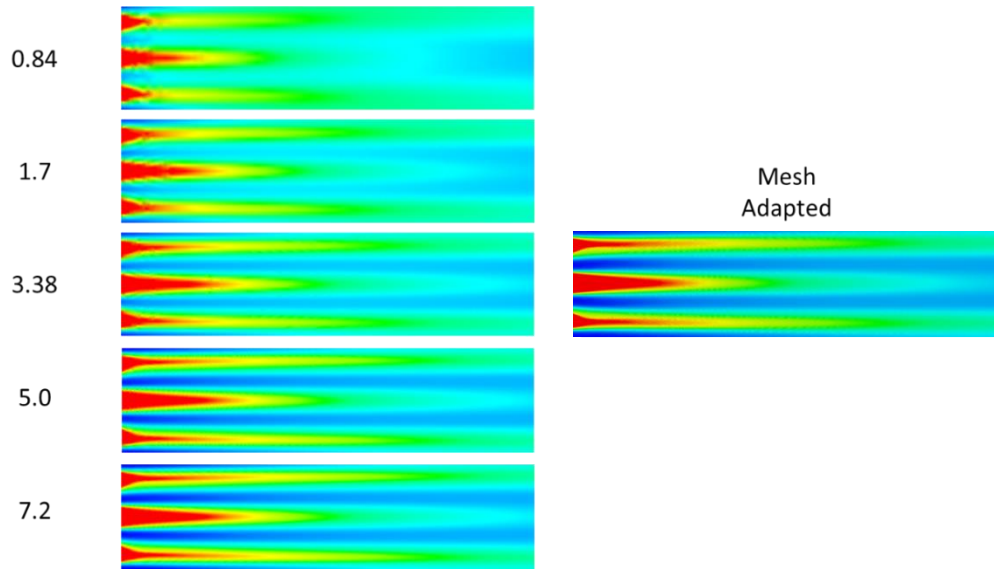

Figure 38 Effect of GIS and mesh adaption on adiabatic effectiveness

5.2.2 Effect of mesh adaption on adiabatic effectiveness

Figure 39 shows the effect of choice of adapted variable on the distribution of adiabatic effectiveness on the flat plate. The contoured mesh column shows the region where local refinement was done. As clearly seen from this result, the effectiveness distribution was not captured accurately

when mesh was not adapted. The diffusion due to mesh coarseness can be noticed in the contours. Similar results were obtained when the mesh was adapted based on 'vorticity', Figure 39c. Expect for the very fine refinement on the hole exit trailing edge, the surface mesh sees no change in size. Even though the coolant jet as such suffers from CRVPs, vorticity values on a surface is almost negligible. It is not surprising that the surface mesh could not be refined. Adiabatic effectiveness is simply normalized wall temperature. At this point, it is obvious that the choice of temperature as an adaption variable clearly captures the gradient and results in an improved coolant jet coverage (Figure 39b). Combining adaption variables also showed equal potential as long as temperature was one of the adapted variables. The major takeaway from Figure 39 would be that either temperature alone or a combination of temperature and another variable can be a good choice of the variable to adapt.

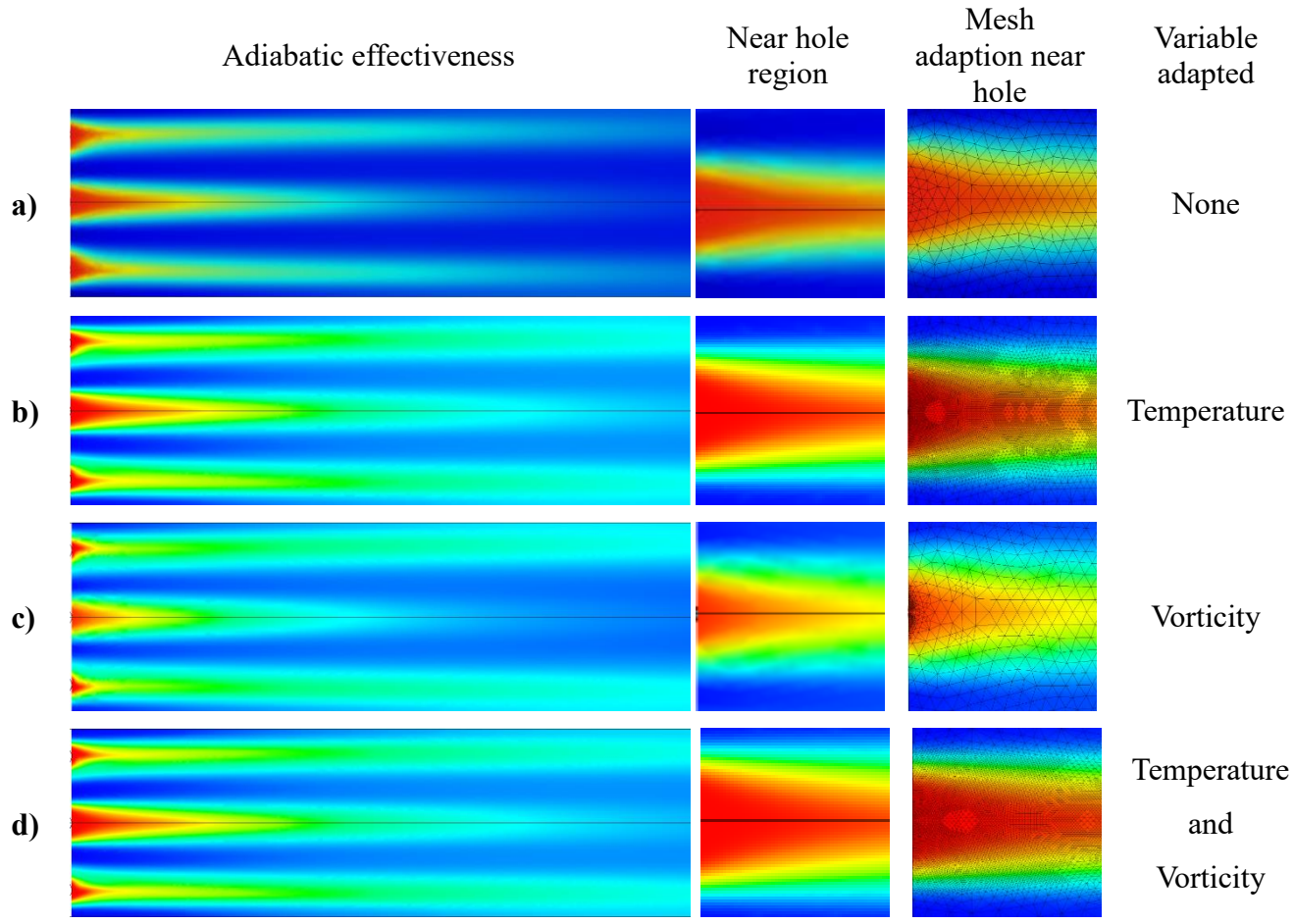

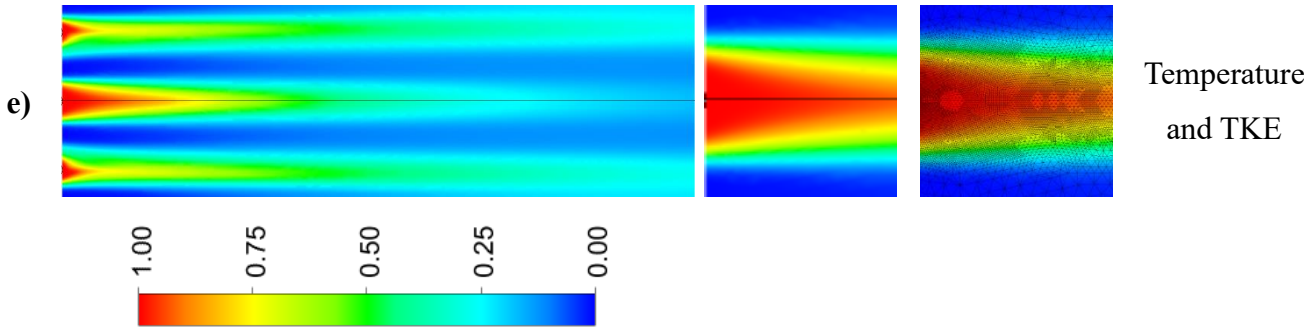

Figure 39 Effect of adaption on adiabatic effectiveness distribution on the flat plate

5.2.3 Effect on hot gas – coolant mixing

Figure 40a shows the coolant exiting the film cooling hole and interacting with the mainstream. The original mesh (without adaption) is unable to capture this large gradient as it is confined to a tiny region. The width of this thin line region is roughly one tenth of the hole diameter. A highly refined mesh capable of capturing this gradient would result in more than 12 million tetrahedral elements. For a steady state simulation solving RANS equations on a domain that covers half a hole pitch, this huge mesh and the resultant computational run time are undesirable. It can be noticed that all variables chosen for adaption were capable of resolving this temperature gradient.

In a study involving prediction of flat plate temperature or cooling effectiveness, as mentioned before, choice of temperature as an adaption variable is implicit, especially when it involves resolving temperature gradients. But since gradients in velocity and turbulent kinetic energy are also equally important in determining the flow temperature and heat transfer coefficient, including these variables for mesh adaption makes sense. However, combination of a number of adaption variables need not perform better than the case with a single adaption variable. This was verified by running a case where more than 5 variables were chosen but the mesh refinement after adaption was not better than case where ‘temperature alone’ or combination of ‘temperature and TKE’ were used as adaption variables. In the next section, the effect of adaption inside the film cooling hole will be examined.

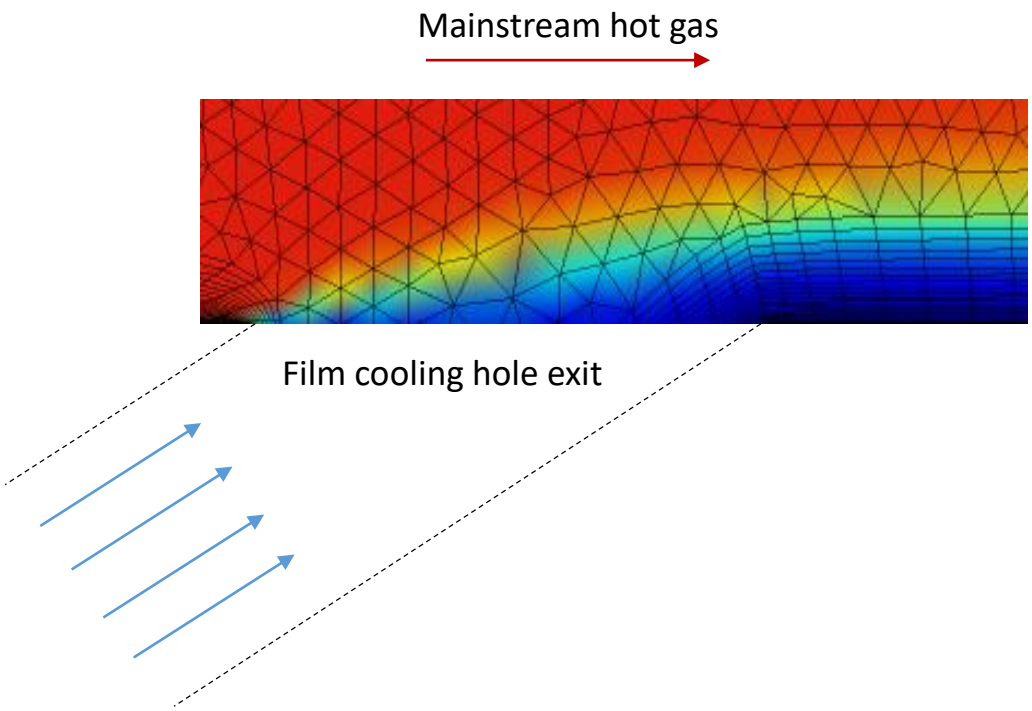

a)

	Temperature distribution near coolant hole exit	Adaption variable
b)	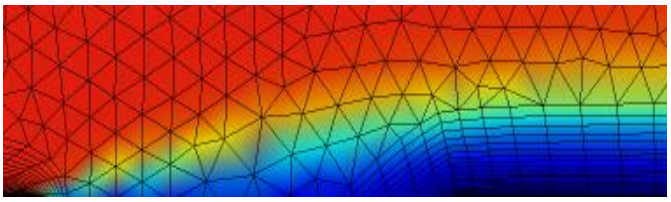	None
c)	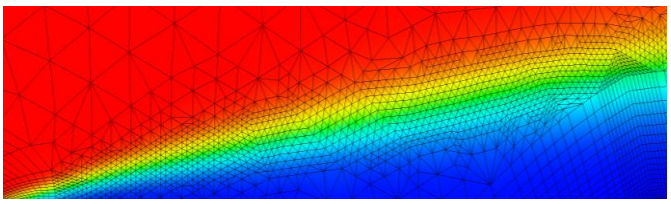	Tempearture
d)	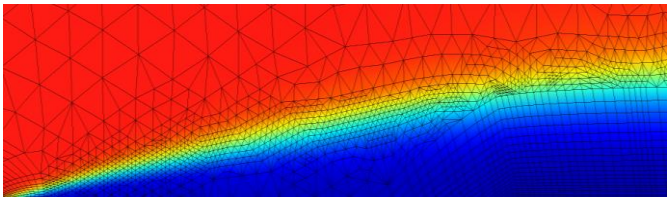	Vorticity

e)

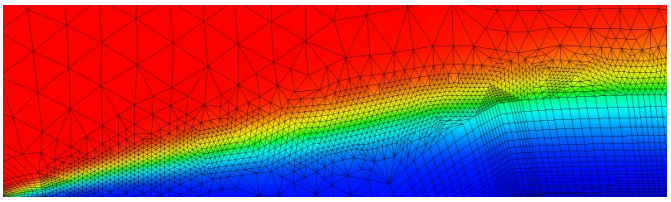

Vorticity and Temperature

f)

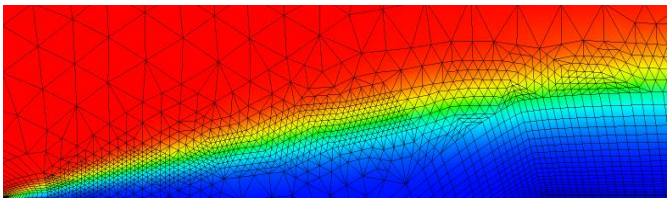

Temperature and TKE

Figure 40 Effect of adaption on hot gas – coolant mixing

5.2.4 Effect on turbulent kinetic energy inside coolant hole

Figure 41 shows the meshed contour of turbulent kinetic energy inside the film cooling hole and the effects of mesh adaption. The apparent turbulent kinetic energy generated by the turning coolant seems to be under predicted except when TKE is also adapted. Significance of this region and the role of turbulence has been discussed in the earlier studies. A detailed analysis on the amount of turbulence produced or the thickness of the mixing layer will not be discussed. The focus here is quick implementation of the mesh adaption technique to successfully capture large gradients in the solution which otherwise could not be resolved satisfactorily. Successful implementation of this mesh adaption technique by evaluating permutation/combinations of the critical variables and other relevant factors, can itself result in a miniature thesis. On that note, key variables like velocity, velocity components, shear stress, turbulent energy dissipation rate, specific dissipation, etc. can be examined. But as mentioned above, the overall objective of the numerical analysis was to make sure that complicated flow features present in film cooling does not suffer due to a mesh that is fine enough to result in solution independent of the grid but not capable of resolving critical gradients in the flow, without making the simulation computationally expensive. From that perspective, the combination of temperature and TKE serves our interest in the best way. However, one important parameter that is not presented here is the flow velocity. Regions inside the film cooling do observe large gradients and mesh adaption based on velocity certainly refines this region. Similar to vorticity, its effect on the surface effectiveness was however lackluster. But the combination of

temperature and velocity definitely resolved this region as well. In spite of this, it was decided to proceed with temperature and TKE since appreciable difference in film cooling performance was not noted between these two cases.

None

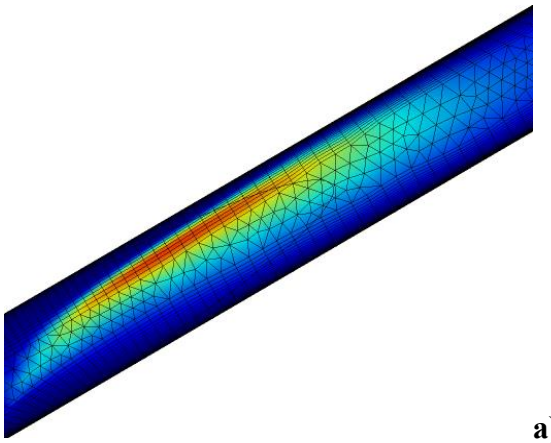

a)

Temperature

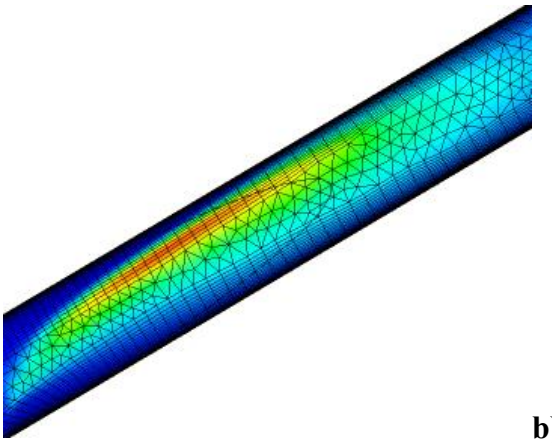

b)

Vorticity

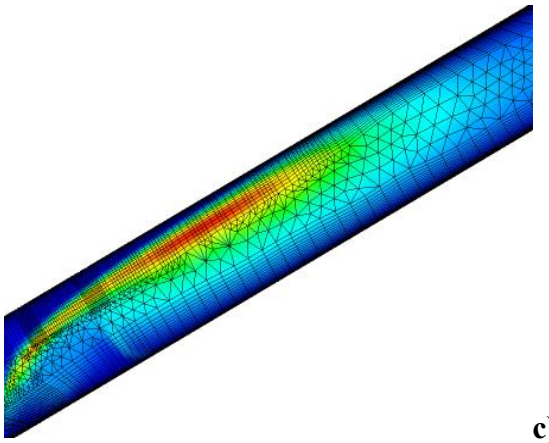

c)

Temperature and Vorticity

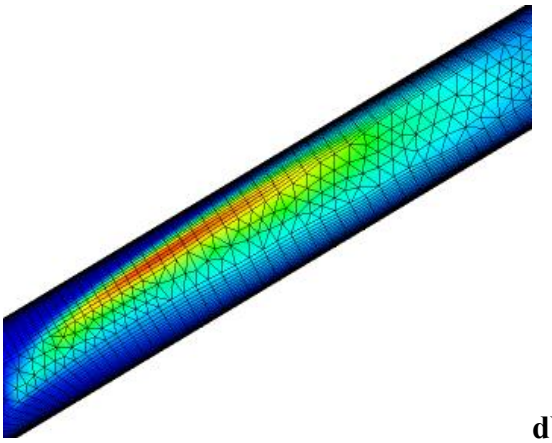

d)

Temperature and TKE

TKE

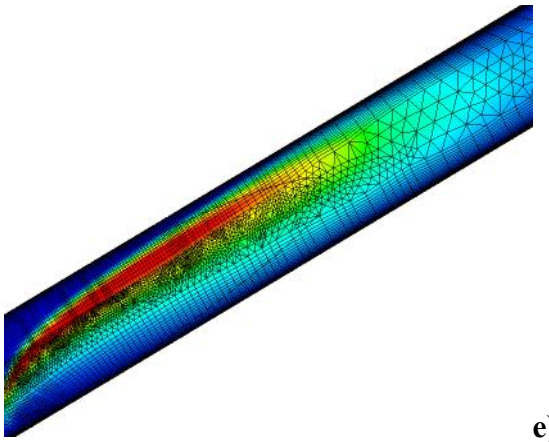

e)

Figure 41 Effect of adaption on turbulent kinetic energy inside the film cooling hole

5.3 Results and discussion

The following section will focus on the key results related to the performance of film cooling holes. Adiabatic effectiveness at various blowing ratios are compared for CY and AV. Later, the counter rotating vortices causing lift off coolant jet exiting the cylindrical hole and the effect of tripod hole's anti-kidney vortices will be discussed. As mentioned before, the current tripod hole has a branching angle of 15°. The effect of this branching angle on anti-kidney vortex pair with constant l/d and constant p/d will be discussed.

5.3.1 Comparison of film cooling performance of various hole shapes

A summary of the numerical analysis of performance of CY and AV is presented in Figure 42 and Figure 43. Variation of laterally averaged effectiveness with downstream location at different blowing ratios can be observed in Figure 42. As observed in the experiments, AV holes clearly outperform the CY holes at all blowing ratios. The significance of studying AV holes however lies in the CY hole effectiveness at very high blowing ratios. The high momentum flux ratio causes the coolant jet exiting the cylindrical hole to lift off from the surface. This phenomenon can be observed by the sudden dip in effectiveness in the region $1 < x/d < 5$. The fact that the AV holes also possess cylindrical hole exits, results in a similar jet lift off behavior at higher blowing ratios. The effect, however, is not as significant as what was observed in case of the cylindrical hole. The reason for higher effectiveness in spite of jet lift off is the reduced exit momentum owing to branching of the coolant into the individual holes of the tripod unit. The effect of anti-vortex hole cannot be felt in

this region. The effect of CRVPs and anti-kidney vortices is explained in the next section. Figure 43 shows adiabatic effectiveness contours for cylindrical and tripod hole at different blowing ratios. The effect of blowing ratio on effectiveness of a cylindrical hole, seen in the experimental result, was predicted in the numerical simulations as well. With the increase in blowing ratio, the adiabatic effectiveness close to the cooling hole exit decreases. As explained in the literature, the low effectiveness is attributed to the jet lift off owing to the high exit momentum flux ratio at BR 1.5 and 2.0.

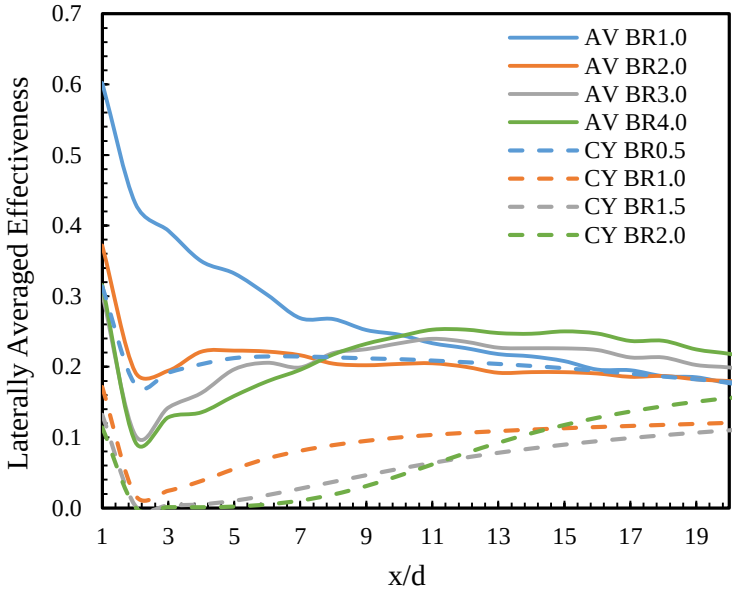

Figure 42 Numerically predicted laterally averaged effectiveness for CY and AV holes at different blowing ratios

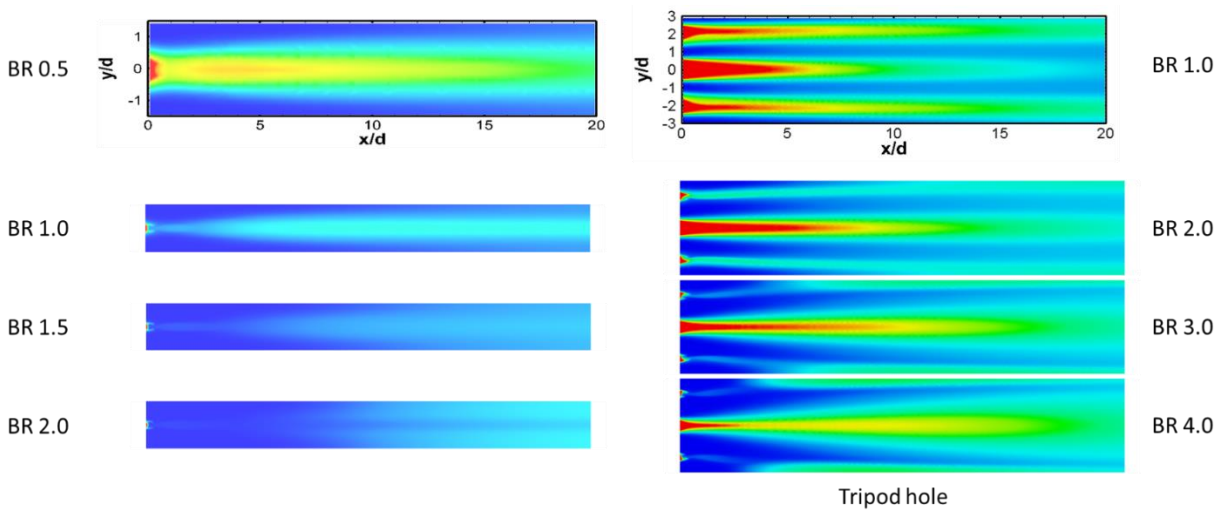

Figure 43 Adiabatic effectiveness contours for cylindrical and tripod hole at different blowing ratios

Tripod hole on the other hand, was found to yield very high effectiveness even at the highest blowing ratio. The effect of blowing ratio on tripod hole effectiveness is not as pronounced as what was observed for the cylindrical hole. In fact, there seems to be a very little effect of blowing ratio on the film cooling performance of the tripod hole. Apart from having a lower exit momentum due to the coolant hole branching, the side holes of the tripod hole unit interact with the mainstream and the coolant jet from the central hole in a way such that the central hole does not lift off even at very high blowing ratios. Film cooling performance predicted by using the SST-KW model certainly shows higher adiabatic effectiveness than what was observed with the flat plate experiments. This trend has been observed by other researchers as well and is applicable even for the tripod holes. CFD simulations using RANS models have a tendency to under predict the lateral diffusion of the coolant jet. As a result, very high effectiveness can be seen even at far downstream locations.

5.3.2 Effect of CRVPs and anti-kidney vortex

Cylindrical holes are known for low effectiveness at higher blowing ratios. This is due to the jet lift off caused by the counter rotating vortex pairs, CRVPs in short. Figure 44 shows normalized temperature contours of coolant jet as it moves downstream. It can be seen that the coolant jet grows in size, both vertically and in the spanwise direction, as it travels downstream of the hole. The spanwise spread of the coolant is a desirable feature as more turbine blade surface would be under

the cover of the coolant, thus protected from the hot gas exiting the combustor. The vertical penetration on the other hand, is an undesirable feature. The CRVPs, causing this lift off, not only causes the coolant jet to grow but also results in hot gas entrainment. This can be observed at BR 1.0 and above. At the highest BR, and at x/d = 11, the coolant jet thickness covers a distance of y/d = 3 (vertical) and z/d = 3 in the spanwise direction.

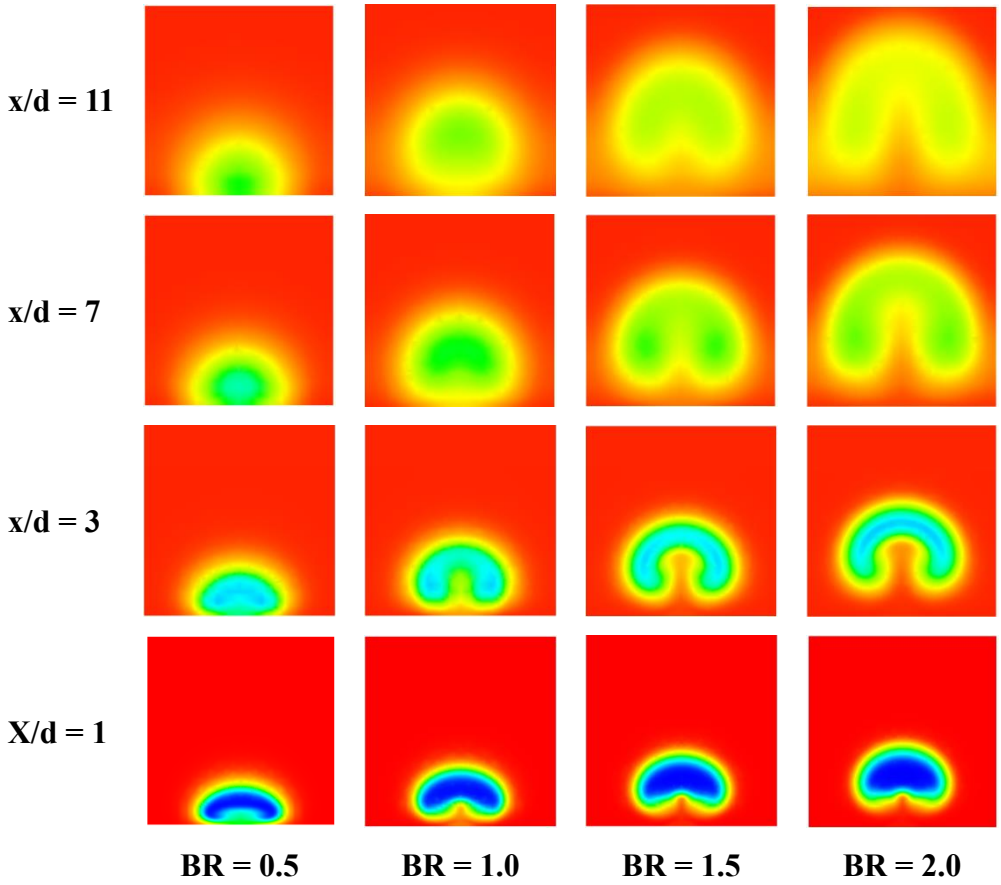

Figure 44 Contours showing effectiveness or normalized jet temperature to illustrate coolant jet penetration from a cylindrical hole at different blowing ratios

The tripod hole was originally designed to suppress the growth of the CRVP that were shown in Figure 44. Figure 45 shows similar normalized coolant jet temperature as it travels downstream. At the lowest blowing ratios, AV BR 1.0 and 2.0, which correspond to the coolant mass flow rate of CY BR 0.5 and BR 1.0, the coolant jet from the central hole does not seem to grow. The effect of the anti-kidney vortex from the side holes also does not seem to interact with the central hole until x/d = 7. In these conditions (low BR), the effect of the anti-kidney seems to be present farther

from the hole exit. At *x/d* =11, the growth of the central hole coolant jet seems to be restricted by the vortices from the side holes. Another important reason for this kind of behavior is the coolant getting branched, resulting in a lower exit momentum. A coolant jet with lower exit momentum will have the tendency to remain attached to the surface. This behavior was observed in the cylindrical holes as well. It is not surprising, as a result, that the film cooling performance of the tripod holes are better than the standard cylindrical holes. The combined effect of reduced blowing ratio at the hole exit and the anti-kidney vortices in the downstream region makes the tripod hole superior to the conventional cylindrical holes. But as mentioned above, it is at higher blowing ratios, where tripod hole completely outperforms the cylindrical hole. Figure 45 also shows coolant jet penetration at higher blowing ratios. The effect of anti-kidney vortex on the central hole CRVP is more apparent at *x/d* = 7 and farther, at BR 3.0 and 4.0. The central hole coolant jet spreads in the spanwise direction because of the suppression of the central hole jet due to the side hole vortices. This increases the coolant coverage and also causes the coolant to stay attached to the flat plate thereby increasing the laterally averaged adiabatic effectiveness.

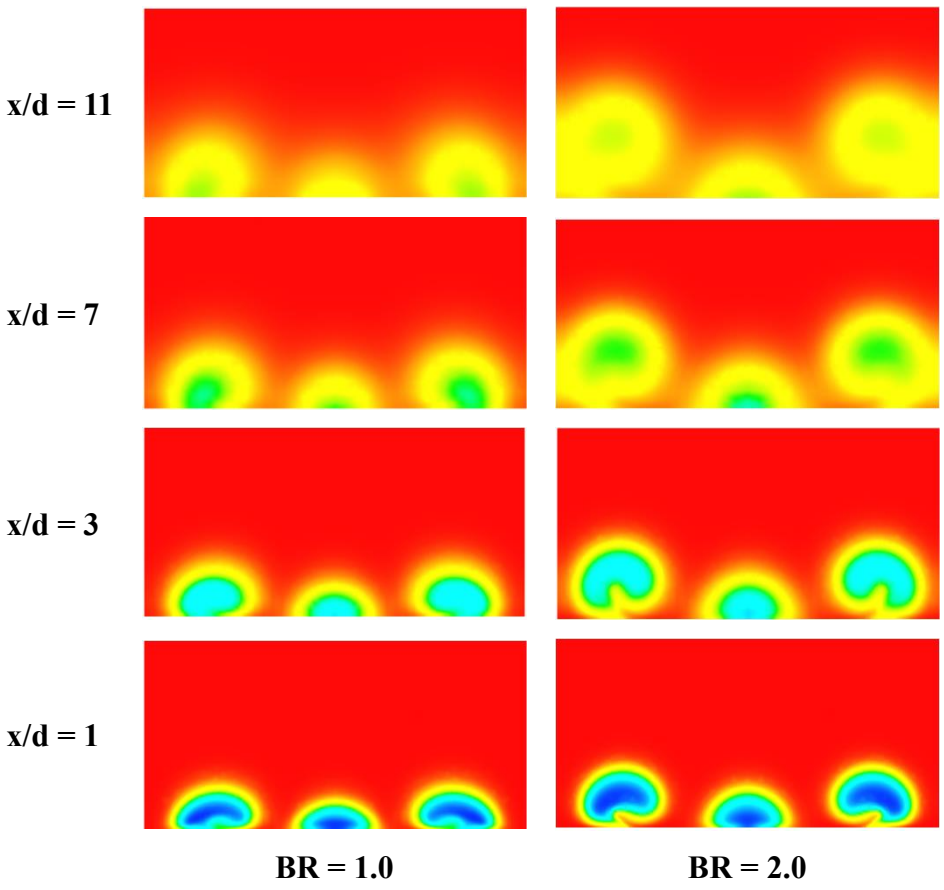

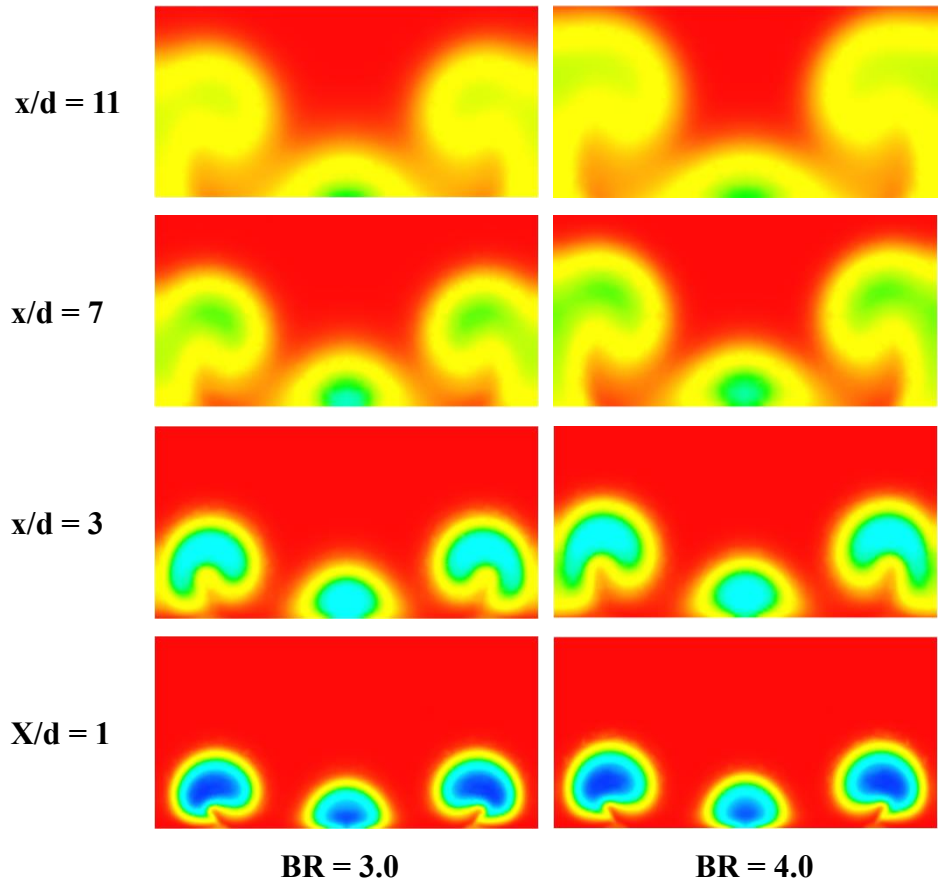

Figure 45 Contours showing effectiveness or normalized jet temperature to illustrate coolant jet penetration from a tripod hole at different blowing ratios

5.3.3 Effect of tripod hole branching angle on adiabatic effectiveness

The effect of branching angle on the performance of the tripod hole was studied via two different approaches. In the first study, the hole *l/d* was fixed at one value (= 8) while the branching angle was varied from 5° to 30° in steps of 2.5°. As a result, with increasing branching angle, the lateral spacing between the central hole and the side holes increased. This in turn weakens the interaction between the vortices generated by the coolant jet exiting the side holes and the central holes. It was expected that with increasing branching angle, the laterally averaged film cooling effectiveness would decrease (Figure 46). But interestingly, increasing the spacing between the central and side hole also increases the overall pitch of *p/d* of the tripod hole, i.e., *p/d* of AV30° > *p/d* of AV15°. As

a result, the blade or flat plate would have fewer AV30° holes as compared to AV15°. For the same blowing ratio, the total amount of coolant flow rate required to the cool the blade or flat plate would decrease with increasing branching angle.

In order to account for the coolant flow rate consumed, the laterally averaged effectiveness were normalized w.r.t. to coolant mass flow rate which in turn depends on the coolant mass flow rate per hole and pitch. Using same blowing for all branching angle cases ensures same coolant mass flow rate per hole, leaving the pitch or *p/d* to be the only varying factor. Figure 47 shows laterally averaged effectiveness times the pitch at different branching angles. Surprisingly, the AV30° whose actual effectiveness is considerably lower than the AV5° ends up providing better cooling for the amount of coolant consumed.

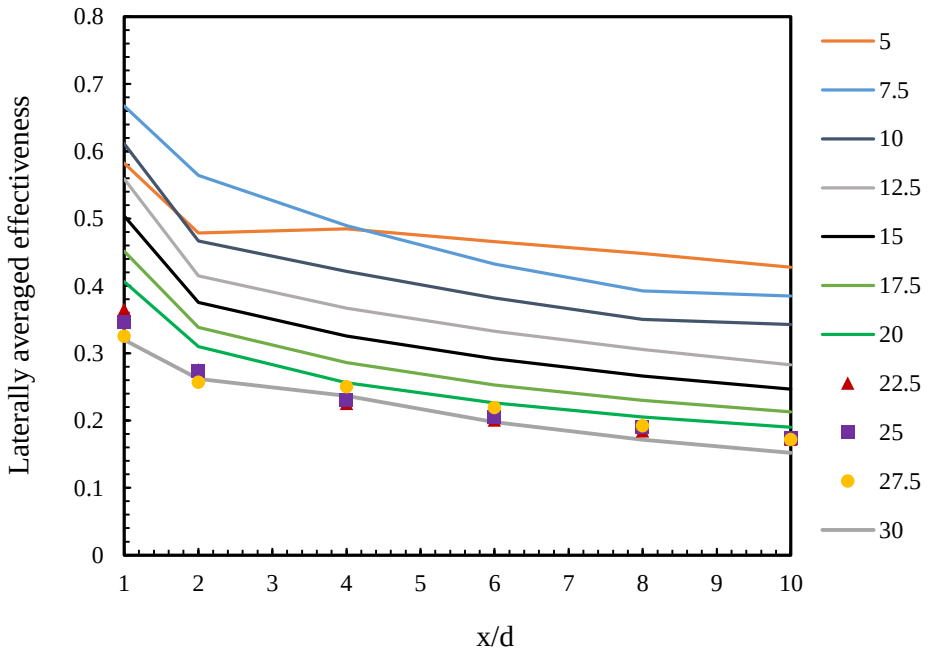

Figure 46 Effect of tripod hole branching angle on laterally averaged effectiveness

The trends observed in Figure 46 and Figure 47 may seem contradictory at first. AV5° is capable of delivering very high effectiveness but has a lower pitch that AV15° and AV30°. Though it is not consistent to compare owing to the difference in pitch, the ultimate objective of the gas turbine cooling is to maximize the effectiveness. The difference in performance arises purely from the pitch rather than the anti-kidney vortex effect. Even though the study does not achieve the intended

objective of optimizing the performance by varying the branching angle, it does throw light on the merits of having a smaller branching angle.

From the perspective of an actual gas turbine blade, it might be easier to accommodate a tripod film cooling hole with a smaller branching angle. For a given blade thickness, the AV30° will result in a large *p/d* which might be undesirable due to lower effectiveness. The AV30° can really shine in situations that put strict restrictions on coolant consumption. Low pressure turbine vanes and blades are not subjected to harsh environments unlike the first stage vanes and blades. As a result, these might require very little or no cooling at all. In these types of scenarios, the AV30° will be capable of delivery a higher performance.

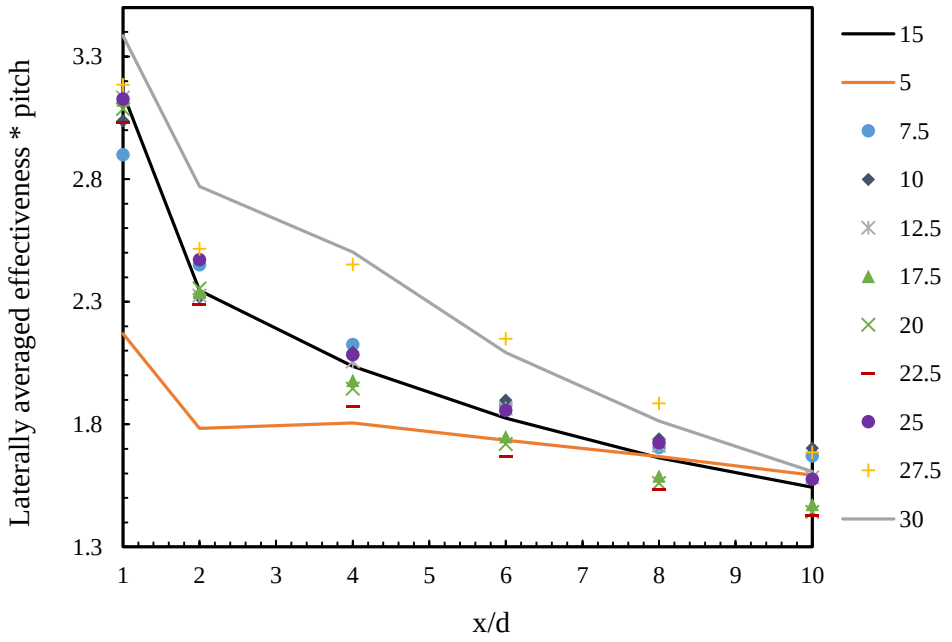

Figure 47 Effect of tripod hole branching angle on laterally averaged effectiveness normalized w.r.t. total coolant mass flow rate

In the second study, the spacing between the central hole and the side hole was kept constant (= 2*d*) while varying the branching angle. As a result, the hole length or *l/d* had to vary between tripod holes with different branching angle. Four different angles were chosen for this particular study. The hole length or *l/d* corresponding to the branching angles 15°, 20°, 25°, and 30° were 8.33, 6.36, 5.16 and 4.33 respectively. The focus was on studying the effect of side hole compound angle and

its effect of the central hole performance. From Figure 48 we can observe that increasing the branching angle lowered the laterally averaged effectiveness.

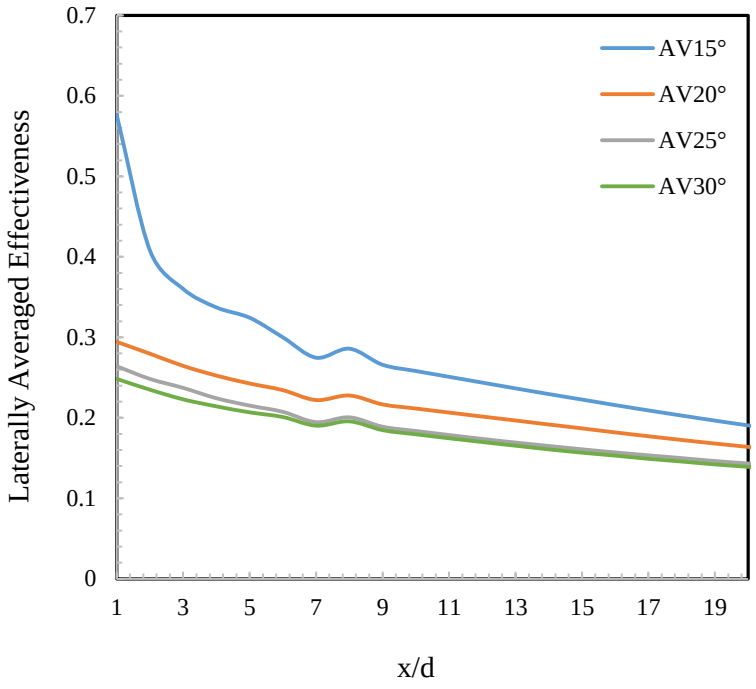

Figure 48 Effect of side hole compound angle on laterally averaged effectiveness at BR 1.0

5.3.4 Comparison with Experimental Data

Numerical results obtained for CY and AV15° with the mesh adaption technique are compared against the experimental data discussed in Chapter 1. Figure 49 and Figure 50 compares laterally averaged effectiveness vs. normalized downstream distance x/d at different blowing ratio for CY and AV15° respectively. Excellent match was observed for the cylindrical hole at BR 1.0 and 2.0. The trend at the lowest blowing was captured until x/d = 3 beyond which the SST KW model over predicted the effectiveness. Stratton and Shih [40] have reported a similar behavior in the performance of SST KW to over predict laterally averaged effectiveness at lower blowing ratios. They mentioned that SST KW model could not predict the swirling present inside the hole and in cases where the swirl inside the hole is considerably smaller compared to other components of velocity, as in the case of higher blowing ratios, the error becomes negligible.

Excellent match at higher blowing ratios is more important since the tripod hole is proposed as an alternative that can address the lingering problems of the cylindrical hole at those high blowing

ratios. Since the SSTKW model had shown to over predict cooling at lower blowing ratios (BR1.0), mismatch observed in Figure 50 was expected. Again, excellent match at BR 1.0, similar to the CY, showed promise for the turbulence model used. Surprisingly, at BR 4.0, the numerical simulation predicted a jet lift off near $x/d = 3$. This can be observed by the drastic dip in the laterally averaged effectiveness plot in Figure 50a. This drastic difference in effectiveness was quite unexpected even though there seems to be almost perfect overlap past 11d. The blowing ratio at the exit of each hole of the tripod hole is little over 1, 1.33 to be accurate. In these conditions, the coolant exiting the cylindrical holes have shown the tendency of lift off the flat plate and reattach at a later point. The flat plate experimental results discussed in Chapter 2 did show certain lift off and it lies around the same region $2 < x/d < 3$. The reasons for this behavior are unknown at this point and needs to be studied further. RANS turbulence models have always been criticized for the isotropic eddy viscosity assumption and it's under prediction of jet diffusion. As a result, it might be possible that while the laterally averaged values measured and predicted are closer, the effectiveness contours could still be appreciably different.

Figure 49b and Figure 50b display the same comparison between experimental and numerical results but also include experimental uncertainty as error bars. This bridges the gap between the two and assures the usage of the turbulence model at higher blowing ratios.

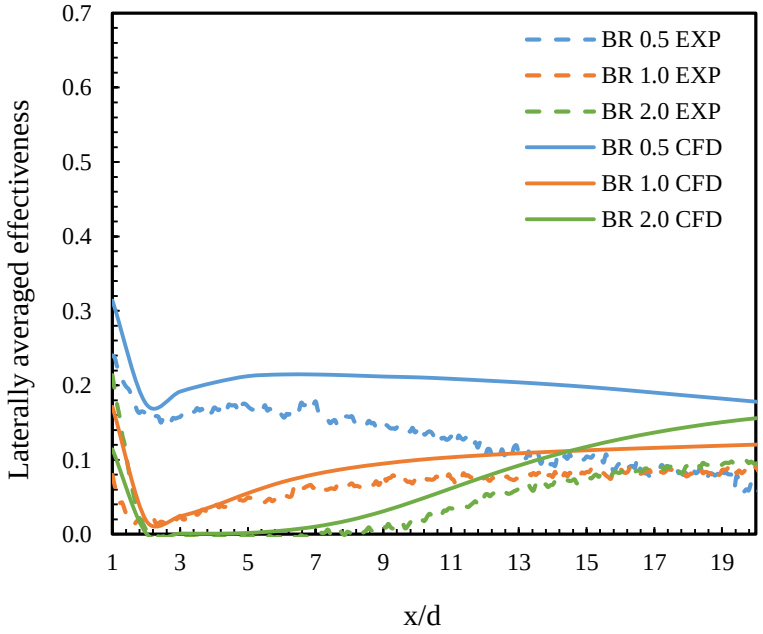

a)

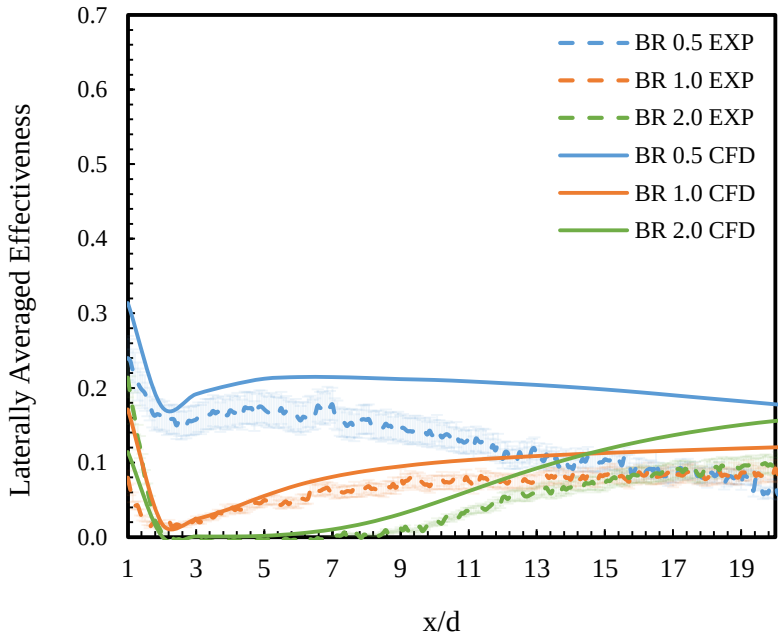

b)

Figure 49 Cylindrical hole laterally averaged effectiveness comparison at different blowing ratios: a) CFD vs Exp.; b) CFD vs Exp. with uncertainty

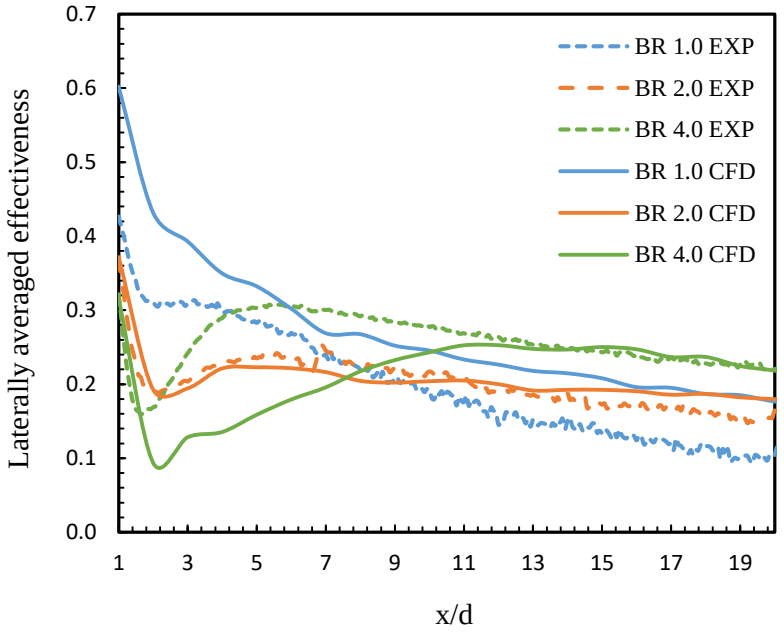

a)

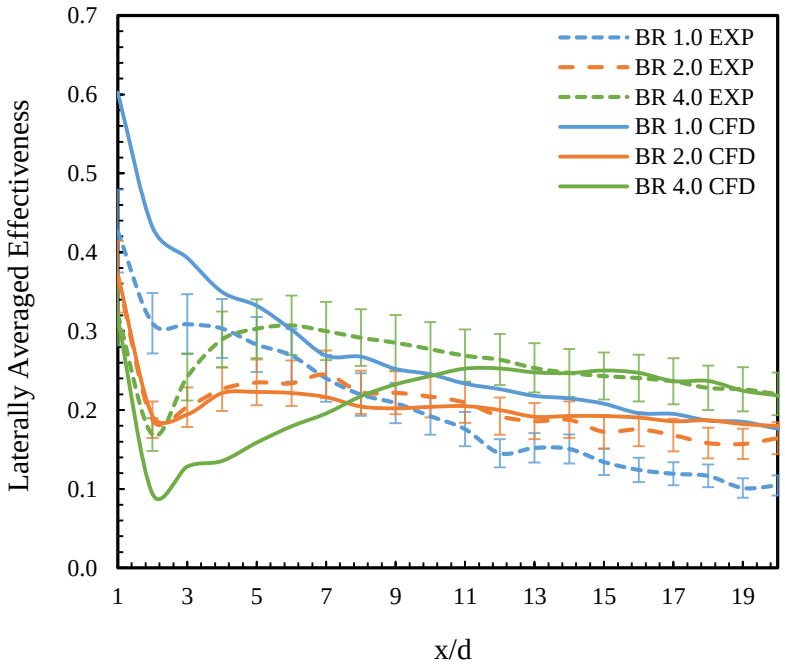

b)

Figure 50 Tripod hole laterally averaged effectiveness comparison at different blowing ratio: a) CFD vs Exp.; b) CFD vs Exp. with uncertainty

5.3.5 Effect of hole pitch on cylindrical hole effectiveness and comparison with tripod hole

It is known that the CY pitch or *p/d* is half of that of the AV hole. For every AV hole, there will be two cylindrical holes on the flat plate. But since the AV hole consists of 3 individual holes (tripod), the superior performance of the AV hole compared to the CY hole cannot be solely attributed to the anti-vortex concept. The additional holes present in the tripod unit, causes a difference in exit blowing or momentum flux ratio. The anti-vortex concept and the reduced exit momentum ratio are responsible for higher effectiveness of the AV hole. This has be adequately discussed in this Chapter. This section attempts to compare the AV tripod hole with a cylindrical hole whose pitch is 2d. This reduced pitch causes the flat plate to have same number of CY hole as the holes in the tripod unit. Figure 51 compares the laterally averaged effectiveness for these two cases. Except at the lowest blowing ratio, AV hole provides better performance until $1 < x/d < 7$. At the highest blowing ratios, cylindrical hole with p/d=2 produces very low effectiveness near the hole exit due to jet lift off.

Beyond this region, the AV hole does not provide any benefit. Interestingly, the CY hole with the reduced pitch results in a better cooling in the far downstream region.

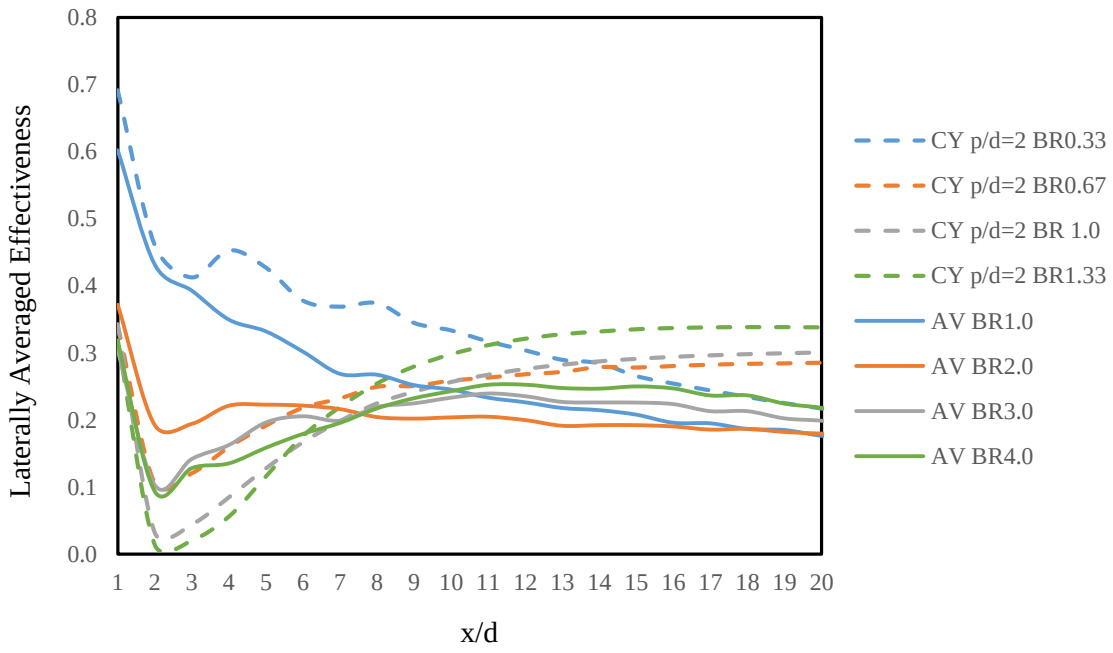

Figure 51 Comparison of laterally averaged effectiveness for AV and CY with p/d=2

CHAPTER 6

NUMERICAL ANALYSIS OF TRIPOD HOLE FILM COOLING AT ENGINE LIKE CONDITIONS

6.1 Preliminary Work

The results described in this chapter have been collected from a high temperature and high pressure test facility at the National Energy Technology Laboratory (NETL). This facility was originally designed to conduct combustion related studies, so the natural gas premixer and swirl vane assembly is similar to a commercial gas turbine premixer. The hot gas flow path transitions from a circular cross-section to a rectangular duct. Flat plate test articles are instrumented and positioned downstream of the combustor section and flush with the walls of the rectangular duct. These test samples are subjected to a swirling, highly turbulent flow field at temperatures of 1450K and pressures from 1 - 5 bar. By conducting tests at high temperature conditions, it is possible to directly measure overall effectiveness, φ, and the heat flux reduction. Results will be presented for two different test specimens. The first test specimen is a flat-plate with no cooling holes. This test specimen is subjected to the same cooling air flow conditions on the back-side, but the coolant flow does not effuse through the test specimen surface. The second test specimen is a flat-plate with eight cylindrical cooling holes drilled at a 30° angle to the surface in the streamwise direction. Additional details on the test specimens will be provided in the next section. Both of these test samples will provide the basis from which future results from the anti-vortex, or tripod cooling geometries can be compared.

For the computational analysis, ANSYS CFX 14.5 was used to perform all numerical simulations. RANS models are most commonly used as they are cost effective [4]. There are also studies which usually compare different turbulence models. One such study by Harrison et al. [38] predicted film cooling performance under different turbulence models: Realizable k-ε, standard k-ω and Reynolds Stress Model turbulence model. They found that RKE model predicted centerline effectiveness while SKW model yielded better laterally averaged adiabatic effectiveness, concluding that choice of any turbulence model would depend upon the application under examination. Sidwell et al. [56] conducted a conjugate heat transfer model simulation study for this

particular test section. After an extensive study where different meshes, discretization schemes and turbulence models were evaluated, it was concluded that the SST k-ω turbulence model can be used to adequately predict heat transfer in film cooling. For this study, Shear Stress Transport (SST) k-ω model was chosen for turbulence closure. In general, the objective was to develop a numerical model that can replace these experiments and still provide a reasonable estimate for the overall effectiveness. There are three benefits associated with numerical modeling. First, the cost involved in manufacturing these Haynes 230 test specimens is high. Secondly, with an acceptable numerical model, it is easier to estimate the film cooling performance of complex film cooling hole geometries which are usually difficult to manufacture. Finally, the thermo-mechanical analysis of a film cooling hole becomes simpler.

6.1.1 Experimental and Numerical setup

As mentioned above, conjugate film cooling experiments at engine like conditions were carried out at the NETL test facility in Morgantown. A comprehensive description of the experimental test setup and the film cooling results obtained can be found here [56]–[58]. The following section will focus on the conjugate heat transfer numerical modelling work carried out at Virginia Tech.

The design model for conjugate heat transfer simulation shown in Figure 52 comprises of fluid and solid domains.

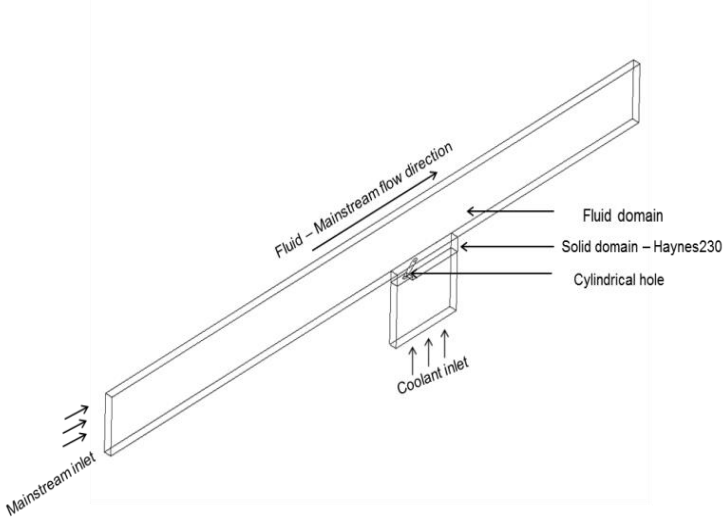

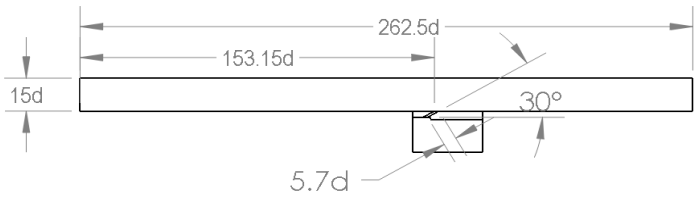

Figure 52 CFX Design Model

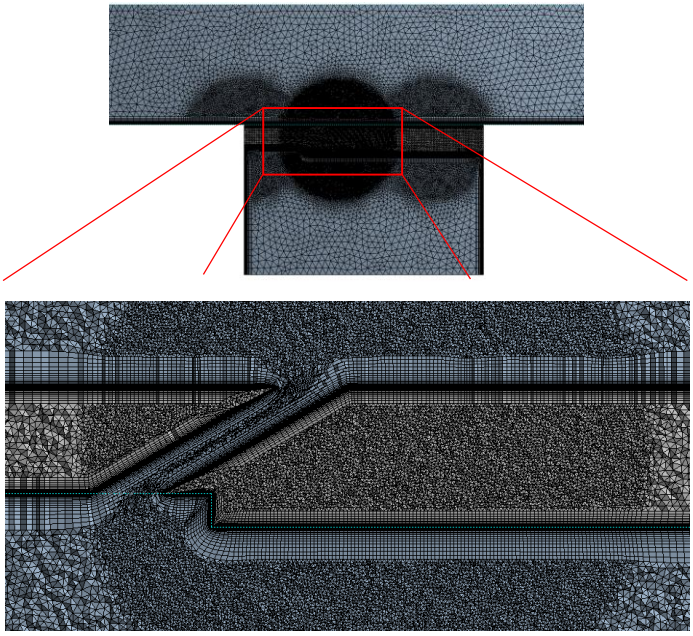

Figure 53 Unstructured Tetrahedral Mesh with Inflation Layers

Mainstream gas and coolant constitute the fluid part where air, treated as an ideal gas, is used. The solid domain is made of Haynes230 alloy material. This design focuses on the performance of a single cylindrical film cooling hole and hence the width of both domains is the same as the pitch (= 3d). As mentioned in the experimental section, cylindrical holes of l/d = 5.7 are inclined 30° to the surface in the streamwise direction. Mainstream inlet is located roughly 153 hole diameters (~0.260 m) upstream from the leading edge of the hole so that the velocity boundary layer developed will be representative of the one calculated for the experiments. The boundary layer development distance was estimated to be around 0.244 m. Other details are presented in Figure 52.

Both these domains are meshed with unstructured tetrahedrons using patch conforming method, which results ~5 million elements. In Figure 53, near the film cooling holes, mesh is refined further in an attempt to capture coolant jet-mainstream interaction. To resolve the boundary layer, inflation layers are added on both domains. Addition of inflation layers replaces default tetrahedrons with hexahedral elements that align in the flow direction. RANS equations were solved with SST model providing closure for turbulence. Also the y+ value was kept ~1 since shear stress model would tend to behave like k-omega turbulence scheme in those regions.

Table 6: Design Data for Computation

Parameter	Input
Hole: CY	d – 1.7 mm; l/d – 5.7; p/d – 3
Boundary condition: mainstream inlet	Fluid: air (ideal gas); Velocity = 71 m/s; Temperature = 1175 °C; Tu = 20%; Fluid: air (ideal gas)
Boundary condition: plenum inlet	CY: M = 0.5, 1.0 and 1.5; Temperature = 260°C; Tu = 5%
Boundary condition: outlet	Pressure – atmospheric pressure
Material	Haynes 230 alloy

During the experiment, the hot combustion gases enter the inlet at 1175 °C with a velocity of 65 m/s. However, simulations were conducted prior to the experiments and an estimated velocity of 71 m/s was used at the mainstream inlet. A turbulence intensity of 20 %, which was estimated from the experiments, was used in the computation. The length scale was determined using the hydraulic diameter of the test section. Coolant is injected at 260 °C and its mass flow rate is varied in accordance with blowing ratio. Turbulence intensity levels in the coolant were assumed to be around 5 %. In order to avoid the effect of boundary layer formation in the mainstream, the top wall was also prescribed a velocity in the streamwise direction with the same magnitude as the inlet velocity. A summary of details can be found in Table 5. Periodic boundary conditions were used on all side walls, including the solid domain as well. The biggest challenge in modeling was the solid domain. As mentioned above, the coupons are constrained in one direction by a compressive load. Upon close observation of the surface temperature distribution shown in Figure 55, we can note

that the average temperature on all borders is around 900 K, with certain exceptions which are discussed later. Hence in the current CFD model, these walls were held at a constant temperature of 900 K. All the cases were run until the required convergence was achieved. For the mass and momentum equations, RMS residual value was set to $1e^{-6}$ and $5e^{-6}$ for the energy equation.

6.1.2 Results

The test conditions that have been investigated are summarized in Table 7. The blowing ratio is not a well-defined quantity for the test specimen without film cooling. So, the blowing ratio is defined for the film-cooled test specimen and the test specimen without film cooling is exposed to the same cooling air flow rate. Therefore, the test specimen without film cooling receives convective cooling on the cold-side that should be the same as the film cooled test specimen.

Table 7: Summary of Test Conditions

Hot Gas Temperature (C)	Bulk Gas Velocity (m/s)	Density Ratio	Operating Pressure (bar)	Blowing Ratio
1175	65	2.8	3	0.5
1175	65	2.8	3	1.0
1175	65	2.8	3	1.5
1175	65	2.8	3	2.0

Figure 54 shows line averaged (spanwise) overall effectiveness measurements for the film cooled test specimen at an operating pressure of 3 bar. Local thermocouple values are also plotted as individual points. The cooling effectiveness over this area of the surface is reasonably smooth or has subtle gradients at low blowing ratio conditions and variations increase as the blowing ratio increases. The experimental results: surface temperature and overall effectiveness of the cylindrical hole and blank coupon at different blowing ratios are shown in Figure 55a and Figure 55b. The surface temperature of the blank coupon appears to be lower than the coupon with the cylindrical film cooling holes. It must be noted that the coolant plenum is located beneath the blank coupon and at BR 0.5 and 1.0, corresponding coolant mass flow rates are supplied to the coolant plenum. Since the coolant cannot flow through the holes in the case of the blank coupon, it enters the plenum and exits through a port that is connected to the hot gas path at a farther downstream location.

Essentially, the coolant plenum acts a heat sink in the case of the blank coupon and cylindrical hole coupon apart from the heat losses that occur due to conduction and radiation. This explains the lower temperature for the blank coupon. The test rig design shows that coolant is supplied to the plenum through four small tubes whose exit is located 6 in away from the coupon. The coolant mass flow rate though small, behaves like an impingement jet in the case of the blank coupon. In the case of the cylindrical hole, the coolant flow path inside the plenum is dictated by the hole inlet location. Close to the coupon surface, coolant flow is redirected towards the hole. Though the plenum acts as a heat sink, the actual behavior of the coolant inside the plenum in the case of a blank coupon and a cylindrical coupon will not be similar.

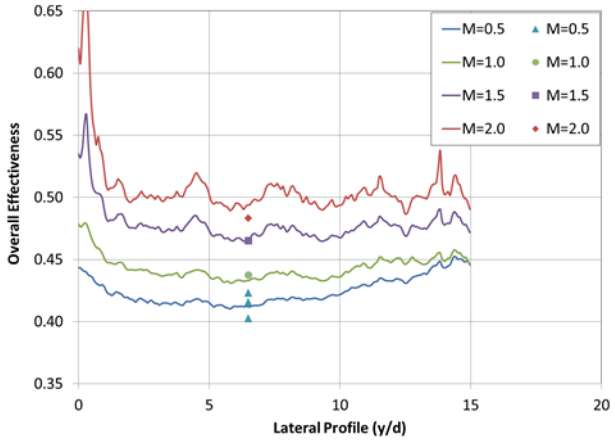

Figure 54 Variation in overall effectiveness along the spanwise direction at different blowing ratios

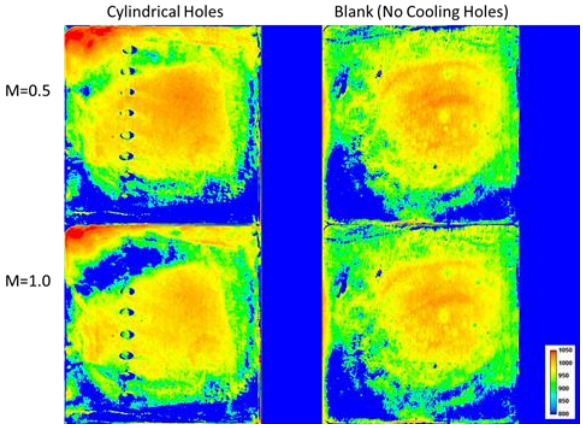

a)

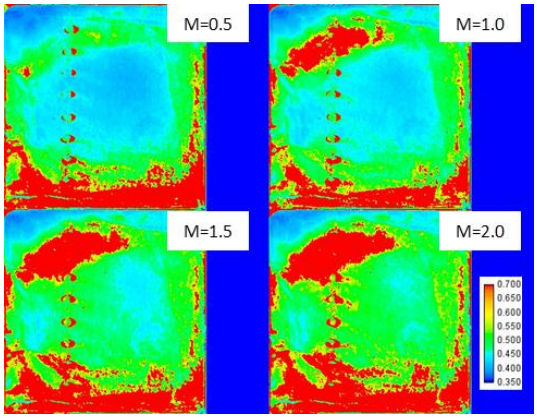

b)

Figure 55 Experimental results from NETL: a) surface temperature distribution for CY and Blank coupon; b) Effect of blowing ratio on overall effectiveness of CY coupon

Figure 56 presents surface temperature distribution for the cylindrical hole coupon at different blowing ratios. For comparison the experimental results for the corresponding blowing ratios are also provided. Conjugate heat transfer CFD results indicate that the effect of cooling is more pronounced and uniform for the lowest blowing ratio of M=0.5 as compared to M=1.5. The experimental results, on the contrary, showed an opposite trend, indicating lower surface temperatures at higher blowing ratios. Figure 57 provides a side-by-side comparison for the laterally averaged surface temperatures. Only for a blowing ratio of 1.0 there seems to be a reasonable agreement between experimental and numerical results. It must be remembered that the velocity profile at the inlet of the experimental test section and numerical test section are quite different. The swirled vane combustor assembly present before the aero-thermal experimental test section wasn't modeled in the CFD.

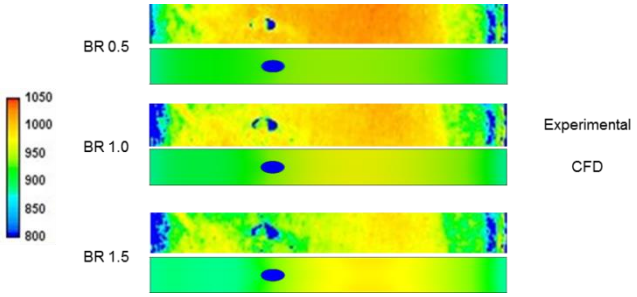

Figure 56: Overall effectiveness contours at different blowing ratios

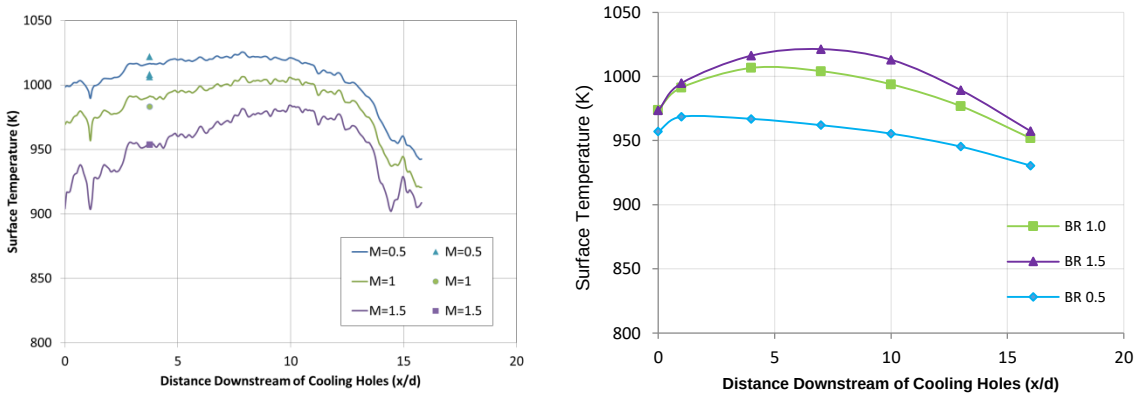

Figure 57 Effect of blowing ratio on laterally average surface temperature: a) Experimental and b) CFD results

6.1.3 Conclusive remarks: Reasons for mismatch

It was experimentally observed that as more coolant was pushed through the holes, the surface temperature of the coupon decreased, contrasting to the expected behavior and with the experimental results discussed in Chapter 1. Cylindrical hole performance peaks at blowing ratios 0.5 - 0.8. Further increase in blowing ratio or coolant mass flow causes the jet to lift off resulting in lower adiabatic effectiveness. This jet lift off was quantified using the momentum flux ratio in the review paper [4]. At lower coolant flow rates, effectiveness scales with blowing ratio while at higher flow rates, scales with momentum flux ratio [59]. The density ratio for these film cooling experiments were considerably higher than those at lab conditions (DR ~ 1.0 - 1.2) or even at engine conditions (DR ~ 1.8 - 2.0). Typical density ratio at the NETL test facility is around 3.8. The low exit momentum ratio being should able to keep the coolant attached to the surface even at blowing ratios as high as 2.0. The plausible reason for the unexpected trend in the effectiveness could arise from two sources:

a) Mainstream turbulent intensity of 20 % which is significantly higher than expected. Even high turbulence levels in mainstream results in an intensity of 10%. Higher freestream turbulence has the tendency to disrupt the coolant jet at lower blowing ratios. At higher blowing ratios, however, the coolant jet is probably able to withstand the turbulent mixing from the mainstream.

b) Other modes of heat transfer: conduction losses to the coupon holder and radiation from the surrounding refractory walls. The coupon surface temperature now is a resultant of combined heat transfer mechanism occurring inside the test rig. Figure 58 shows the effect of these heat transfer modes on a blank coupon. The radiating refractory walls also contribute to the heat input apart from the convective combustor exhaust gas. Conduction losses are inevitable as the coupon is made of Haynes230 alloy, a nickel based super alloy, with a thermal conductivity of ~ 20 W/m-K at 1000K. The coupon holder system is made of stainless steel, another high thermal conductivity material. The viewport on either side of the coupon, that captures the surface temperature through a CCD camera fitted with a band pass filter, is constantly cooled to a temperature < 600K. As a result, the refractory walls and coupon surface emit radiation to the hot side and cold side viewport windows.

Owing to these two reasons, the mismatch in overall effectiveness obtained from numerical simulations and experimental results could be understood. It should be noted that the numerical model used does not include radiation heat flux or accurately capture the conduction losses.

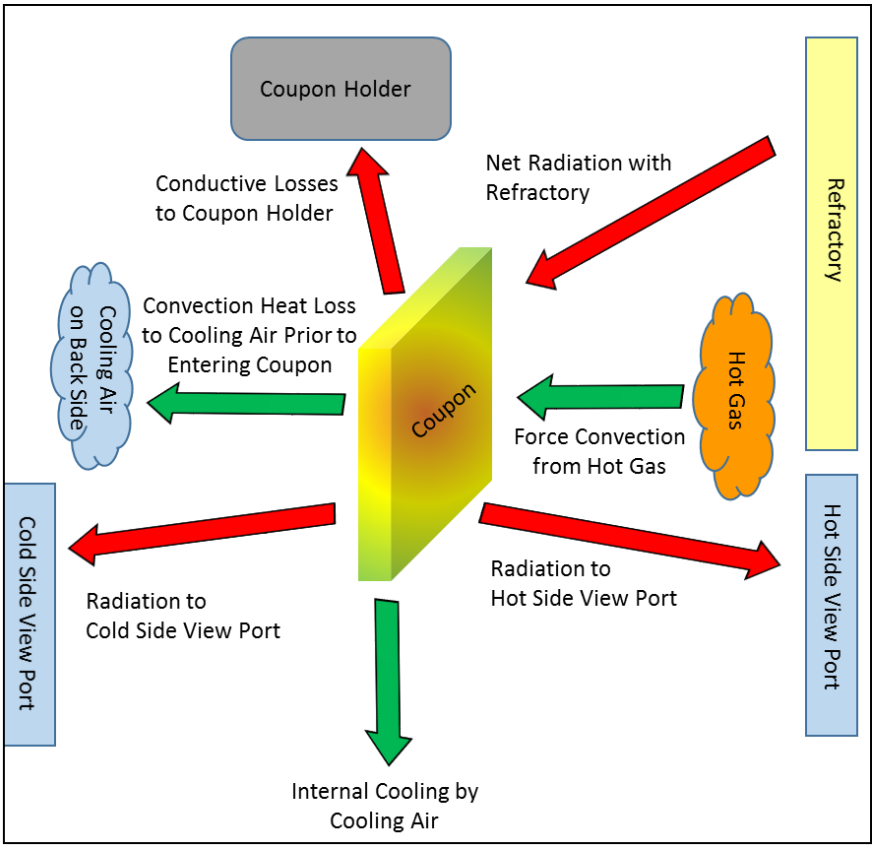

Figure 58 Various heat fluxes entering and leaving the film cooling coupon

6.2 Experimental Methodology

The experimental methodology used to evaluate film cooling performance at engine like condition is revisited here. The surface temperature obtained from the CCD camera is normalized with respect to the hot gas temperature and coolant temperature. The details of the experimental test facility can be found in these papers [56]–[58]. The coupon surface temperature either by the CCD camera with filter or with the help of the embedded thermocouple, is a resultant of the incoming radiation heat transfer and conduction losses apart from the film cooling process. The normalized film cooled coupon surface temperature will provide the overall effectiveness instead of adiabatic effectiveness which is usually reported in film cooling studies. Since the film cooled coupons do not sport any internal cooling features, backside cooling cannot be quantified accurately as it varies with coolant mass flow rate as well. Typical experimental studies involving measurement of overall effectiveness, maintain Bi similar to the engine conditions. The heat transfer coefficient on the backside of the coupon does not represent the internals of the turbine blade. Since the objective of this study is only to evaluate film cooling hole shapes, overall effectiveness is not the best parameter to compare the performance. Needless to say that the temperature of the coupon is affected by radiation heat fluxes as well. The equations used so far to obtain film cooling performance are given below:

Coupon (center) effectiveness, $\varphi = \frac{T_m - T_w}{T_m - T_{c,internal}}$ (6.1)

Heat transfer, $q = kA\frac{T_{c1} - T_{c3}}{dx}$ (6.2)

Overall heat transfer coefficient, $q^{"} = H(T_m - T_w)$ (6.3)

$H \ni \{h_{convection}, h_{radiation}\}$ (6.4)

$q_f^{"} = h_f\left(T_f - T_{w2}\right)$ (6.5)

$\mathrm{q_0^{"}} = \mathrm{h_0(T_m - T_{w1})}$ (6.6)

Net heat flux reduction, $\frac{\Delta q^{"}}{q_0^{"}} = 1 - \frac{h_f}{h_0}\left(1 - \frac{\eta}{\varphi}\right)$ (6.7)

As mentioned above, in order to evaluate the film cooling performance of the coupons, an energy balance equation involving all possible heat transfer mechanism is developed. The equations given below is the summation of net heat entering and leaving the film cooled coupon.

$$h_f A_w \left(\mathrm{T}_\infty - \eta(\mathrm{T}_\infty - \mathrm{T}_{c,\,exit}) - T_w\right) = \sigma\varepsilon_w A_w F_{w\to v}(T_w^4 - T_v^4) + \sigma\varepsilon_w A_w F_{w\to p}\left(T_w^4 - T_p^4\right) +$$

$$\dot{m}C\left(T_{c,exit} - T_{c,inlet}\right) + \sum kA_i \frac{dT}{dx} + Q_{h,naturalconv} - \sigma\varepsilon_r A_r F_{r\to w}(T_r^4 - T_w^4) \qquad (6.8)$$

where f = film; c = coolant; w = wall / coupon surface; v = viewport; p = plenum; coolant; r = refractory; h = convection; ∞ = mainstream

Owing to the nature of the experiments, only certain quantities and parameters are known a priori. These include: T_∞ $T_{c,\,inlet}$ K A_i A_c A_r m C_p σ. The unknown variables or quantities with limited information include: ε_c ε_r $F_{c\to v}$ $F_{c\to p}$ $T_{c,\,exit}$ dT/dx T_r and T_v. The above energy balance equation is solved for h_f and η. Since we have a one equation and two variables to solve, two separate experiments have been conducted such that the heat transfer coefficient and adiabatic effectiveness remain the same between the experiments. This requires the blowing ratio and density ratio to remain the same for these two experiments. Additionally, radiation heat transfer and conduction losses that are difficult to measure experimentally, had to be modelled using a conjugate heat transfer CFD analysis that also models radiation.

6.3 Conjugate CFD with radiation modelling

The numerical design shown in Figure 59 includes only the aero-thermal part of the test rig. This design has the same dimensions as the physical experimental test setup. Additional details are provided in Table 8. The numerical model was meshed with unstructured tetrahedral elements, shown in Figure 60. Since the design was 1x scaled version of the test rig, inclusion of multiple layers of the refractory wall results in a huge mesh, making the simulation computationally expensive. As a result, it was decided to model the refractory walls using shell conduction feature available in fluent. Typically, walls can be replaced by the shell conduction model when the thickness of the wall layers are comparatively smaller than the size of the domain. In that case, adding finer element causes huge increase in mesh size. Shell conduction tackles this issue by assuming 1D conduction along the thickness of the walls. In the case of aero-thermal test rig, the refractory walls are made of very low thermal conductivity materials and conduction across must be uniform and assuming 1D heat transfer for the sake of computation time will not be a huge violation of this feature or deviation from experiments. The shell conduction feature in fluent allows user to provide number of layers and thickness and material properties for each layer.

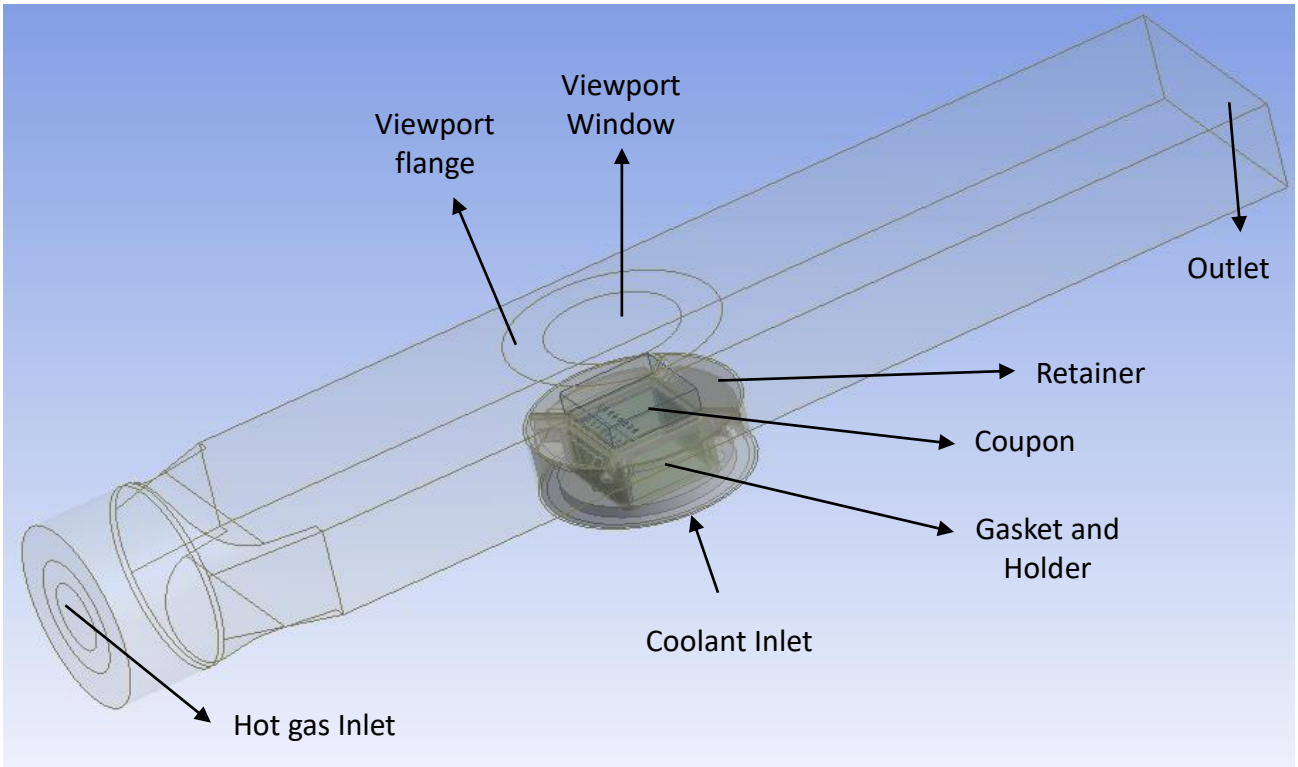

Figure 59 Conjugate numerical model including refractory walls and viewport windows

Table 8 Conjugate numerical model: Aero thermal test rig

Variable	**Value**
Fluid domain	hot gas and coolant
Solid domain	Coupon (Haynes230 alloy), coupon holder assembly: retainer (SS316), holder (Haynes230) and gasket (Cotronics)
Refractory walls	Inner and outer walls: Plicast series Outer shell: carbon steel
Viewport	Window: quartz Holder flange: SS316

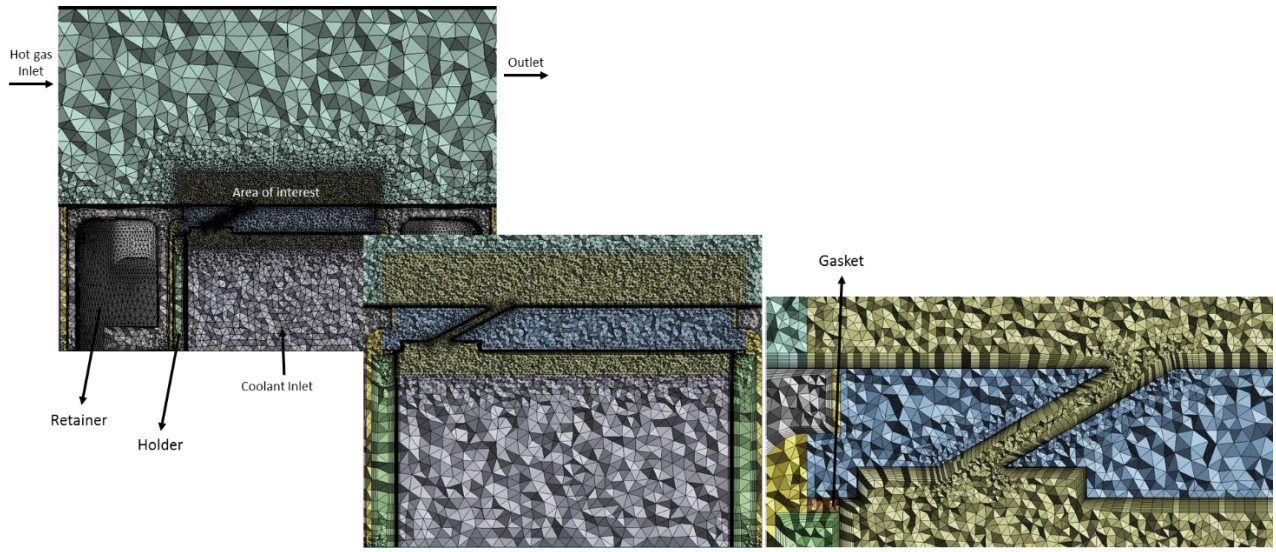

Figure 60 Unstructured tetrahedral elements with refined mesh in the region of interest

In spite of removing the refractory layers and treating the inner wall with shell conduction model, the resultant mesh was made of huge ~ 9-10 million elements. The model was further simplified by the removing the water domain that was used in the experiments to cool the coupon holder assembly and keep their temperature below the safe working limits. Based on the numerical results from the original/initial/actual aero-thermal rig model, it was observed that the difference between water inlet and outlet temperature was less than 1°C. The amount of heat gained by water was negligible and as a result, the other walls of the coupon holder assembly was fixed at a constant temperature same as water inlet temperature.

With these two assumption, a new ***"simplified rig (numerical model)"*** was developed. But before evaluating the performance of the film cooling holes, it was necessary to compare this simplified numerical model with an aero-thermal model that included the layered refractory wall and water domain: ***"actual aero-thermal rig (numerical model)"***. Since the actual aero-thermal model required more than 9 million tetrahedral elements, the unstructured tetra mesh was converted to a polyhedral mesh using fluent in built process. Thus the number of elements reduced from 9 million tets to 5 million polyhedras. The boundary conditions used for all the test cases are shown in Table 9. Typical inlet temperature and tangential velocity profile can be seen in Figure 61.

Table 9 Boundary conditions

Location	Value
Inlet	Velocity – Axial, Radial and Tangential; Static Temperature and TKE and ε: from Combustor CFD run performed by researchers at NETL
Outlet	pressure set to zero
Operating Pressure	3 bar
Surface Emissivity	Holder ε = 0.23; Coupon ε = 0.67; Retainer ε = 0.5; Refractory ε = 0.15; Viewport Flange ε = 0.5; Viewport Window ε = 0.75; Gasket ε = 0.5
Simplified rig	Refractory: Simplified using shell wall conduction Retainer Cooling: Water used to maintain retainer temperature has been simplified using a constant Temp = 300 K Viewport: Air used to cool viewport is not included in the current model
Actual Aero Thermal Rig	Refractory: included in the model Retainer cooling: water domain included in the model Viewport: not included in the current version

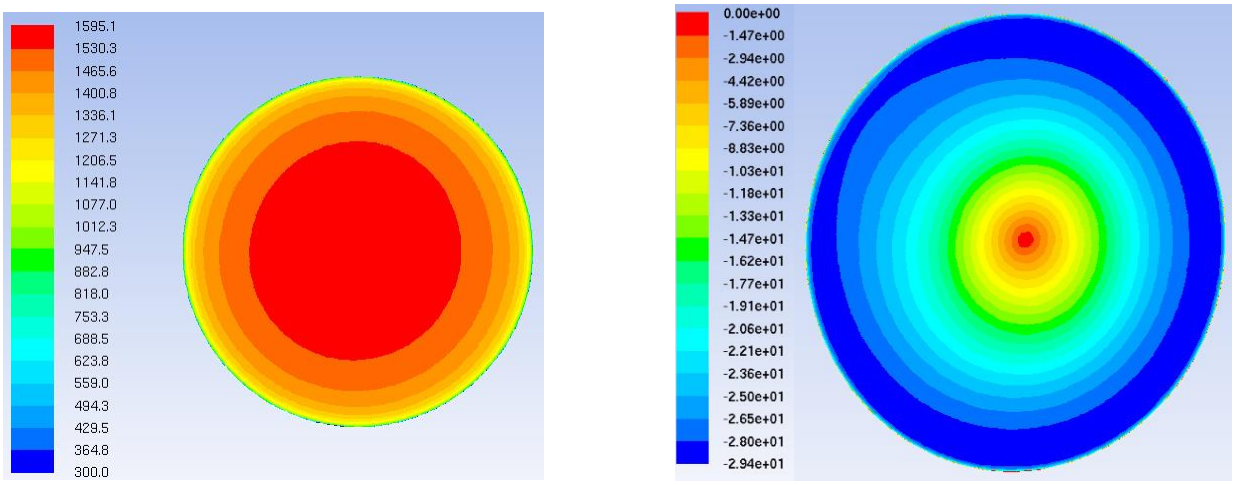

Figure 61 Inlet Boundary Condition: a) Temperature; b) Tangential Velocity

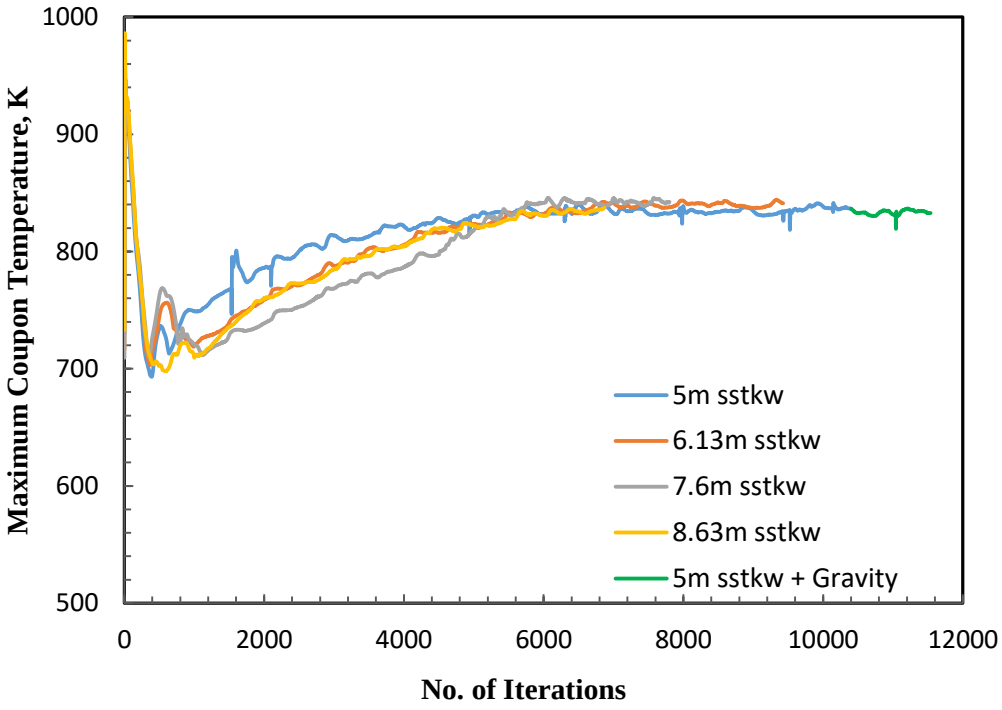

Figure 62 Grid independent study: Comparison of maximum coupon temperature

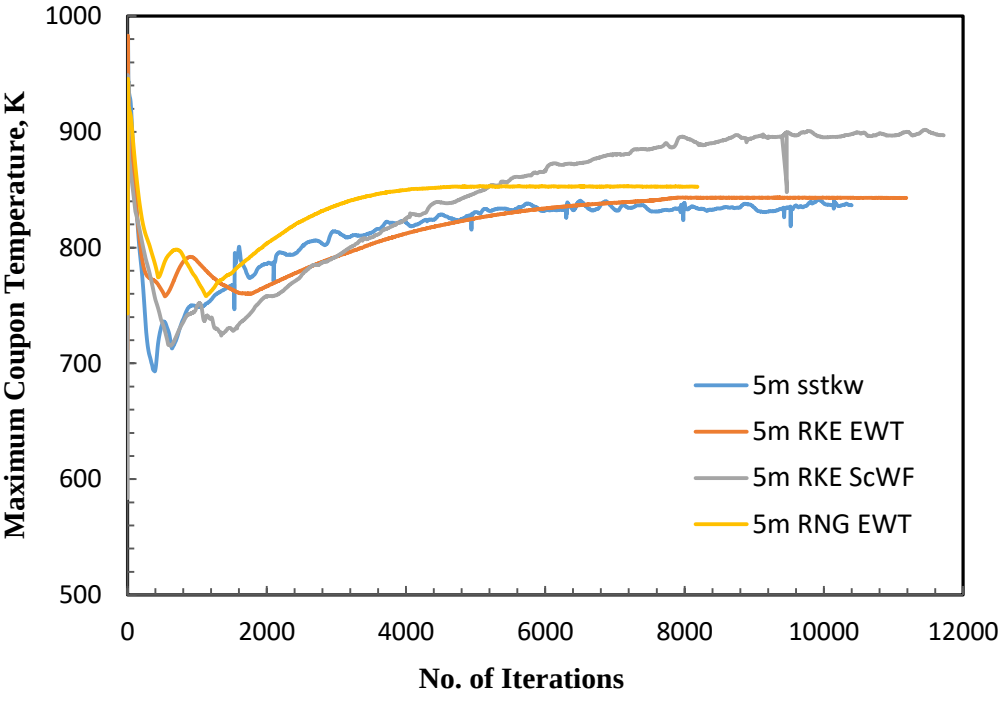

Figure 63 Effect of turbulence model

The results of the grid independent study is shown in Figure 62. The coarsest mesh used in the study with 5 million tetrahedral elements, provided same coupon temperatures as the finer mesh. The effect of turbulence model on film cooling performance needed to studied as it has proven to be significant in the past literature studies. The most commonly used (RANS) turbulent models were RKE and SST-KW. The RNG-KE model, usually recommended for swirling flows, was also compared. Since wall treatment is critical for RKE and RNG-KE models, two different variants: enhanced wall treatment and scalable wall functions were studied. From Figure 63, it can be observed that all models except RKE-SWF resulted in similar coupon surface temperature. Past studies have shown that SST-KW model could predict the laterally averaged effectiveness better, it was chosen as the choice of turbulence model for all test cases.

6.4 Results and Discussion

6.4.1 Comparison of "simplified rig" and "actual aero-thermal rig"

Table 9 shows a comparison of area averaged surface temperature at various locations in the simplified rig and actual aero-thermal (AT) rig model. Marginal decrease in temperature was observed on all locations except the retainer surface that was exposed to the hot mainstream gas (22%). This difference arises from constant temperature wall boundary condition on the outer walls of the retainer. It appears that though the mass averaged water temperature does not rise more than 1 °C, the outer retainer walls are considerable higher than 300 K. The difference in temperature in the regions of interest: coupon hot side and film cooling holes (2.55% and 3.8 % resp.) was considerably lower than the retainer hot side. Though magnitude in difference seems high, this value was smaller than the variability and uncertainty observed in the experiments. Moreover, the predicted temperature difference in the refractory wall surface was close to 1%. It must be noted that these walls were treated with shell conduction in the simplified rig model and this assumption was proven to be valid.

The temperature distribution along a vertical traverse line was also observed between these two models (Figure 64). The difference in hot gas peak temperature and line averaged temperature was: 13 K, 0.86 % and -43 K, -3.4 % respectively. Film temperature distribution also shows agreeable match but difference in lowest temperature is roughly about 40 K, 0.8%.

Table 10 Difference in area averaged surface temperature between the simplified rig and actual AT rig model

Location	Temperature Difference (K)	% difference (increase)
Retainer hot side	100	22
Coupon hot side	21	2.55
Holes	30	3.8
Refractory	-14	-1
Viewport window	36	2.9

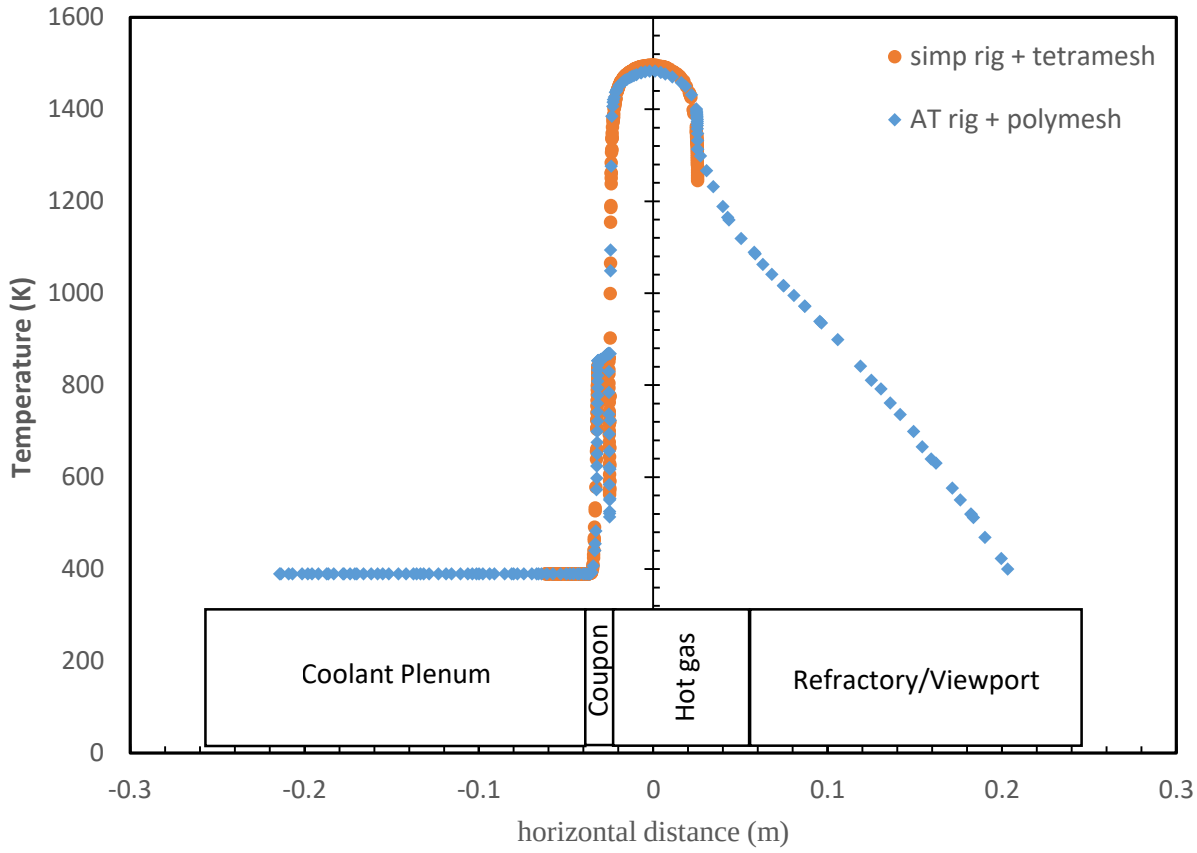

Figure 64 Temperature distribution along a horizontal traverse line: Comparison in prediction

Table 11 shows the magnitude and difference in total heat transfer rates at few critical locations. These are area averaged quantities. The difference in retainer temperature observed in Table 8 was found to offset the balance in heat transfer rates. Since the experimental methodology relies on numerically measured heat fluxes, difference more than 15% could not be accepted. As a result, all numerical simulations were continued with "actual AT rig model".

Table 11 Difference in heat transfer rates between simplified and actual AT rig models

Location	Total heat transfer rate difference (W)	% difference (increase)
Coupon – Retainer Contact	50	26.3
Coupon – Gasket Contact	-6	-20.6
Coupon hot side	62	15.6

6.4.2 Comparison of CFD with experiments

As shown in Figure 65, numerically predicted temperature matches with experiment only at very high blowing ratios: BR 3.0. Effect of blowing ratio on overall effectiveness was not observed in the CFD data: Possible reasons include: a) Experimentally measured turbulence intensity was roughly ~ 15-20% (high uncertainty); b) Film cooling performance at low blowing ratios decreases with increases in mainstream TI; c) Thermocouple radiation correction might explain some differences in temperature in the coolant plenum.

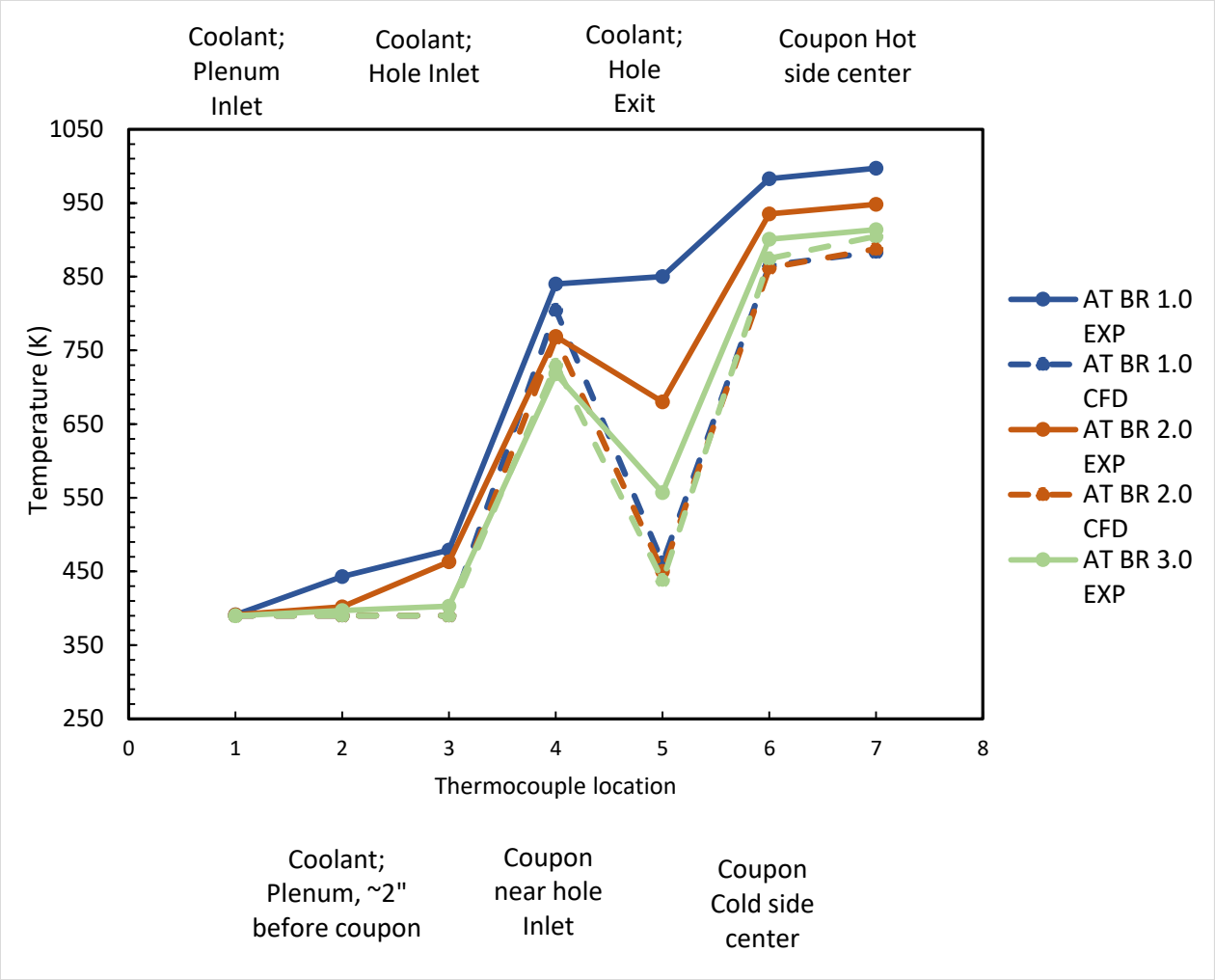

Figure 65 Comparison in temperature between experiments and CFD

CONCLUSION AND FUTURE WORK

Conclusion

Transient heat transfer experiments were conducted on a flat plate test rig with the objective of analyzing the thermal performance of tripod film cooling holes with and without manufacturing features, and comparing this innovative hole geometry to that of traditional film cooling hole geometries used in industry. The film cooling hole geometries analyzed included cylindrical, shaped cylindrical, tripod, shaped tripod, and an additional set of tripod holes with realistic manufacturing features. This study, in agreement with previous work by [14], found that tripod holes are capable of delivering a higher film cooling effectiveness than traditional cylindrical holes at almost half the coolant usage. The experimental results showed that adding realistic manufacturing features to the tripod holes actually improves the overall thermal performance of the hole geometry. Anti-vortex film cooling holes, with and without manufacturing features, were shown to outperform their traditional cylindrical counterparts; adding further evidence of the thermal management advantages that anti-vortex designs can bring if implemented in industrial designs.

Experiments were also conducted on a vane airfoil to evaluate coolant hole designs with an aim to lower the blade metal temperature as much as possible. Different geometries including Cylindrical (CY), Shaped (SH-10°), Tripod (AV-15°) and Shaped-Tripod (SH 5° - AV15°) hole geometries were tested. It was observed that:

a) Shaping improves film cooling effectiveness at lower coolant mass flow rates. However, at higher flow rates, there was no significant improvement expect in the far downstream region. Near the holes, shaping results in higher effectiveness.
b) Tripod holes were better than shaped and cylindrical in the far downstream region at all blowing ratios. Near the holes, roughly 10 hole diameters, AV design results in lower effectiveness region.
c) Shaped-tripod holes provided very high effectiveness compared to other geometries at low flow rate conditions (BR = 1.0 and 2.0 with respect to AV hole). At higher blowing ratios, effect of shaping resulted in low effectiveness region when compared with AV (15°) design.

d) Overall, Anti-Vortex holes (with shaping) serves as the best design at lower blowing ratios (BR = 1.0 and 2.0 with respect to an AV hole) and Anti-Vortex (without shaping) at higher blowing ratios (BR = 3.0 and 4.0).

Tripod holes have already been tested for better film cooling performance. Application of such cooling method would also require careful consideration of its impact on aerodynamic losses and induced thermal stresses. A relatively new technique for studying thermal stress was implemented in this paper. While CFD provided agreeable comparison between experimental and numerical results, stress analysis showed that cylindrical holes can be replaced with tripod holes but the performance depends on working conditions. For both working conditions (CY: BR 0.5 and 2.0), CFD predicts safe function of cooling holes. But caution must be exercised while using these data since CFD over predicted temperature distribution. Moreover, the test section is a simplified version of a gas turbine engine. Even for flat plate testing, usage of actual inlet Reynolds numbers, thermal barrier coating and variation in any parameter attributed with a film cooling hole might have huge implications on thermal stress behavior. For the current study, at any blowing ratio, maximum stress region was seen inside the hole and cylindrical holes seems to create more stress on the blade compared to the tripod holes.

Future work

Experiments conducted so far have provided a good estimate of film cooling performance under laboratory testing conditions. These experiments act as proof of concept studies and helped in identifying optimal film cooling configurations. In order to evaluate the performance of these holes at engine realistic conditions like higher hot gas path temperatures, higher mainstream pressure, metal coupons etc., steady state experiments are being conducted at the aero thermal rig facility at NETL.

The numerical models used until now were developed from models that were validated against laboratory experiments. Moreover, during the validation process it was observed that the trend for the laterally averaged effectiveness was found to be the same as that of experiments but the values were offset. Since then, continuous efforts were taken to improve the numerical predictions. Matching numerical predictions of this conjugate system at engine realistic condition will be a part of the future work as well. A successful prediction of surface temperature also causes

the thermal load on the coupon to be more accurate which in turns results in more precise prediction of thermal stress.

This project focuses on advanced film cooling techniques involved in a thermal management of a gas turbine. It is sponsored by National Energy Technology Laboratory of the Department of Energy. Virginia Tech's collaborators in this project include University of Pittsburg, NETL lab at Morgantown and Pennsylvania State University who work on other fields of research in gas turbine cooling like internal cooling, effects of rotation, effects of high temperature, high pressure conditions etc. The overall objective of this initiative is to develop advanced cooling techniques for a gas turbine vane/blade. As mentioned before, this involves studying film cooling on an airfoil where surface curvature and flow conditions will affect the performance of a film cooling hole. The numerical models developed for the flat plate can also be tested here and film cooling performance can be evaluated.

REFERENCES

[1] R. J. Goldstein, E. R. G. Eckert, and F. Burggraf, "Effects of hole geometry and density on three-dimensional film cooling," *Int. J. Heat Mass Transf.*, vol. 17, no. 5, pp. 595–607, May 1974.

[2] V. L. Eriksen and R. J. Goldstein, "Heat Transfer and Film Cooling Following Normal Injection Through a Round Hole," *J. Eng. Gas Turbines Power*, vol. 96, no. 4, pp. 329–334, Oct. 1974.

[3] D. R. Pedersen, E. R. G. Eckert, and R. J. Goldstein, "Film Cooling With Large Density Differences Between the Mainstream and the Secondary Fluid Measured by the Heat-Mass Transfer Analogy," *J. Heat Transfer*, vol. 99, no. 4, pp. 620–627, Nov. 1977.

[4] D. G. Bogard and K. a. Thole, "Gas Turbine Film Cooling," *J. Propuls. Power*, vol. 22, no. 2, pp. 249–270, Mar. 2006.

[5] R. S. Bunker, "A Review of Shaped Hole Turbine Film-Cooling Technology," *J. Heat Transfer*, vol. 127, no. 4, p. 441, 2005.

[6] J.-C. Han, S. Dutta, and S. Ekkad, *Gas turbine heat transfer and cooling technology*. Taylor & Francis, 2012.

[7] S. Baldauf, a. Schulz, and S. Wittig, "High-Resolution Measurements of Local Effectiveness From Discrete Hole Film Cooling," *J. Turbomach.*, vol. 123, no. 4, p. 758, 2001.

[8] S. Baldauf, a. Schulz, and S. Wittig, "High-Resolution Measurements of Local Heat Transfer Coefficients From Discrete Hole Film Cooling," *J. Turbomach.*, vol. 123, no. 4, p. 749, 2001.

[9] A. K. Sinha, D. G. Bogard, and M. E. Crawford, "Film-cooling effectiveness downstream of a single row of holes with variable density ratio," *J. Turbomach.*, vol. 113, no. 3, pp. 442–449, 1991.

[10] D. L. Schmidt, B. Sen, and D. G. Bogard, "Film Cooling With Compound Angle Holes: Adiabatic Effectiveness," *J. Turbomach.*, vol. 118, no. 4, pp. 807–813, Oct. 1996.

[11] M. Gritsch, A. Schulz, and S. Wittig, "Adiabatic Wall Effectiveness Measurements of Film-Cooling Holes With Expanded Exits," *J. Turbomach.*, vol. 120, no. 3, pp. 549–556, Jul.

1998.

[12] J. D. J. J. D. Heidmann and S. Ekkad, “A novel antivortex turbine film-cooling hole concept,” *J. Turbomach.*, vol. 130, no. 3, p. 31020, 2008.

[13] A. Dhungel, Y. P. Lu, W. Phillips, S. V. Ekkad, and J. Heidmann, “Film Cooling From a Row of Holes Supplemented With Antivortex Holes,” *J. Turbomachinery-Transactions Asme*, vol. 131, no. 2, p. 021007, 2009.

[14] C. LeBlanc, D. P. Narzary, S. Ekkad, C. LeBlanc, and S. Ekkad, “Film-Cooling Performance of Antivortex Hole on a Flat Plate,” *J. Turbomach.*, vol. 135, no. 6, p. 61009, Sep. 2013.

[15] P. L. P. Johnson, J. Kapat, V. Krishnan, H. Zuniga, M. Ricklick, and G. Brown, “The Impact of Manufacturing Techniques on Film Cooling Effectiveness,” in *AIAA/ASME/SAE/ASEE Joint propulsion conference*, 2013, pp. 1–23.

[16] M. B. Jovanović, H. C. de Lange, and a. a. van Steenhoven, “Effect of hole imperfection on adiabatic film cooling effectiveness,” *Int. J. Heat Fluid Flow*, vol. 29, no. 2, pp. 377–386, Apr. 2008.

[17] M. A. Alvin, J. Klinger, B. McMordie, M. Chyu, S. Siw, N. Miller, B. V. K. Reddy, B. Gleeson, I. Anderson, A. Heidloff, S. Ekkad, S. Ramesh, and B. Kang, “NETL Research Efforts on Development and Integration of Advanced Material Systems and Airfoil Cooling Configurations for Future Land-Based Gas Turbine Engines,” in *ASME Turbo Expo 2014: Turbine Technical Conference and Exposition*, 2014, pp. V006T22A006–V006T22A006.

[18] S. Ito, R. J. Goldstein, and E. R. G. Eckert, “Film cooling of a gas turbine blade,” *J. Eng. Power*, vol. 100, no. 3, pp. 476–481, 1978.

[19] U. Drost and A. Bölcs, “Investigation of detailed film cooling effectiveness and heat transfer distributions on a gas turbine airfoil,” in *ASME 1998 International Gas Turbine and Aeroengine Congress and Exhibition*, 1998, pp. V004T09A003–V004T09A003.

[20] L. J. Zhang and R. Pudupatty, “The Effects of Injection Angle and Hole Exit Shape on Turbine Nozzle Pressure Side Film Cooling,” in *ASME Turbo Expo 2000: Power for Land, Sea, and Air*, 2000, pp. V003T01A053–V003T01A053.

[21] M. I. Ethridge, J. M. Cutbirth, and D. G. Bogard, “Scaling of performance for varying density ratio coolants on an airfoil with strong curvature and pressure gradient effects,” in *ASME Turbo Expo 2000: Power for Land, Sea, and Air*, 2000, pp. V003T01A047–V003T01A047.

[22] J. Chappell, P. Ligrani, S. Sreekanth, and T. Lucas, “Suction-side gill region film cooling: effects of hole shape and orientation on adiabatic effectiveness and heat transfer coefficient,” *J. Turbomach.*, vol. 132, no. 3, p. 31022, 2010.

[23] J. R. Winka, J. B. Anderson, E. J. Boyd, D. G. Bogard, and M. E. Crawford, “Convex Curvature Effects on Film Cooling Adiabatic Effectiveness,” *J. Turbomach.*, vol. 136, no. 6, p. 61015, 2014.

[24] S. Yamawaki, T. Maya, B. A. Haven, D. K. Yamagata, M. Kurosaka, S. Yamawaki, and T. Maya, “Anti-kidney pair of vortices in shaped holes and their influence on film cooling effectiveness,” in *ASME 1997 International Gas Turbine and Aeroengine Congress and Exhibition*, 1997, pp. V003T09A007–V003T09A007.

[25] T. I. P. Shih, Y.-L. Lin, M. K. Chyu, and S. Gogineni, “Computations of film cooling from holes with struts,” in *ASME 1999 International Gas Turbine and Aeroengine Congress and Exhibition*, 1999, pp. V003T01A085–V003T01A085.

[26] S. S. Papell, “Vortex generating flow passage design for increased film-cooling effectiveness and surface coverage,” *NASA STI/Recon Tech. Rep. N*, vol. 84, p. 22909, 1984.

[27] K. B. M. Q. Zaman and J. K. Foss, “The effect of vortex generators on a jet in a cross-flow,” *Phys. Fluids*, vol. 9, no. 1, pp. 106–114, 1997.

[28] R. S. Bunker, “Film cooling effectiveness due to discrete holes within a transverse surface slot,” in *ASME Turbo Expo 2002: Power for Land, Sea, and Air*, 2002, pp. 129–138.

[29] Y. Lu, D. Faucheaux, and S. V Ekkad, “Film Cooling Measurements for Novel Hole Configurations,” in *ASME 2005 Summer Heat Transfer Conference collocated with the ASME 2005 Pacific Rim Technical Conference and Exhibition on Integration and Packaging of MEMS, NEMS, and Electronic Systems*, 2005, pp. 59–66.

[30] K. Kusterer, A. Elyas, D. Bohn, T. Sugimoto, R. Tanaka, and M. Kazari, “Film Cooling Effectiveness Comparison Between Shaped-and Double Jet Film Cooling Holes in a Row Arrangement,” *ASME Turbo Expo 2010 Power Land, Sea, Air. Am. Soc. Mech. Eng.*, pp. 1503–1515, 2010.

[31] J. S. Liu, M. F. Malak, L. A. Tapia, D. C. Crites, D. Ramachandran, B. Srinivasan, G. Muthiah, and J. Venkataramanan, “Enhanced film cooling effectiveness with new shaped holes,” in *ASME Turbo Expo 2010: Power for Land, Sea, and Air*, 2010, pp. 1517–1527.

[32] S. Ramesh, D. G. Ramirez, S. V Ekkad, and M. A. Alvin, “Analysis of film cooling

performance of advanced tripod hole geometries with and without manufacturing features," *Int. J. Heat Mass Transf.*, vol. 94, pp. 9–19, 2016.

[33] R. S. Bunker, "Film Cooling: Breaking the Limits of Diffusion Shaped Holes," in *ICHMT DIGITAL LIBRARY ONLINE*, 2009.

[34] B. B. K. Hunley, A. C. Nix, W. Virginia, and J. D. Heidmann, "A preliminary numerical study on the effect of high freestream turbulence on anti-vortex film cooling design at high blowing ratio," in *ASME Turbo Expo 2010: Power for Land, Sea, and Air*, 2010, pp. 1313–1322.

[35] D. M. Kercher, "A film-cooling CFD bibliography: 1971–1996," *Int. J. Rotating Mach.*, vol. 4, no. 1, pp. 61–72, 1998.

[36] J. D. J. Ferguson, D. K. D. Walters, and J. J. H. Leylek, "Performance of turbulence models and near-wall treatments in discrete jet film cooling simulations," in *ASME, International Gas Turbine & Aeroengine Congress & Exhibition, 43 rd, Stockholm, Sweden*, 1998.

[37] D. K. Walters and J. H. Leylek, "Computational Study of Film-Cooling Effectiveness on a Low-Speed Airfoil Cascade: Part II—Discussion of Physics," in *ASME 2002 International Design Engineering Technical Conferences and Computers and Information in Engineering Conference*, 2002.

[38] K. L. Harrison and D. G. Bogard, "Comparison of RANS turbulence models for prediction of film cooling performance," in *ASME Turbo Expo 2008: Power for Land, Sea, and Air*, 2008, pp. 1187–1196.

[39] S. Ravelli and G. Barigozzi, "Application of Unsteady CFD Methods to Trailing Edge Cutback Film Cooling," *Vol. 5B Heat Transf.*, vol. 136, no. December 2014, p. V05BT13A012, 2014.

[40] Z. T. Stratton, T. I. P. Shih, G. M. Laskowski, B. Barr, and R. Briggs, "Effects of crossflow in an internal-cooling channel on film cooling of a flat plate through compound-angle holes," in *ASME Turbo Expo 2015: Turbine Technical Conference and Exposition*, 2015, pp. V05BT12A022–V05BT12A022.

[41] J. W. McClintic, S. R. Klavetter, J. R. Winka, J. B. Anderson, D. G. Bogard, J. E. Dees, G. M. Laskowski, and R. Briggs, "The effect of internal crossflow on the adiabatic effectiveness of compound angle film cooling holes," *J. Turbomach.*, vol. 137, no. 7, p. 71006, 2015.

[42] R. Schroeder and K. Thole, “Adiabatic Effectiveness Measurements for a Baseline Shaped Film Cooling Hole,” in *ASME Turbo Expo 2014, GT2014-25992*, 2014, pp. 1–13.

[43] T. W. Repko, A. C. Nix, S. C. Uysal, and A. T. Sisler, “Flow Visualization of Multi-Hole Film-Cooling Flow under Varying Freestream Turbulence Levels,” *J. Flow Control. Meas. Vis.*, vol. 4, no. January, pp. 13–29, 2016.

[44] K. Kusterer, D. Bohn, T. Sugimoto, and R. Tanaka, “Double-Jet Ejection of Cooling Air for Improved Film Cooling,” *J. Turbomach.*, vol. 129, no. 4, p. 809, 2007.

[45] C. Han, J. Ren, and H. De Jiang, “Multi-parameter influence on combined-hole film cooling system,” *Int. J. Heat Mass Transf.*, vol. 55, no. 15–16, pp. 4232–4240, 2012.

[46] C. Han, Z. Chi, J. Ren, and H. Jiang, “Optimal Arrangement of Combined-Hole for Improving Film Cooling Effectiveness,” *J. Therm. Sci. Eng. Appl.*, vol. 7, no. 1, p. 11010, Mar. 2015.

[47] Z. Chi, C. Han, X. Li, J. Ren, and H. Jiang, “Geometrical Optimization and Experimental Validation of a Tripod Film Cooling Hole With Asymmetric Side Holes,” in *ASME Turbo Expo 2014: Turbine Technical Conference and Exposition*, 2014, pp. V05BT13A005–V05BT13A005.

[48] C. LeBlanc, S. Ramesh, S. Ekkad, and M. A. Alvin, “Effect of Breakout Angle on Tripod Injection Hole Geometries on Flat Plate Film Cooling,” in *ASME 2012 International Mechanical Engineering Congress and Exposition*, 2012, pp. 1995–2002.

[49] S. Kline and F. McClintock, “Describing uncertainties in single-sample experiments,” *Mechanical engineering*. 1953.

[50] A. P. Rallabandi, J. Grizzle, and J.-C. Han, “Effect of Upstream Step on Flat Plate Film-Cooling Effectiveness Using PSP,” *J. Turbomach.*, vol. 133, no. 4, p. 041024, 2011.

[51] M. Gritsch, A. Schulz, and S. Wittig, “Film-cooling holes with expanded exits: Near-hole heat transfer coefficients,” *Int. J. Heat Fluid Flow*, vol. 21, no. 2, pp. 146–155, 2000.

[52] N. Hay, D. Lampard, and C. L. Saluja, “Effects of Cooling Films on the Heat Transfer Coefficient on a Flat Plate With Zero Mainstream Pressure Gradient,” *J. Eng. Gas Turbines Power*, vol. 107, no. 1, p. 105, 1985.

[53] J. H. Leylek and R. D. Zerkle, “Discrete-jet film cooling: a comparison of computational results with experiments,” *J. Turbomach.*, vol. 116, no. July 1994, p. 358, 1994.

[54] S. W. S. Burd and T. T. W. Simon, “The influence of coolant supply geometry on film

coolant exit flow and surface adiabatic effectiveness," *ASME Pap.*, no. 97-GT, p. 25, 1997.

[55] J. D. Heidmann, "A Numerical Study of Anti-Vortex Film Cooling Designs at High Blowing Ratio," *Vol. 4 Heat Transf. Parts A B*, no. November, pp. 789–799, 2008.

[56] T. G. Sidwell, S. A. Lawson, D. L. Straub, K. H. Casleton, and S. Beer, "Conjugate Heat Transfer Modeling of a Film-Cooled, Flat-Plate Test Specimen in a Gas Turbine Aerothermal Test Facility," in *Volume 3B: Heat Transfer*, 2014, pp. 1–16.

[57] S. Ramesh, S. V Ekkad, D. L. Straub, S. A. Lawson, and M. A. Alvin, "Experimental and Computational Analysis of Film Cooling Hole Performance on a High Temperature Test Rig," in *ASME 2014 International Mechanical Engineering Congress and Exposition*, 2014, pp. V08BT10A007–V08BT10A007.

[58] S. a. Lawson, D. L. Straub, S. Beer, K. H. Casleton, and T. Sidwell, "Direct Measurements of Overall Effectiveness and Heat Flux on a Film Cooled Test Article at High Temperatures and Pressures," in *Volume 3C: Heat Transfer*, 2013, p. V03CT14A008.

[59] W. F. Colban, K. A. Thole, and D. Bogard, "A Film-Cooling Correlation for Shaped Holes on a Flat-Plate Surface," *J. Turbomach.*, vol. 133, no. 1, p. 011002, 2011.